Effects of the Jimpy mutation on retinal structure and function

Dissertation

zur Erlangung des Grades eines

Doktors der Naturwissenschaften

der Mathematisch-Naturwissenschaftlichen Fakultät

und

der Medizinischen Fakultät

der Eberhard-Karls-Universität Tübingen

vorgelegt

von

Hovhannisyan Anahit

aus Yerevan, Armenia

September 2014

Tag der mündlichen Prüfung:	Oktober 27th, 2014
Dekan der Math.-Nat. Fakultät:	Prof. Dr. W. Rosenstiel
Dekan der Medizinischen Fakultät:	Prof. Dr. I. B. Autenrieth
1. Berichterstatter:	Dr. T. Münch
2. Berichterstatter:	Prof. Dr. U. Schraermeyer
Prüfungskommission:	Dr. T. Münch
	Prof. Dr. U. Schraermeyer
	Dr. M. Kukley
	Prof. Simone Di Giovanni

I hereby declare that I have produced the work entitled: “Effects of the Jimpy mutation on retinal structure and function”, submitted for the award of a doctorate, on my own (without external help), have used only the sources and aids indicated and have marked passages included from other works, whether verbatim or in content, as such. I swear upon oath that these statements are true and that I have not concealed anything. I am aware that making a false declaration under oath is punishable by a term of imprisonment of up to three years or by a fine.

Tübingen, September 17th 2014

Anahit Hovhannisyan

Publications

Published

J Anat. 2011 Jul;219(1):18-32. doi: 10.1111/j.1469-7580.2011.01392.x. Epub 2011 May 17.

Fate of neuron-glia synapses during proliferation and differentiation of NG2 cells.

Fröhlich N, Nagy B, Hovhannisyan A, Kukley M.

Author information

Group of Neuron-Glia Interactions, Werner Reichardt Centre for Integrative Neuroscience, University of Tübingen, Germany.

ABSTRACT

Progenitor cells expressing proteoglycan NG2 (also known as oligodendrocyte precursor cells or polydendrocytes) are widespread in the grey and white matter of the CNS; they comprise 8-9% of the total cell population in adult white matter, and 2-3% of total cells in adult grey matter. NG2 cells have a complex stellate morphology, with highly branched processes that may extend more than 100 μm around the cell body. NG2 cells express a complex set of voltage-gated channels, AMPA/kainate and/or γ-aminobutyric acid (GABA)(A) receptors, and receive glutamatergic and/or GABAergic synaptic input from neurons. In every region of the brain NG2 cells are found as proliferative cells, and the fraction of actively cycling NG2 cells is quite high in young as well as in adult animals. During development NG2 cells either differentiate into myelinating oligodendrocytes (and possibly also few astrocytes and neurons) or persist in the brain parenchyma as NG2 cells. This review highlights new findings related to the morphological and electrophysiological changes of NG2 cells, and the fate of synaptic input between neurons and NG2 cells during proliferation and differentiation of these cells in the neonatal and adult nervous system of rodents.

Submitted

Journal of comparative neurology, 2014 August

Effects of the jimpy mutation on mouse retinal structure and function

Anahit Hovhannisyan[1,2], Boris Benkner[1], Antje Biesemeier[3], Ulrich Schraermeyer[3], Maria Kukley[2], Thomas A. Münch[1,*]

1 Retinal Circuits and Optogenetics, Centre for Integrative Neuroscience, University of Tübingen, 72076 Tübingen, Germany

2 Neuron Glia Interactions, Centre for Integrative Neuroscience, University of Tübingen, 72076 Tübingen, Germany

3 Section of Experimental Vitreoretinal Surgery, Centre for Ophthalmology, 72076 Tübingen, Germany

* Corresponding Author

ABSTRACT

The Jimpy mutant mouse has a point mutation in the proteolipid protein gene (plp1). The resulting misfolding of the protein leads to oligodendrocyte death, myelin destruction and failure to produce adequately myelinated neurons in the central nervous system (CNS). It is not known how the absence of normal myelination during development influences neural function. For this reason I characterized the Jimpy mouse retina in order to find out if lack of myelination in the optic nerve during development has an effect on normal functioning and morphology of the retina.

Optokinetic reflex measurements showed that Jimpy mice had, in general, a functional visual system. Both PLP1 antibody staining and RT-PCR for plp1 mRNA showed that plp1 is not expressed in the wild type retina. However, in the optic nerve, plp1 is normally expressed, and consequently, in Jimpy mutant mice, myelination of axons in the optic nerve was mostly absent. Nevertheless, neither axon count nor axon ultrastructure in the optic nerve was affected. Physiological recordings of ganglion cell activity using microelectrode arrays revealed a decrease

of stimulus-evoked activity at mesopic light levels. Morphological analyses of the retina did not show any significant differences in the gross morphology, such as thickness of retinal layers or cell number in the inner and outer nuclear layer. The cell bodies in the inner nuclear layer, however, were larger in the retina of Jimpy mutant mice. Antibody labeling against cell type specific markers showed that the number of rod bipolar and horizontal cells was increased in Jimpy mice. In conclusion, while the Jimpy mutation has dramatic effects on the myelination of retinal ganglion cell axons, it has moderate effects on retinal morphology and function.

Link between publications and thesis

The published review I have used in my introduction, for introducing the oligodendrocyte precursor cells. These are precursors of oligodendrocytes which die because of Jimpy mutation.

The findings in this thesis are included in the submitted publication.

Content

PUBLICATIONS ..... - 4 -

CONTENT ..... - 9 -

LIST OF TABLES ..... - 12 -

LIST OF FIGURES ..... - 13 -

1. ABSTRACT 3

2. EXTENDED SYNOPSIS 4

2.1. PURPOSE AND BACKGROUND: 4

2.2. AIM OF THE PROJECT: 6

2.3. WORK DESCRIPTION: 6

2.3.1. Find out if Jimpy mutation has direct effect on the retina. 7

2.3.2. Effect of Jimpy mutation on function of retina. 7

2.3.3. Effect of Jimpy mutation on morphology of retina. 8

2.4. CONCLUSION 8

3. GENERAL INTRODUCTION 9

3.1. SIGNAL TRANSDUCTION AND CELL TYPES IN NERVOUS SYSTEM 9

3.2. OLIGODENDROCYTES DURING DEVELOPMENT 13

3.3. MYELINATION IN THE OPTIC NERVE DURING DEVELOPMENT 17

3.4. RETINA GANGLION CELL AXONS IN THE RETINA AND OPTIC NERVE 18

3.5. MYELIN BASED AND PROTEOLIPID PROTEINS 19

3.6. DEMYELIANTION AND DYSMYELINATION DISEASES 22

3.6.1. General description 22

3.6.2. Dysmyelination and Jimpy mouse model 23

3.7. RETINA AND VISUAL SYSTEM DURING DEVELOPMENT 26

4. METHODS 30

4.1. ANIMALS 30

4.2. MOLECULAR BIOLOGY 32

4.2.1. Genotyping 32

4.2.2. plp1 gene expression *36*
4.3. Electron Microscopy 38
4.4. Immunohistochemistry 44
4.5. MEA recordings: Experimental procedure 49
4.6. MEA recordings: Stimuli 50
4.7. MEA recordings: Light Intensity Measurements 54
4.8. MEA recordings: Spike sorting and data analyses 55
4.9. Behavioral tests: Optokinetic drum 57
5. EFFECT OF JIMPY MUTATION ON RETINAL GANGLION CELLS AND OPTOKINETIC REFLEX 58
5.1. Introduction 58
5.2. Results 58
5.2.1. Myelin based protein and proteolipid protein expression in the retina *59*
5.2.2. Effects of the Jimpy mutation on the ganglion cells body and axons morphology *61*
5.2.3. General functional characterization of visual system *64*
5.3. Discussion 65
6. EFFECTS OF THE JIMPY MUTATION ON RETINAL FUNCTION 67
6.1. Introduction 67
6.2. Results 67
6.2.1. Spontaneous spike rate *68*
6.2.2. Stimulus evoked spike rate *70*
6.2.3. Linear filter *71*
6.2.4. Spatial and Temporal preference of retinal ganglion cells *72*
6.3. Discussion 74
7. EFFECTS OF THE JIMPY MUTATION ON RETINAL MORPHOLOGY 75
7.1. Introduction 75
7.2. Results 76
7.2.1. Retina gross morphology *76*
7.2.2. Cell type-specific comparison *79*
7.3. Discussion 83
8. GENERAL DISCUSSION 84

9. REFERENCES..89

List of tables

Table 4-1: RT-PCR primer details 34

Table 4-2 Overview table of animals with their genetic background included in the experiments. 36

Table 4-3: RT-PCR primer details 38

Table 4-4: Antibody list 46

List of Figures

Figure 2-1. Schematic presentation of visual system development 6

Figure 3-1. Signal transduction between neurons. 10

Figure 3-2. Types of the neurons and their functional components. 11

Figure 3-3. Different types of glia cells. 13

Figure 3-4. Oligodendrocyte development in the wild type mouse optic nerve. 14

Figure 3-5. Electron micrographs of the synaptic relationships of OPC with an axon in the hippocampus. 15

Figure 3-6. Morphological comparison of the oligodendrocyte lineage cells. 16

Figure 3-7. The myelination by oligodendrocyte. 17

Figure 3-8. The axons bundles in the optic nerve. 19

Figure 3-9. The structure of myelin. 20

Figure 3-10. Myelinated axons in the mouse optic nerve (P21). 21

Figure 3-11. Example of myelin sheaths from dysmyelination models. 23

Figure 3-12. PLP1 protein and its role in myelination. 24

Figure 3-13. The myelination in wild type and Jimpy mutant mice. 25

Figure 3-14. Diagram of time course of development of different cell types in the retina, and schematic representation of the retina. 28

Figure 4-1. The phenotype of Jimpy mutant mouse. 30

Figure 4-2. Genotyping results of wild type and Jimpy mutant mice for $plp1^{jp}$ and Eda^{Ta} mutations. 35

Figure 4-3. Eyecup and optic nerve preparation for EM analyses. 39

Figure 4-4. The cross section of the retina for light microscopy analyses..... 40

Figure 4-5. Measuring the thicknesses of retina layers and counting of the cells in the ONL, INL and GCL. 41

Figure 4-6. Measuring the cell body size in the ONL, INL and GCL. 43

Figure 4-7. Cell count examples for horizontal, rod bipolar, starburst amacrine and Müller cells..... 48

Figure 4-8. Retina preparation for MEA recordings. 50

Figure 4-9. Experimental setup of MEA recordings. 51

Figure 4-10. Stimulus used during MEA recordings, and included in the thesis. 52

Figure 4-11. The time course of used stimuli during experiments. 53

Figure 4-12. The raw data high pass filtering..... 55

Figure 4-13. The optokinetic reflex measurement. 57

Figure 5-1.: Expression and localization of MBP and PLP in the retina and optic nerve..... 61

Figure 5-2.: Electron micrographs of optic nerve cross-sections. 62

Figure 5-3. Electron micrographs of ganglion cell bodies from retina cross-sections of wild type (left) and Jimpy mutant mice (right). 63

Figure 5-4.: Tested animals that show optokinetic reflex. 65

Figure 6-1. Spontaneous firing rate of retinal ganglion cells. 69

Figure 6-2. Stimulus evoked spike rate of retinal ganglion cells to white noise full flicker stimulation. 70

Figure 6-3. Linear filters latencies of retinal ganglion cells. 72

Figure 6-4. Spatial and temporal preference of retinal ganglion cells. 73

Figure 7-1. General morphology of wild type and Jimpy mutant retinas. 77

Figure 7-2. Mean cell body size from the individual retinas. 78

Figure 7-3. EM micrograph of Müller cell in the retina cross section. 79

Figure 7-4. Density of horizontal and rod bipolar cells in wild type and Jimpy mutant ventral and dorsal retina. 81

Figure 7-5. Density of Müller cells and starburst cells in wild type and Jimpy mutant ventral and dorsal retina. 82

1. Abstract

The Jimpy mutant mouse has a point mutation in the proteolipid protein gene (*plp1*). The resulting misfolding of the protein leads to oligodendrocyte death, myelin destruction and failure to produce adequately myelinated neurons in the central nervous system (CNS). It is not known how the absence of normal myelination during development influences neural function. For this reason I characterized the Jimpy mouse retina in order to find out if lack of myelination in the optic nerve during development has an effect on normal functioning and morphology of the retina.

Optokinetic reflex measurements showed that Jimpy mice had, in general, a functional visual system. Both PLP1 antibody staining and RT-PCR for *plp1* mRNA showed that *plp1* is not expressed in the wild type retina. However, in the optic nerve, *plp1* is normally expressed, and consequently, in Jimpy mutant mice, myelination of axons in the optic nerve was mostly absent. Nevertheless, neither axon count nor axon ultrastructure in the optic nerve was affected. Physiological recordings of ganglion cell activity using microelectrode arrays revealed a decrease of stimulus-evoked activity at mesopic light levels. Morphological analyses of the retina did not show any significant differences in the gross morphology, such as thickness of retinal layers or cell number in the outer nuclear layer. The cell bodies in the inner and outer nuclear layer, however, were larger in the retina of Jimpy mutant mice. Antibody labeling against cell type specific markers showed that the number of rod bipolar and horizontal cells was increased in Jimpy mice. In conclusion, while the Jimpy mutation has dramatic effects on the myelination of retinal ganglion cell axons, it has moderate effects on retinal morphology and function.

2. Extended Synopsis

2.1. Purpose and background:

Nerve cells communicate by sending electrical signals (action potentials, or spikes) down through the axons. To increase the speed of conduction, and to isolate neighboring axons from each other, many axons in the central and peripheral nervous system are wrapped by myelin (Baumann and Pham-Dinh 2001; Nave 2010). Loss of myelin can result in severe neurological diseases (Baumann and Pham-Dinh 2001; Butt, Pugh et al. 2004). There are diverse causes of myelin loss, including autoimmune disorders (e.g. multiple sclerosis) (Baumann and Pham-Dinh 2001; Trapp and Nave 2008) or genetic mutations in the glial cells that form the myelin sheaths (Baumann and Pham-Dinh 2001).

During the recent decades many aspects of demyelination and remyelination have been investigated in detail. Yet an important question which still remains open is whether a neuron, whose axon gets demyelinated, “knows” about the demyelination event, and whether it changes its morphological and/or functional properties, and/or its connectivity with other cells, in response to demyelination. To start addressing this question I used a retina-optic nerve preparation as a model system. The optic nerve consists of axons of retinal ganglion cells, the output neurons of the retina. While these axons are myelinated inside the optic nerve, they remain unmyelinated while they are still transversing the retina, from the cell body to the optic disk. In fact, there is no myelination at all inside the retina. Because of this arrangement, ganglion cells do not receive synaptic input from neurons that are normally myelinated, but they may be affected directly by dysmyelination.

As an animal model I have chosen the Jimpy mouse mutant, which carries a spontaneous point mutation in the the gene coding for proteolipid protein 1 (*plp1*). In humans, mutations in *plp1* underly the Pelizaeus-Merzbacher disease, where different forms of the genetic defect (duplication, deletion) lead to different degrees of disease severity (Greer and Lees 2002). PLP1 is a membrane protein with four

transmembrane domains. It is expressed by oligodendrocytes, the glial cells responsible for axon myelination (Gow, Friedrich et al. 1994; Jung, Sommer et al. 1996; Thomson, Montague et al. 1997; Gow, Southwood et al. 1998; Kramer, Schardt et al. 2001; Southwood and Gow 2001; Ghandour, Feutz et al. 2002; Dhaunchak and Nave 2007; Bradl and Lassmann 2010). Its extracellular domain is thought to make tight homotypic connections with other PLP1 proteins. PLP1 thus contributes to stability and structural integrity of myelination by cross linking the many layers of the myelin sheath as it wraps around an axon (Kalwy and Smith 1994). In the Jimpy mutant, the mutation does not disrupt expression of the protein, but the protein gets trapped in the Golgi apparatus and eventually causes the death of the oligodendrocytes.

The Jimpy mutation is X-linked and recessive. Affected male mice have a severe phenotype: they have muscular spasms, they shake, and usually die by the age of postnatal day 22-24 (P22-P24) due to respiratory problems (Klugmann, Schwab et al. 1997; Vela, Gonzalez et al. 1998). Consistent with the suggested disease pathogenesis, most axons in the central nervous system remain unmyelinated in Jimpy mice. This includes the axons in the optic nerve (Meier and Bischoff 1975; Omlin and Anders 1983).

To investigate the effect of dysmyelination on the neurons, I have looked at the physiological and morphological properties of the wild type and Jimpy mutant mouse retinas. As the mutant mice are dying around P22, I was restricted with the time window that I could perform investigations.

Below is the schematic diagram of retina, optic nerve and LGN development (Figure 2-1). The red frame on the diagram represents the latest time window that I can use for my experiments. As you can see the retina has already all cell types and connections developed. Around P20-P22, the light evoked responses of the retina are also present. The connections with the upper brain regions has been also established (for more details see section 3.7 of the introduction). This means the P20-P21 age group, where I have performed all my investigations, can mimic the behavior of mature retina.

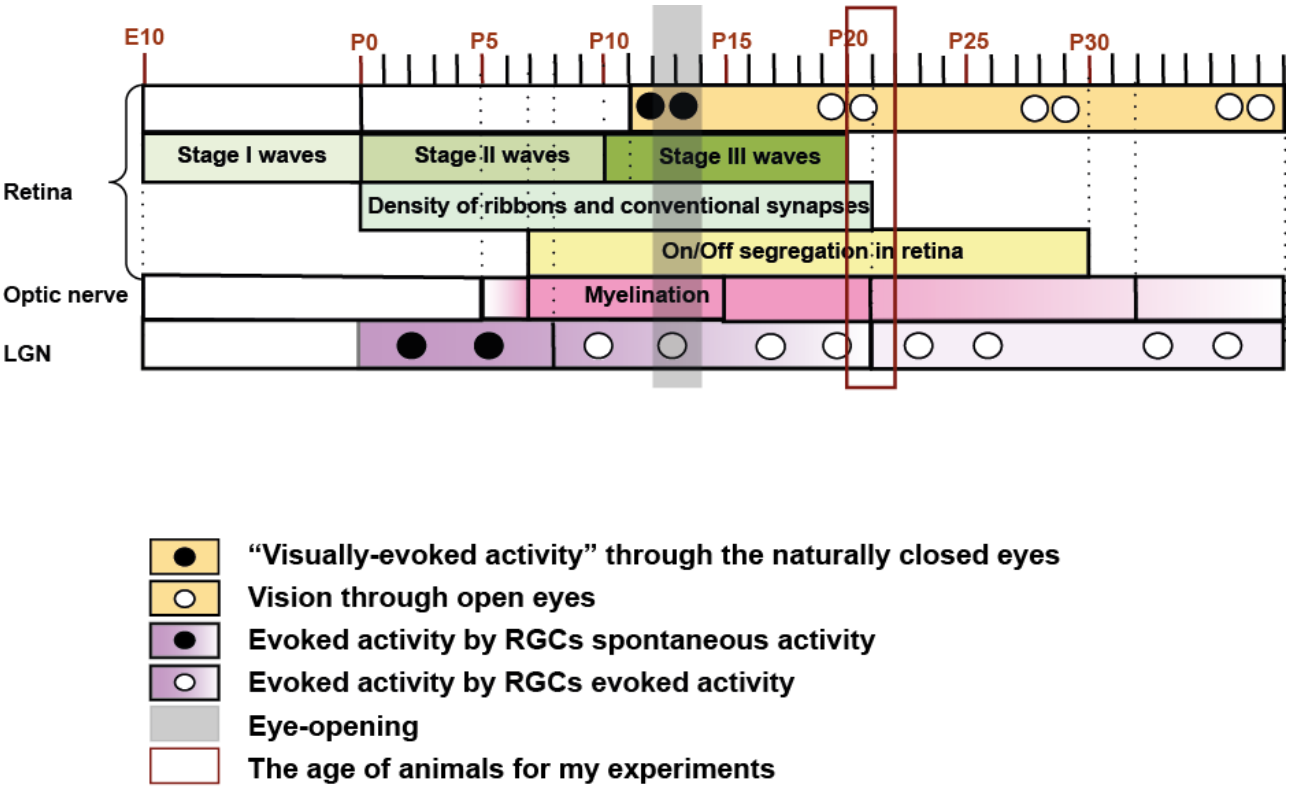

Figure 2-1. Schematic presentation of visual system development

2.2. Aim of the project:

The aim of my Ph.D project is to study whether dysmyelination has an effect on dysmyelinated neurons morphology and function.

2.3. Work description:

For this project I have used 20 to 22 day old male wild type and Jimpy mutant mice. I have performed morphological measurements, MEA recordings, optokinetic reflex measurements. Here are my ***objectives:***

2.3.1. Find out if Jimpy mutation has direct effect on the retina.

PLP1 antibody staining and RT-PCR for *plp1* mRNA showed that there is no PLP1 expression in the wild-type retina. This suggests that it is unlikely for the mutated Jimpy protein to have a direct effect on cells in the retina.

In order to check whether the number of retinal ganglion cells is reduced in Jimpy mutant, and as well whether retinal ganglion cell axons have been damaged I have analyzed the optic nerve on the EM level. I found that, as previous studies have shown, only very few axons are myelinated in the mutant mice and that myelin sheaths are less compact than in wild type mice. The axon and cell count, however, and the axon and the cell body morphology themselves, didn't show any significant difference.

In addition, I have checked if the Jimpy mutation has an effect proper visual information transduction. For this we have made optokinetic reflex measurements in Jimpy mutant and wild type mice. The results show that 50% of tested Jimpy mutant mice and 86% of wild type mice have the optokinetic reflex.

2.3.2. Effect of Jimpy mutation on function of retina.

The aim of this objective was to find out if the functional properties of retinal ganglion cells have been affected because of Jimpy mutation. For this I have performed micro electrode array (MEA) recordings. The results didn't show an obvious change of response properties of the various RGCs types (ON, OFF, direction selective), although I have found that in the mesopic ambient luminance stimulus evoked spike rate was significantly lower in Jimpy mutants retina compared to the wild type mice.

2.3.3. Effect of Jimpy mutation on morphology of retina.

The aim of this objective was to check whether the retina morphology has been affected because of Jimpy mutation. The analyses didn't show any significant differences in the gross morphology of the retina, such as thickness of retinal layers or cell number in inner and outer nuclear layer. However, the cell bodies in the inner nuclear layer were larger in the Jimpy mutant mice.

Specific antibody labeling showed that the number of Rod bipolar cells and horizontal cells increased in Jimpy mice.

2.4. Conclusion

I confirmed the previously reported severe dysmyelination of axons within the optic nerve. However, the dysmyelinated axons show normal ultrastructure, and they do not decline in number. The processing of light stimuli by the retina was altered in a way that suggests that some neurons (that are not normally myelinated) have altered properties in the Jimpy mutant retina. Consistent with these physiological findings, I found subtle changes in the gross retinal morphology, and I found that the number of certain interneurons in the retina (rod bipolar cells and horizontal cells) was increased in the Jimpy mutant mouse.

The thesis contains detailed explanation of my findings. In the discussion part I discuss possible reasons for the changes observed in Jimpy mutant mice.

3. General Introduction

3.1. Signal transduction and cell types in nervous system

The nervous system is a complex collection of special cell types, *neurons* and *glia* ("glue" in Greek) cells.

Neurons are cells in the nervous system and their main function is to process and transmit information.

Both in central, and in peripheral nervous systems of vertebrates neurons are responsible for input of the signal from outside and as well inside, its transduction, processing and according behavior formation. Neurons are communicating with each other by sending signals (action potentials, or spikes) down axons and through the synapses (electrical and chemical) (Figure 3-1). The signal transduction in the axons is very fast and happens in milliseconds scale.

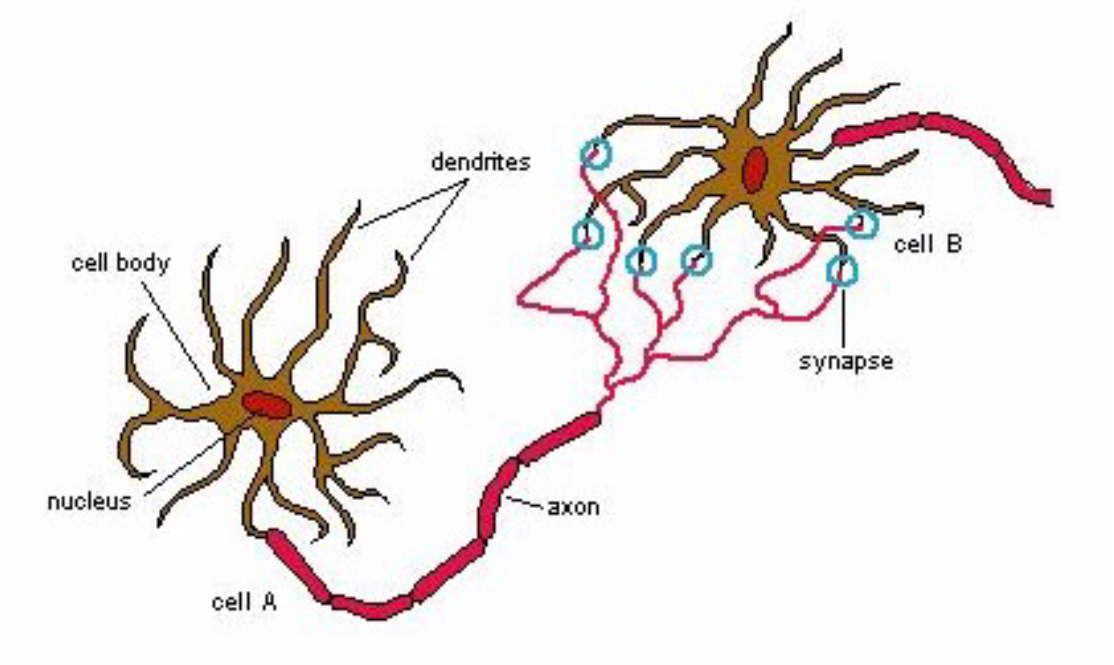

Figure 3-1. Signal transduction between neurons.
Evoked action potential (signal) in neuron A propagates through its axon and reaches to the synapses (blue circles). Via synaptic connections between neuron A axon and neuron B dendrites, signal transits to the neuron B. The figure is from (Hsieh-Wilson 2002).

The neurons are classified into three main functional groups*: sensory neurons, motor neurons* and *inter neurons*.

Sensory neurons allow us to receive information from the outside world through our sensory organs (eye, ear, inner ear, skin, tongue, nose). These neurons evoke the sensation of touch, pain, vision, hearing and taste, which allow us to perceive our surrounding.

Motor neurons are neurons that receive impulses from the spinal cord or the brain and send them to the muscles causing muscular contraction and gland secretion.

Interneurons are the largest class of the neurons. There are subdivided into two classes: *relay or projection interneurons*, which have long axons and send signals from one brain region to another, and *local interneurons,* which have short axons and process information within local circuits (like in the retina) (Figure 3-2).

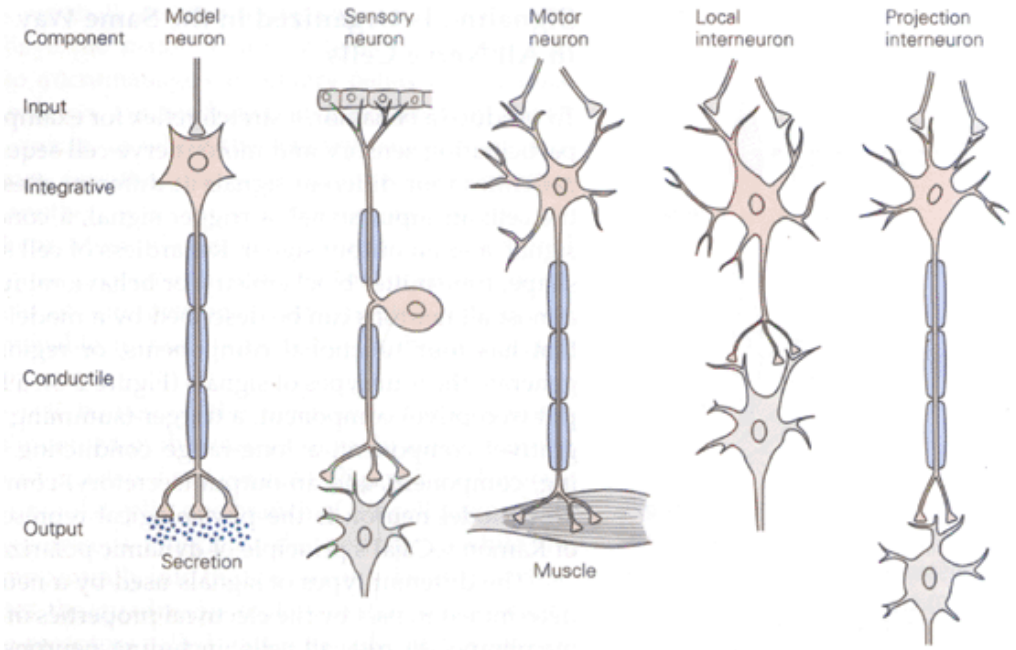

Figure 3-2. Types of the neurons and their functional components.
The functional components of neurons: input component, a trigger or integrative component, a conductile component, and an output component. They all produce a characteristic signal: the input, integrative, and conductile signals are all electrical, the output signal consists of the release of a chemical transmitter into the synaptic cleft. Not all neurons share all these features; for example, local interneurons often lack a conductile component. The cartoon is from (Eric R. Kandel 2000).

The *glia* cells are supporting neurons and hold them in place. There are 5 distinct glia cell types in the nervous system: *astrocytes, microglia cells, Müller glia cells, oligodendrocytes* and *schwann cells*. Each of this cells has specific function characteristic to their type.

Astrocytes are star-shaped types of glial cells, which are the largest and most numerous neuroglial cells in the nervous system (Peters, Josephson et al. 1991). They build up the microarchitecture of the brain parenchyma, are important for blood–brain barrier formation, maintain brain homeostasis, store and distribute ATP (Coco, Calegari et al. 2003), control the synaptogenesis and synaptic maintenance and provide for brain protection (Abbott, Ronnback et al. 2006; Diniz, Almeida et al. 2012).

The *microglia cells* are the resident macrophages of the nervous system. Their main function is to provide support to the neurons, by removing the leftovers of dead cells and organelles (Rock, Gekker et al. 2004).

The *Müller cells* are special glia cells in the retina, which are responsible for the homeostatic and metabolic support of retinal neurons. Müller cells control the transcellular ion, water, and bicarbonate transport, provide trophic and anti-oxidative support of photoreceptors and neurons, regulates the blood-retinal barrier, uptake glutamate and regulate the synaptic activity in the inner retina. Müller cells are as well guiding light through the inner retinal tissue and by that enhancing the signal/noise ratio. (Reichenbach and Bringmann 2013).

The *oligodendrocytes* in central nervous system (CNS) and *schwann cells* in peripheral nervous system (PNS) are the glia cells responsible for myelination. They provide support to axons and produce the myelin sheath, which isolate axons from each other (Bradl and Lassmann 2010) (Figure 3-3).

To properly function, the nervous system needs tight cooperation of all neural and glia cell types, and disturbance of any of the system component brings the nervous system to an imbalance, resulting in different neurological diseases. Many of these diseases are related to the myelin and myelination, and as it has been mentioned above, oligodendrocytes are responsible for that in the central nervous system.

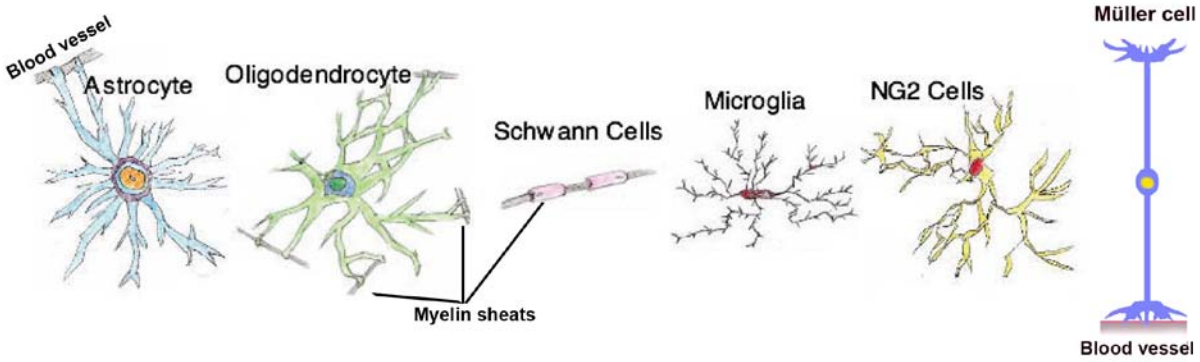

Figure 3-3. Different types of glia cells.
Astrocytes and their end feet on the blood vessel. Oligodendrocytes and their processes (myelin sheaths) surrounding the axons. Schwann cells are sitting on the axons and perform myelination. Microglia cells. NG2 cells or oligodendrocyte precursor cells (OPCs). Müller cells, prolong through length of the retina, on the bottom are associated with blood vessel. The cartoons are modified from ((Witkovsky 2006; Jabr 2012)). The description of each glia cells is presented in the text.

3.2. Oligodendrocytes during development

Oligodendrocytes are glia cells responsible for CNS myelination. They are appearing in the central nervous system postnatally. The first oligodendrocytes appear shortly after birth, e.g. in rat from P7-P10 and mouse from P4-P7 (Skoff, Price et al. 1976; Billon, Jolicoeur et al. 2002) (Figure 3-4).

The oligodendrocytes develop from oligodendrocyte precursor cells (OPCs) (Rivers, Young et al. 2008; Frohlich, Nagy et al. 2011). These cells are widely distributed throughout the whole central nervous system in both gray and white matter. They exist in every postnatal developmental stage (Nishiyama, Lin et al. 1996; Dawson, Polito et al. 2003; Frohlich, Nagy et al. 2011) and play important role in the normal functioning of the CNS.

OPCs initially arise in restricted regions of the neuroepithelium and migrate relatively long distances to their final destinations (Tsai and Miller 2002). In the adult brain there is also a pool of proliferating/cycling OPCs (Psachoulia, Jamen et al. 2009; Young, Psachoulia et al. 2013). These cells may generate new

oligodendrocytes which could restore myelin-sheaths after pathological conditions or injuries resulting in their loss, but their exact function is unknown (Young, Psachoulia et al. 2013).

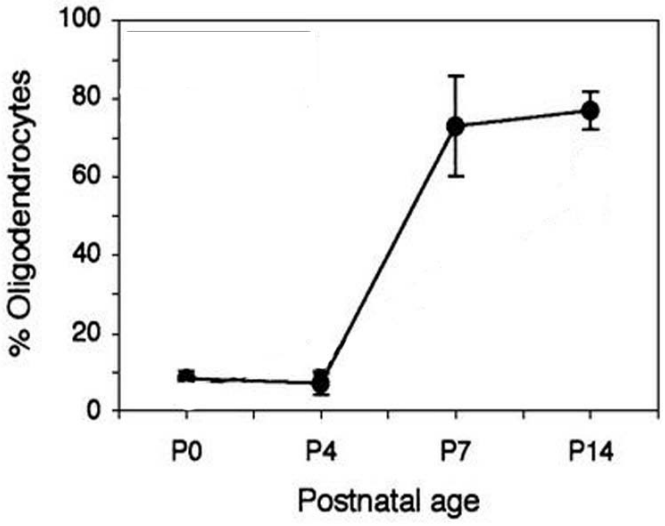

Figure 3-4. Oligodendrocyte development in the wild type mouse optic nerve. The percentage of oligodendrocytes from the population of the isolated cells from optic nerve. The cell count is based on the Galactocerebroside immunostaining (specific marker for oligodendrocytes (Raff, Mirsky et al. 1978)).The figure is modified from (Billon, Jolicoeur et al. 2002).

OPCs express several types of neurotransmitter-receptors, e.g. ionotropic receptors for GABA, glutamate and acetylcholine (Bergles, Roberts et al. 2000; Lin and Bergles 2004; Velez-Fort, Audinat et al. 2009). GABA and glutamate ionotropic receptors are located in synapses between non-myelinated neurons and OPCs, both in gray and white matter, at every developmental stage (Bergles, Roberts et al. 2000; Lin and Bergles 2004; Kukley, Capetillo-Zarate et al. 2007; Ziskin, Nishiyama et al. 2007), but the function of these synapses is unknown (Frohlich, Nagy et al. 2011).

OPCs maintain their synapses during division (Kukley, Kiladze et al. 2008; Ge, Zhou et al. 2009). Synapses between axons and OPCs are ultrastructurally similar to neuronal synapses (Ziskin, Nishiyama et al. 2007; Nishiyama, Komitova et al. 2009; De Biase, Nishiyama et al. 2010; Frohlich, Nagy et al. 2011), suggesting that

OPCs are uniquely positioned within the oligodendrocyte lineage to monitor the firing patterns of surrounding neurons. Figure 3-5 shows an example of such a synaptic connection, where the axon cross section contains vesicles and the biocytin labeled OPC process is closely associated with it.

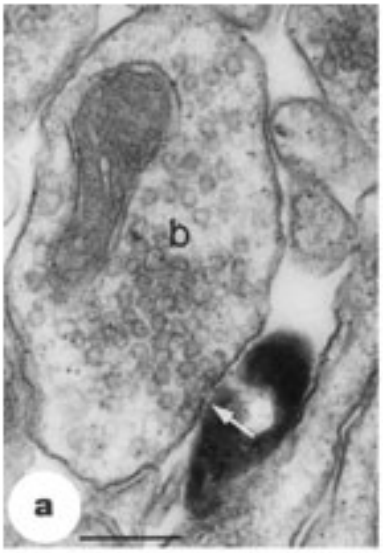

Figure 3-5. Electron micrographs of the synaptic relationships of OPC with an axon in the hippocampus.
Section of a process (black, peroxidase reaction) from a physiologically identified, biocytin labelled OPC receiving a synapse (arrow) from a bouton (b). Scale bars 0.2 µm. The figure is modified from (Bergles, Roberts et al. 2000).

It is tempting to speculate that these synapses play an important role in regulating the cell cycle, and influence the proliferation properties (speed, division frequency, ratio of proliferating cells, etc.) and/or the differentiation of OPCs to oligodendrocytes.

While differentiating to oligodendrocytes, OPCs lose their synaptic connections and first become premyelinating oligodendrocytes and then oligodendrocytes. Figure 3-6 shows a cartoon demonstrating differences between cells of the oligodendrocyte linage based on markers being expressed (Frohlich, Nagy et al. 2011).

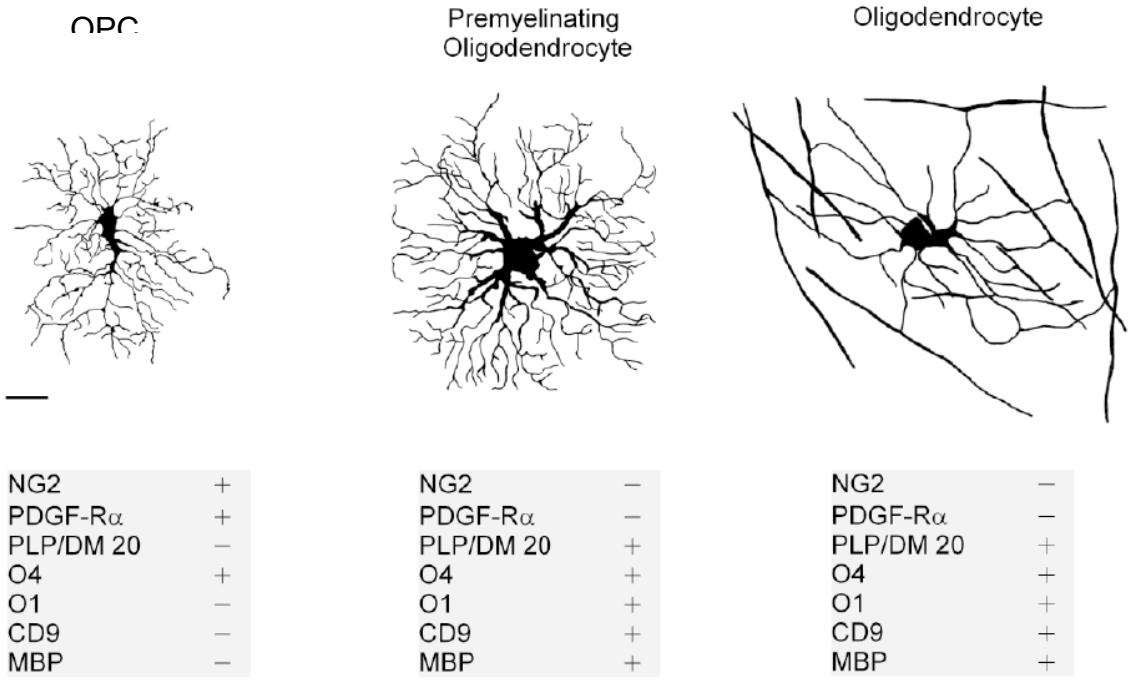

Figure 3-6. Morphological comparison of the oligodendrocyte lineage cells. Drawings of an OPC, a premyelinating oligodendrocyte and a myelinating oligodendrocyte. The drawings are traced from Lucifer-Yellow-filled cells in brain slices, and represent the typical morphology of oligodendrocyte lineage cells at different stages of differentiation. The grey panels beneath the drawings list some of the important molecular markers that are present (+) or absent (-)) in the oligodendrocytes lineage cells. Scale bar: 10µm (applies to all three drawings). Upper panel is modified from (Kukley, Nishiyama et al. 2010). The figure is from (Frohlich, Nagy et al. 2011).

Differentiated oligodendrocytes form myelin sheaths around axons and perform myelination as it is shown in Figure 3-7. In case of oligodendrocytes absence or dysfunction, several neurological diseases can develop.

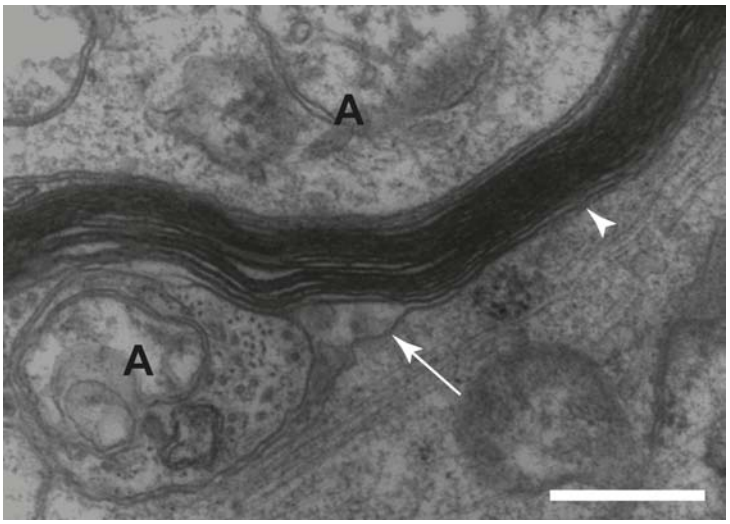

Figure 3-7. The myelination by oligodendrocyte.
EM micrographs of optic nerve cross section. A: axon; arrow head: the myelin sheaths; arrow: the process of oligodendrocyte surrounding the axon. Scale bars 0.5 μm.

3.3. Myelination in the optic nerve during development

The optic nerve is one of the heavily myelinated brain regions. In neonatal mammals, newly grown optic axons are uniformly small in diameter. In the adult, in contrast, axons within the optic nerve can be classified into distinct groups according to their diameter (Colello, Pott et al. 1994). The optic nerve axons are myelinated by oligodendrocytes, which originate from OPCs. In the optic nerve they originate at a focal point on the floor of the third ventricle located just above the optic chiasma (Ono, Yasui et al. 1997) and then migrate distally towards the optic nerve-retina connection part. (Sugimoto, Taniguchi et al. 2001). OPCs don't enter to the retina because of migration stopping factors, as the retina needs to be transparent. The mouse optic nerve becomes myelinated at a distance of 100-150μm from optic disc. (Sugimoto, Taniguchi et al. 2001; May and Lutjen-Drecoll 2002; Gao, Macklin et al. 2006; Sun, Lye-Barthel et al. 2009).

OPCs start to colonize the mouse optic nerve in a chiasmal-to-retinal gradient between E14.5 and E17.5. The number of the cells increases significantly between

E18.5 and P5 (Spassky, de Castro et al. 2002). After a period of proliferation, most OPCs stop dividing and terminally differentiate into oligodendrocytes, which then myelinate the axons in the nerve.

The myelination in the optic nerve starts at P5-P7. It has two periods of growth: the initial - *first* period, when maximum growth of axons occurs (P7-P21), when more than 80% of axons are myelinated. At the point when the mice eye opening takes place (P11-P12), over 50% of optic nerve fibers are myelinated. (Colello, Pott et al. 1994; Billon, Jolicoeur et al. 2002). The *second* period of growth commences during week 5 of postnatal life, and lasts during whole adult life. The rate of the change in the growth of the nerve during this second period is slower than that during the first period, and progressively becomes slower with age. Myelination within the optic nerve is complete during the 2nd period of growth, although the nerve continues to grow in caliber (Dangata, Findlater et al. 1996; Young, Psachoulia et al. 2013).

3.4. Retina Ganglion cell axons in the retina and optic nerve

The ganglion cell axons from the retina nerve fiber layer run toward the optic disk, through the optic nerve and to the higher brain regions. In the mouse the number of ganglion cell axons varies from 32.000-99.000. The variability of axons number is so high as it differs from mouse line to mouse line (Honjin, Sakato et al. 1977; Lam, Sefton et al. 1982; Keenan 2008).

Unmyelinated axons within the retina have a similar range of diameters as the same myelinated axons in the optic nerve. The unmyelinated and myelinated axons diameter within the optic nerve varies 0.3–1.1 μm and 0.4-3,5 μm respectively (Colello, Pott et al. 1994; Perge, Koch et al. 2009).

The axons in the optic nerve, closer to the optic disk, are separated by astrocytes processes to bundles as it is shown in the Figure 3-8. (May and Lutjen-Drecoll 2002; Sun, Lye-Barthel et al. 2009). During some neurological diseases these

separations are disturbed, and the astrocytes processes are all over the optic nerve (Skoff 1976; Vela, Gonzalez et al. 1998).

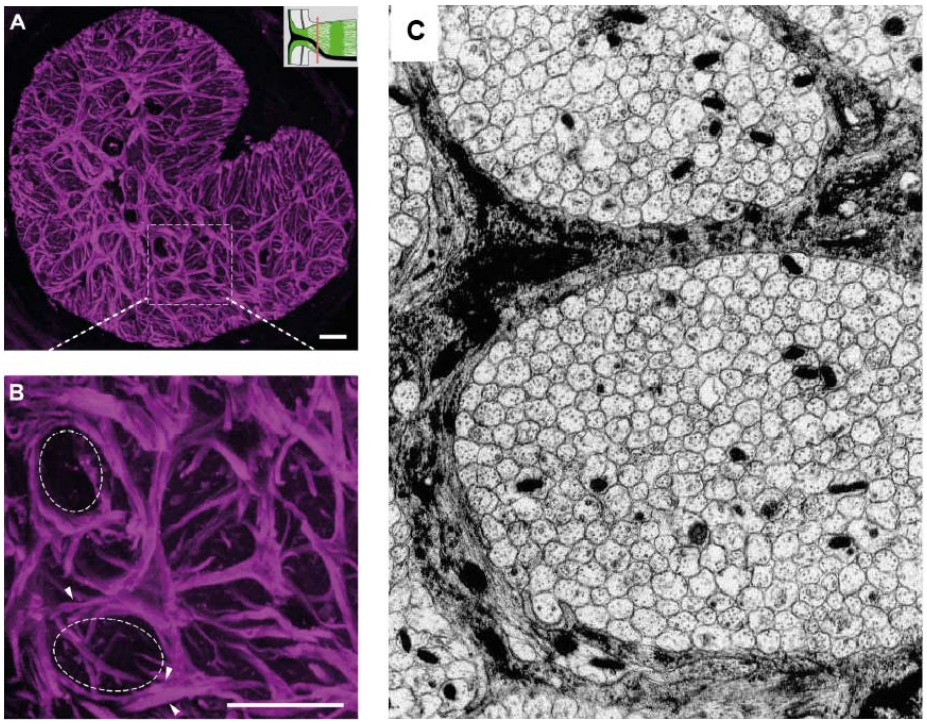

Figure 3-8. The axons bundles in the optic nerve.
A, B: Transverse sections of GFAP-labeled optic nerve showing that each of the glial tubes within the honeycomb structure are ensheathed by many astrocytic processes (A, B, dashed circles and arrowheads). B: An enlargement of the dashed square in A. The figure is modified from (Sun, Lye-Barthel et al. 2009). C: EM micrographs of optic nerve cross sections. The figure is from (Colello, Pott et al. 1994). Scale bar in A and B 20 µm, in C 2 µm.

3.5. Myelin based and Proteolipid proteins

The nervous system gets myelinated during development. In the CNS the myelin is formed from the plasma membrane of oligodendrocytes. The individual oligodendrocytes myelinate up to 50 axon segments (Hildebrand, Remahl et al. 1993). With their own cell membrane oligodendrocytes wrap axons with myelin by spiral shape, which eventually becomes a multilayered sheath (Kalwy and Smith 1994) (Fig. 2.7., Fig. 1.10.).

Myelin consists of 80% lipid and 20% protein, which insulate very sufficiently axons from each other and allows efficient conduction of action potentials (Baumann and Pham-Dinh 2001; Nave 2010) by reducing the transverse capacitance and increasing its resistance (Hartline and Colman 2007). In myelinated axons, action potentials are traveling through the axons by nodes of Ranvier. These myelin free segments are enriched with voltage gated Na^+ and K^+ channels, which amplify the traveling action potentials (Poliak and Peles 2003).

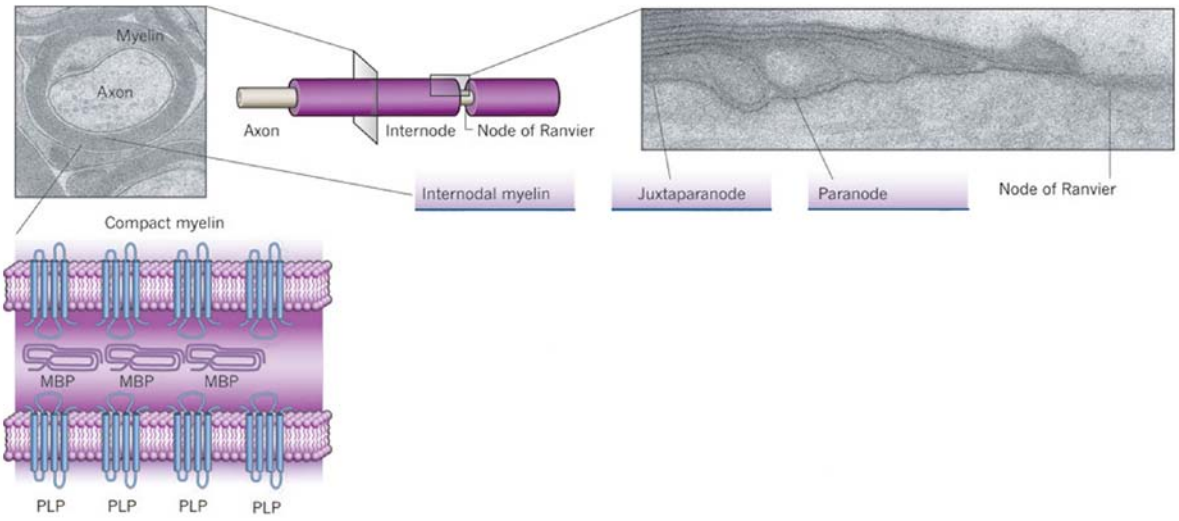

Figure 3-9. The structure of myelin.
From left to right: Axon surrounded with myelin. Along the axon the myelin is distributed in the internodes (consists of the oligodendrocytes processes), and in between this internodes are located the nodes of Ranvier. The internodes by themselves consist of juxtaparanodes and paranodes. Each myelin sheath consists of two main myelinating proteins: myelin basic protein (MBP) and proteolipid protein (PLP). The figure is modified from (Nave 2010).

The structural proteins, such as proteolipid protein (PLP1) and myelin basic protein (MBP), in the CNS are responsible for compact myelination (Kalwy and Smith 1994; Jahn, Tenzer et al. 2009). Myelin compaction is crucial step in the maturation of myelin. This involves removal of cytoplasm from the myelinating process and close association of its membrane surfaces (Kalwy and Smith 1994). Figure 3-9 shows the structure of myelin in the axons and the location of the PLP1 and MBP proteins.

MBP is a highly basic protein which has a net charge of about +20 at physiological pH. It is located on the cytoplasmic side of the myelin membrane. By electrostatic

interactions it binds with the charged lipid-head groups. MBP determines the spacing of lipid membranes in multilayers (Smith 1992; Kalwy and Smith 1994; Jahn, Tenzer et al. 2009) (Figure 3-9).

PLP1 is an intrinsic membrane protein. The amino acid sequence of PLP1 is highly conserved among mammals: e.g. human and mouse PLP are identical (Kitagawa, Sinoway et al. 1993). It has hydrophobic and hydrophilic segments. The PLP1 molecules form homopolymeric aggregates and by this stabilize myelin maintaining correct spacing between apposing extracellular membrane surfaces. PLP1 is involved as well in the regulation of oligodendrocytes maturation (Kitagawa, Sinoway et al. 1993; Kalwy and Smith 1994; Jahn, Tenzer et al. 2009).

When these two main proteins, responsible for proper myelination, are functioning normally, the correct myelin formation is taking place. As it is demonstrated in Figure 3-10, the myelin sheaths are very nicely compact, and axons are separated from each other.

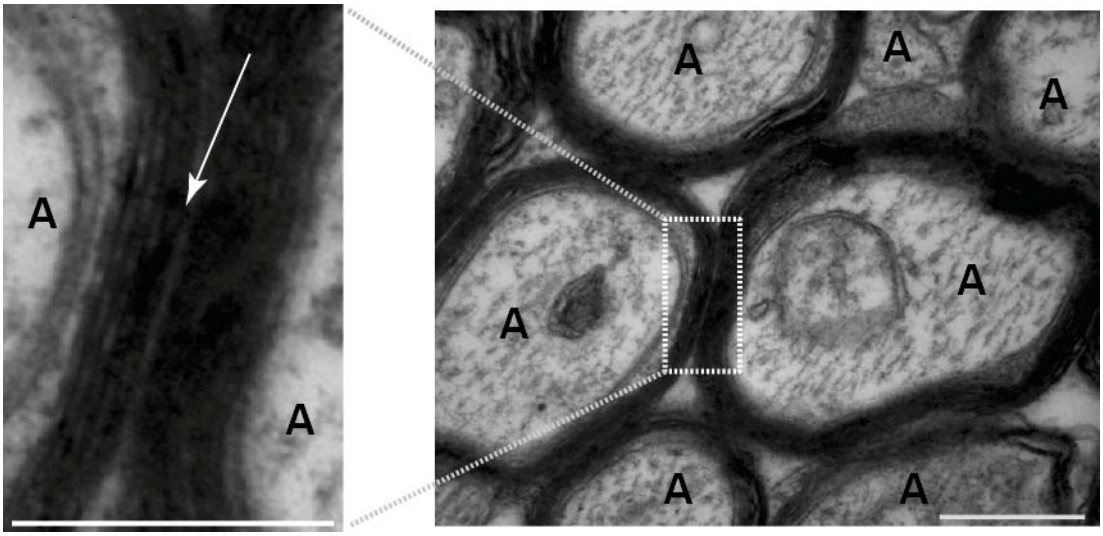

Figure 3-10. Myelinated axons in the mouse optic nerve (P21).
EM micrographs of mouse optic nerve cross section. Axons are surrounded by myelin. A: axons. Arrow: gap between two myelinated axon. Scale bars 0.5 µm.

3.6. Demyeliantion and dysmyelination diseases

3.6.1. General description

Several neurological diseases can result from loss of myelin sheath (Demyelination) and absence or defective myelination (Dysmyelination) (multiple sclerosis, acute disseminated encephalomyelitis, Pelizaeus–Merzbacher disease, etc. (Baumann and Pham-Dinh 2001; Butt, Pugh et al. 2004; Trapp and Nave 2008)). Consequentially myelination is one of the important factors to maintain the normal structure and function of the nervous system.

Demyelination is the pathological process in which myelin sheaths are lost, which normally isolate the nerve fibers. This results in the decreased conduction velocity of electrical signals in the axons (Imaizumi, Kocsis et al. 1998; Imaizumi, Lankford et al. 1998). Demyelination is a reason of many diseases including multiple sclerosis (MS), acute disseminated encephalomyelitis, optic neuritis, leukodystrophies and others (Baumann and Pham-Dinh 2001; Butt, Pugh et al. 2004; Trapp and Nave 2008). In the CNS demyelination is usually the consequence of a direct insult targeted at the oligodendrocytes. Mature oligodendrocytes, as they are postmitotic, cannot contribute to cell replacement when neighboring cells are lost. However, during injury oligodendrocytes may be replaced by proliferating to OPCs (Gensert and Goldman 1997; Young, Psachoulia et al. 2013)).

Dysmyelination is result of defective myelination or absence of myelination. There are number of mutant strains of mouse (Jimpy, quaking, shiverer, myelin synthesis deficiency; twitcher, rumpshaker), rat (myelin deficiency), and dog (shaking pup) created in order to investigate the influence of dysmyelination on the nervous system. The basis of most of these mutations is a human disease Pelizaeus-Merzbacher, which is as well a result of dysmyelination (Gow, Southwood et al. 1998; Greer and Lees 2002). In the CNS of these mutants and as well as humans, the result of dysmyelinetion is hypomyelination, with inappropriately compacted myelin and tremendous decrease of myelination level (Campagnoni and Macklin

1988).Figure 3-11 shows a comparison of normal (Wild type) and two mutant mice (*plp*- and *plp*^{jp}) myelin sheaths. Compared to wild type mice, the two mutants have abnormal compactisation of myelin sheaths. In *plp*- mice it is very compact and in *plp*^{jp} mice the other way around (Klugmann, Schwab et al. 1997).

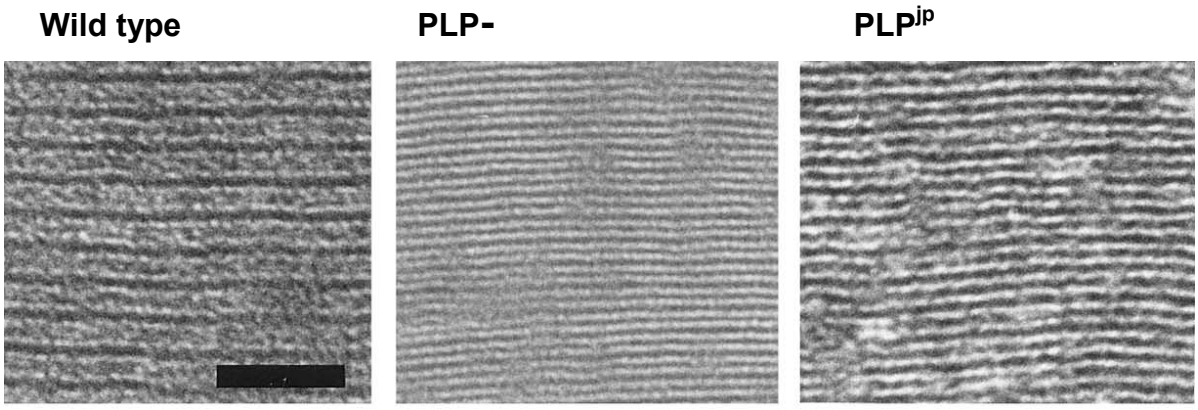

Figure 3-11. Example of myelin sheaths from dysmyelination models. plp-: mice with knocked down of PLP1. plp^{jp}: mice with point mutation in PLP1. The figure is from (Klugmann, Schwab et al. 1997). Scale bar is 50 nm for all tree images.

For several of these mutants, mutations in the *plp1* or *mbp* gene have been described. This may result in poor gene transcription or abnormally spliced mRNAs. The deficiency in one myelin protein is often accompanied by poor incorporation of the other one and lipids into the membrane. Result of this is an abnormal myelination and overall decrease in myelin formation (Kalwy and Smith 1994).

3.6.2. Dysmyelination and Jimpy mouse model

The Jimpy mouse model carries a spontaneous point mutation in the gene coding for *plp1*. *plp1* gene is located on the X-chromosome at Xq22 (Figure 3-12.A).

PLP1 has four transmembrane α-helices which span the myelin membrane and NH_2 and COOH terminals on the cytoplasmic side of the membrane (Greer and Lees 2002; Dhaunchak and Nave 2007). PLP1 is a highly hydrophobic protein, which is

increased further by posttranslational modification by covalent attachment of long chain fatty acids (Figure 3-12. B).

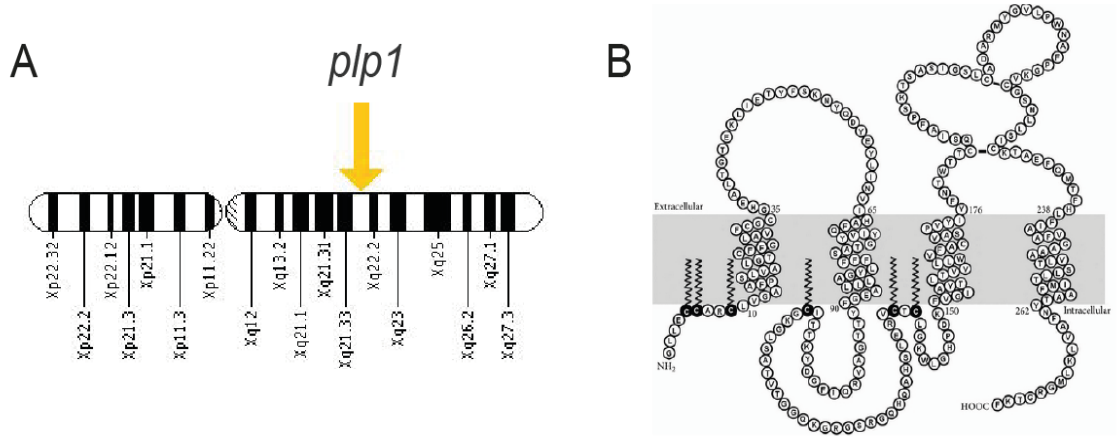

Figure 3-12. PLP1 protein and its role in myelination.
A: The location of plp1 gen in X chromosome at position q22. The cartoon is modified from (Genetics 2008). B: Orientation of PLP1 in the myelin membrane (grey area). Amino acids are indicated using the single letter code. Cysteine residues that are thioacylated in vivo are shown as black circles, with the lipid tail shown as a zigzag line. The figure is from (Greer 2013).

In the Jimpy mutant, the mutation does not disrupt expression of the protein, but the protein gets trapped in the Golgi apparatus and eventually causes the death of the oligodendrocytes (Gow, Friedrich et al. 1994; Jung, Sommer et al. 1996; Thomson, Montague et al. 1997; Gow, Southwood et al. 1998; Kramer, Schardt et al. 2001; Southwood and Gow 2001; Ghandour, Feutz et al. 2002; Dhaunchak and Nave 2007; Bradl and Lassmann 2010). As a result most of the axons in Jimpy mouse CNS are not myelinated (Figure 3-13).

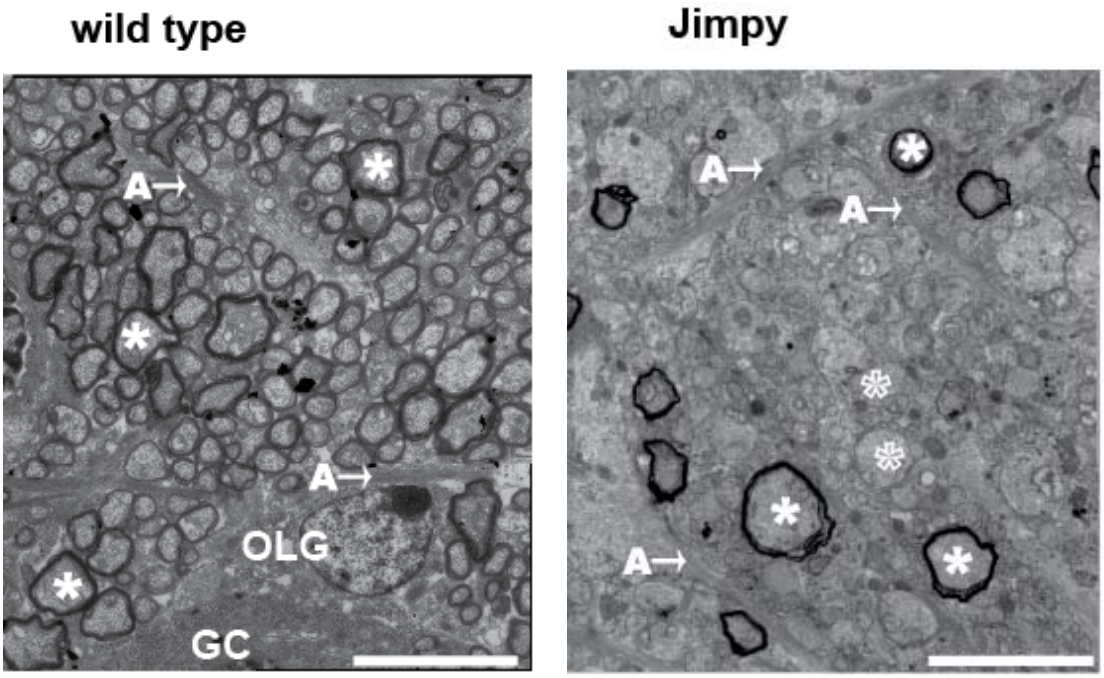

Figure 3-13. The myelination in wild type and Jimpy mutant mice.
The Jimpy mutant mice have very few myelinated axons compares to the wild type mice. A->: astrocytes processes; OLG: oligodendrocytes; GC: Golgi complex; filled stars: myelinated axons; open stars: non-myelinated axons. Scale bars 5 µm.

The result of this mutation is that these mice develop tremor, tonic seizures, with death occurring in the third to fourth postnatal week, when myelination normally reaches its maximum (Klugmann, Schwab et al. 1997; Vela, Gonzalez et al. 1998).

In the CNS of Jimpy mutant mice, the number of mature oligodendrocytes is reduced by 50% in spinal cord (Knapp, Skoff et al. 1986). Thus only 1–3% of Jimpy mutant axons are surrounded by myelin sheaths compared with wild type mice (Duncan, Hammang et al. 1989; Baumann and Pham-Dinh 2001). Myelin sheaths produced by surviving oligodendrocytes are not as compact as in wild type mice (Figure 3-11).

The oligodendrocytes are not the only cell types which are affected by the Jimpy mutation. It is known that astrocytes in the white matter of Jimpy mutant mice are fibrotic. These fibrotic astrocytes undergo morphological changes including hypertrophy of their processes and soma (Skoff, Price et al. 1976; Vela, Gonzalez et al. 1998) and increased expression of the intermediate filament protein Glial

Fibrillary Acidic Protein (GFAP), especially in the spinal cord (Farkas-Bargeton, Robain et al. 1972; Vela, Gonzalez et al. 1998). These changes are similar to alterations seen in astrocytes in other pathological conditions. "Reactive gliosis" or "astrogliosis" are terms used to describe the condition of these astrocytes.

Because of the severe dysmyelination these mice are dying due to respiratory problems (Klugmann, Schwab et al. 1997; Vela, Gonzalez et al. 1998).

3.7. Retina and visual system during development

The retina is part of the CNS. Although no axons inside the retina are myelinated, still ganglion cells, which axons are myelinated in the optic nerve, can die during multiple sclerosis, as multiple sclerosis is an inflammatory and neurodegenerative disorder that leads to a progressive axonal loss and degeneration of neurons (Oberwahrenbrock, Schippling et al. 2012).

The vertebrate retina is a laminated structure, which consists of five major neuronal classes (photoreceptors, horizontal cells, bipolar cells, amacrine cells and ganglion cells) (Figure 3-14). Each of these cell classes is generated from multipotent progenitors that undergo mitosis at the apical surface (Marquardt and Gruss 2002).

In most mammals, retinal neurogenesis and synaptogenesis start before birth and continue during early postnatal development. By eye opening, all retinal cell types are born and most synaptic contacts are established (Fisher 1979; Tian and Copenhagen 2001; Tian 2004).

In the mouse retina from E10 to birth, the retinal ganglion cells, horizontal cells, amacrine cells, and cones develop and gap junctions between retinal ganglion cells form. From birth to P3, bipolar cells and rods develop with immature synapses associate between amacrine cells and retinal ganglion cells. At P3-P5 the outer plexiform layer (OPL) forms and functional synapses between amacrine cells and retinal ganglion cells, and between horizontal cells and cones develop. At P5 photoreceptor outer segments form. At P7 synapses between bipolar cells and retinal ganglion cells develop (Morgan, Dhingra et al. 2006). Ribbon synapses are

first detected at P11. The density of both ribbons and conventional synapses reaches the peak level by the age of P21 (Fisher 1979). A 70% reduction of the retinal ganglion cell dendrites occurs from bi-stratified processes into mono-stratified, during the maturational period, which takes place from just before eye opening to 2 weeks after eye opening (Tian 2004). Consistent with the time course of synaptogesis in the retina the frequency of retinal ganglion cell spontaneous activity is low before and shortly after eye opening, which takes place at P12-P13. The average frequency of spontaneous excitatory postsynaptic currents (sEPSCs) increase with age, and in mouse ganglion cells were recorded as early as P7 (Tian and Copenhagen 2001). Glutamate receptor-mediated sEPSCs and GABA/glycine receptor-mediated spontaneous inhibitory postsynaptic currents (sIPSCs) appear around P10, increasing retinal ganglion cell synaptic inputs over 4-fold in 2 weeks after eye opening and subsiding by P60 (Tian and Copenhagen 2001).

First light-evoked responses in retinal ganglion cells are observed at P11. The maturational changes in light-evoked responsiveness of mouse retinal ganglion cells occur after eye opening at around P14 and older (Tian and Copenhagen 2001).

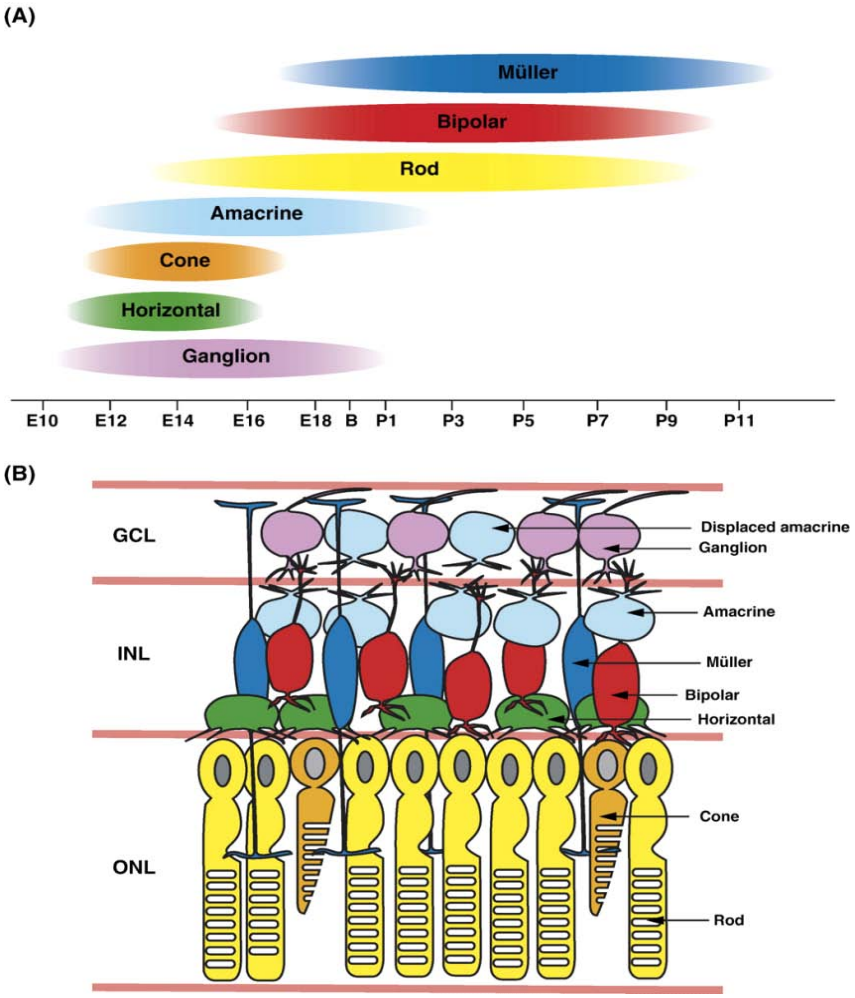

Figure 3-14. Diagram of time course of development of different cell types in the retina, and schematic representation of the retina.

A: Time course of the different cell types in the retina during pre- and postnatal development. B: Cartoon of the retina cross section with the main cell types. The cartoon is from (Ohsawa and Kageyama 2008).

GCL: ganglion cell layer, INL: inner nuclear layer, ONL: outer nuclear layer. The light red lines indicate the plexiform layers, where are located the processes of different retinal cell types.

The development of retinal projections to the dorsal lateral geniculate nucleus (dLGN) and superior colliculus (SC) are present contralaterally just beyond the chiasm at E14. By E16 they have grown into both dLGN and SC. Ipsilateral fibers are limited to the proximal optic tract at E16; their growth into dLGN and SC is delayed until E18-birth. During the first 2 postnatal days, an early population of ipsilateral fibers invades the dLGN and on the third postnatal day they establish a deep and denser projection along the medial and dorsal borders of dLGN. The

segregation of each projection starts on the fourth postnatal day, when crossed fibers begin to disappear from the small region of uncrossed projection. During this period, the ipsilateral fibers withdraw from the deepest layer of dLGN, and their terminal density increases gradually; by the eighth postnatal day, both projections are already well separated (Godement, Salaun et al. 1984).

At P0 (before eye opening and before the formation of the mature innervation pattern, when ganglion cells still can't respond to light) their activity drives LGN neurons to fire action potentials. During the height of the retinally driven synaptic barrage, the almost simultaneous occurrence of many excitatory synaptic events strongly depolarizes the postsynaptic LGN neuron, causing it to fire trains of action potentials. Connections between retinal ganglion cells and LGN neurons are not only potentially capable of working, but they are actually being driven periodically and repeatedly by spontaneous neural activity originating from retinal ganglion cells (Mooney, Penn et al. 1996).

Regarding above mentioned studies ganglion cells are making neurotransmitter release even before they have mature light responses.

4. Methods

All procedures were carried out at room temperature unless otherwise noted. Chemicals were obtained from Sigma Aldrich unless otherwise noted.

4.1. Animals

All experiments were carried out on male B6CBACa Aw-J/A-*plp1*^{jp} *Eda*^{Ta}/J mice (Jimpy mutant, Jackson mouse strain # 000287), which are heterozygous for plp1^{jp} and *Eda*^{Ta} maintained on the same X chromosome. Hemizygous males carrying the spontaneous X-linked Jimpy mutation (*plp1*^{jp}) die by the age of around P22. As a control for Jimpy mice, I used male littermates which did not carry the mutation (Jimpy wild type, simply referred to as "wild type" from now on). The animals were kept at stable humidity and temperature in 12/12h light/dark cycle. Animal use was in accordance with German and European regulations and approved by the Regierungspräsidium Tübingen.

Figure 4-1. The phenotype of Jimpy mutant mouse.
The picture is from Jimpy mutant, Jackson mouse strain # 000287. The mouse looks weak and not healthy.

Jimpy mutant mice were not uniform in their phenotype. All mice had severe tremor by age P10; and they had generalized tonic-clonic seizures without focal onset from P18 of age. During a seizure, the head is arched back, while the extremities are extended and abducted at the distal joints. Most seizures last less than 1 minute, and are followed by total cessation of activity and then by resumption of prior

behavior. These are phenotypic indications for the *plp1*^{jp} mutation, as described by Jackson laboratory. Genotyping of the mice confirmed the *plp1*^{jp} mutation for all animals used in the experiments.

Several Jimpy mutant mice had an additional phenotype. They were smaller than wild type male littermates, lacked fur behind the ears and on the tail. This is a phenotypic indication of the *Eda*^{Ta} mutation, as described by Jackson laboratory, which I confirmed with genotyping.

Some of the mice without *Eda*^{Ta} phenotype (20% of all mice) had yet another additional phenotype; they had weak or completely paralysed hind limbs by P19-P20. It is assumed that this is a particular strong individual phenotype associated with the *plp*^{jp} mutation. Figure 4-1 shows the a phenotypic appearance of Jimpy mutant mouse.

If possible, I have excluded *Eda*^{Ta} mice from my analyses. Most Jimpy mutant data presented in this study are from mice carrying the plp1^{jp} mutation, but lacking the *Eda*^{Ta} mutation, with the following exceptions: Jimpy mutant mice used for (ultra-) structural analyses (Figure 5-2, Figure 5-3, Figure 7-2 and Figure 7-3) contained n=4 samples, with one sample from a *plp1*^{jp} mouse, and 3 samples from *plp1*^{jp} *Eda*^{Ta} mice. The individual micrographs shown in Figure 5-2, Figure 5-3 and Figure 7-3 are from the *plp1*^{jp} mouse. For all other experiments, the sample size was large enough so that I could exclude the Jimpy mutant mice carrying the *Eda*^{Ta} mutation from the analyses. It should be noted, however, that all findings reported here hold true when *plp1*^{jp} *Eda*^{Ta} mice are considered as well.

The control animals – male wild-type litter mates, genotyped as having neither the plp1^{jp} nor the *Eda*^{Ta} mutations – lacked all of the above phenotypes.

4.2. Molecular biology

4.2.1. Genotyping

The nucleic acids isolation for *plp1* and *Eda* genotyping have been performed with the same protocol. For this, ear clips have been taken from mice. For longer storage, they were kept at -20°C. Nucleic acid isolation has been performed with a spin column-based kit, following manufacturer's instructions (high pure PCR template preparation kit, Roche diagnostics GmbH). The isolated products were stored at −20°C and used as templates for polymerase chain reaction (PCR) using specific primers.

4.2.1.1. Genotyping for plp1^{jp} mutation

The primers used for *plp1* genotyping are introduced in Table 4-1. All primers were designed in Dr. Thorsten Schmidt's lab. For negative controls, a reaction with plp1 primers was run in parallel with water as template. The PCR reactions for plp1 contained 13.6µl nuclease-free water, 2µl 10xBiotherm+(Genercraft), 1.6µl 2µM dNTP, 0.8µl R-primer, 0.8µl F-primer, 0.2µl Taq-polymerase (Genecraft), 1µl template DNA. The reaction was set up on ice and run in a thermocycler (BioRad), using a touchdown PCR program: 94°C, 4 min; (94°C, 15 sec; 65°C, 30 sec; 72°C 30s) x 10; Annealing temperature for all primer pairs started at 65°C, decreasing by 1°C per cycle until 55°C for the remaining cycles. (94°C, 15s; 55°C, 30s; 72°C, 30s) x 25; 72°C, 6 min; 9°C;∞. After PCR , the PCR products were digested with 10µl PCR-product, 1,5µl buffer 3, 0,1µl Dde1 (enzyme) 3,4µl nuclease-free water. The reaction was set up on ice and run in a thermocycler (BioRad), using the following program: 37°C, 3 hours; 65°C, 20 min; 10°C, ∞.

The digestion products were run on a 2% agarose gel, containing 4% ethidium bromide (Carl Roth) in tris-borate-EDTA buffer (TBE) and visualized using normal UV excitation and filters for ethidium bromide (Figure 4-2 left). The small 73 and 57bp fragments usually were not visible in the visualized gels.

4.2.1.2. Genotyping for Eda^{Ta} mutation

The primers used for *Eda (exon1 and exon8)* genotyping are described in Table 4-1. Because in Jimpy mutant mice, the Eda allele is characterized by an ~ 2 kb deletion in exon1 (Ferguson, Brockdorff et al. 1997), the genotyping PCR for exon1 should be negative. The Exon8 genotyping of Eda was used as a positive control, as both Jimpy mutant and wild type mice should have it. For negative controls, a reaction with exon1 and exon8 primers were run in parallel with water as template. For exon1 and exon8, PCR was run together and the reaction mix contained: 1µl (10pmol/µl) F-exon1, 1µl (10pmol/µl) R-exon1, 1µl (10pmol/µl) F-exon8, 1µl (10pmol/µl) R-exon8, 10µl, 2µl Phire animal Tissue PCR buffer, 0.4µl Phire hot Start II DNA polymerase, 4.6µl nuclease-free water, 1µl isolated DNA. The reaction was set up on ice and run in a thermocycler (BioRad), using PCR program: 98°C, 5 min; (98°C, 5 sec; 59°C, 5 sec; 72°C, 20 sec) x 40; 72°C, 1 min; 4°C, ∞.

The PCR products were run on a 1.5% agarose gel, containing 2% midori green (BioZym) or 4% ethidium bromide (Carl Roth) in tris-borate-EDTA buffer (TBE) and visualized using normal UV excitation and filters for ethidium bromide (Figure 4-2 right).

Table 4-1: RT-PCR primer details

gene name	primer	sequence (5' --> 3')	Tm (°C)*	primer length	amplicon size (bp)	reference
plp1	PLP1_F PLP1_R	TTAACAACGCAAAGCAGCAC TTCCTCCATGTCTAGCCAATC	60.48 60.93	20 24	342(digestion fragments 209+73+57(mut), 283+57 (wt))	**
Eda exon1	exon1_for exon1_rev	CGCTGTGCTGCTACCTAGAG TCTTCTCCCGGTTCCAAAGG	62.83 61.99	20 20	192	*
Eda exon8	exon8_for exon8_rev	TTGTCCTTCTCCTGTCCTGG GCCTATGTACTTGTAGCTCTGAG	61.33 60.50	20 23	113	*

***calculated by Perl Primer**

**** designed in Dr. Thorsten Schmidt's lab**

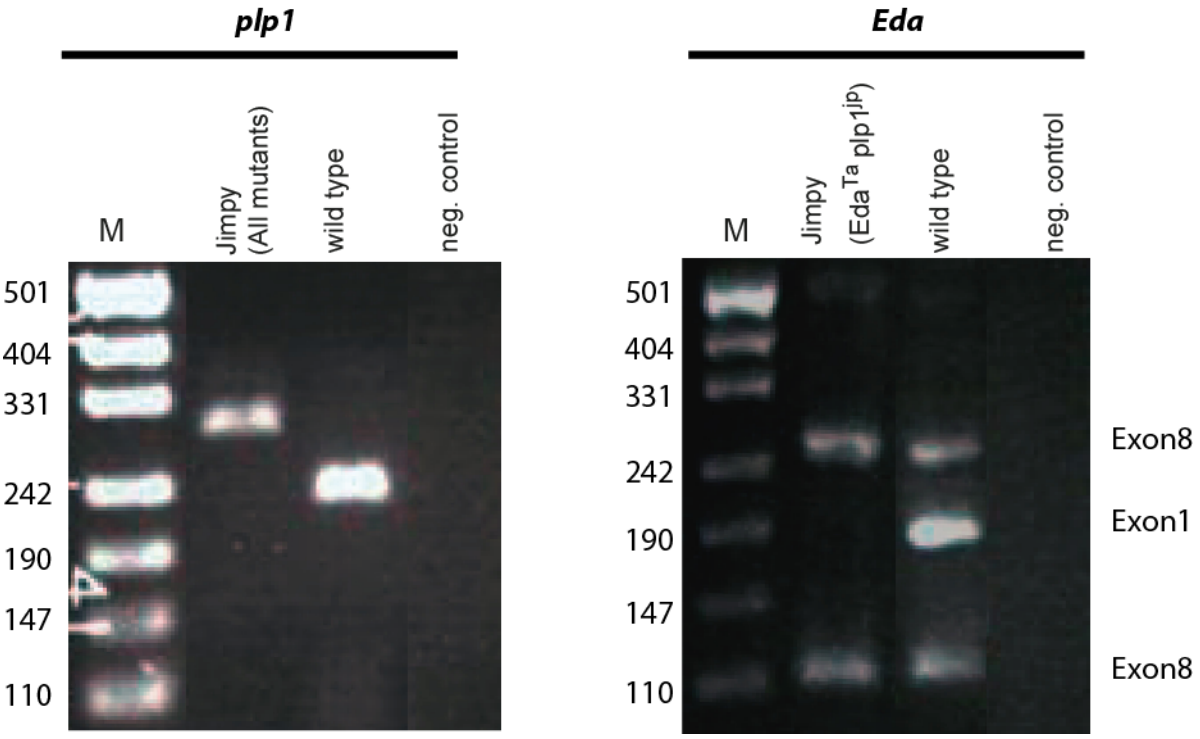

Figure 4-2. Genotyping results of wild type and Jimpy mutant mice for plp1^{jp} and Eda^{Ta} mutations.

On left genotyping for plp1^{jp} mutation, on right genotyping for *Eda^{Ta}* mutation. M: marker. Amplicon sizes: *plp1*: 300 bp for wild type mice and 210 bp for Jimpy mutants, *Eda^{Ta}*: 240 bp and 113 bp for Exon8 (as positive control) 192 bp for Exon1 only for wild type, as *Eda^{Ta}* mutant mice have ~ 2 kb deletion in Exon1.

Below in the Table 4-2, all the mice that have been used for this study are presented.

Table 4-2 Overview table of animals with their genetic background included in the experiments.

	Wild type	**Mutant**
Experiments	***# animals***	***Carrying only plp1^{jp} (# animals)***
Physiology (6.2.1-6.2.4) (MEA recordings)	7 (266 units)	4 (119 units)
Optic nerve axons (5.2.2.)	5	4 (1 plp^{jp} and 3 plp^{jp} & Eda^{Ta})
Retina (7.2.1.) electron and light microscopy	7	4 (1 plp^{jp} and 3 plp^{jp} & Eda^{Ta})
ChAT (7.2.2.) (starburst amacrine cells)	6	4
Calbindin (7.2.2) (horizontal cells)	8	7
GS (7.2.2) (Müller cells)	6	6
PKC_α (7.2.2) (rod bipolar cells)	7	5

4.2.2. plp1 gene expression

RT-PCR (reverse transcription-polymerase chain reaction) of plp1 genes was performed on total retinal RNA. P21 days old Jimpy and wild type mice were killed by CO2 and decapitated. Retinas and optic nerves were dissected out in ice-cold RNase-free phosphate-buffered saline (PBS). Remnants of retinal pigment epithelium (RPE) were removed and both retinas of each animal were put

immediately in lysis buffer (Trizol, Invitrogen), incubated for several minutes, followed by strong vortexing. Unlysed tissue pieces were triturated and dispersed by pipetting. RNA was isolated from the lysates with a spin column-based kit, following manufacturer's instructions (TRIzol® Plus RNA Purification Kit, Qiagen). The RNA was eluted in nuclease-free water and RNA concentration and quality was measured on a Nanodrop ND-1000 (Thermo Scientific). Afterwards, RNA was stored short-term at−20°C or long -term at−150°C or immediately used in a retrotranscription reaction (100 ng RNA with ProtoScript® AMV First Strand cDNA Synthesis Kit, New England Biolabs or SuperScript® III First-Strand Synthesis System, Invitrogen). cDNA products were stored at −20°C and used as templates for polymerase chain reaction (PCR) using cDNA-specific primers for all plp1 transcripts (see Table 4-3 for primer details). All primers were designed in Perl Primer (Marshall 2004). For negative controls, a reaction with plp1 primers was run in parallel with water as template. The PCR reactions contained 0.2 µM forward primer (for), 0.2 µM reverse primer (rev), 200 µM dATP, dTTP, dCTP and dGTP each, 1.5 mM MgCl2, 0.125 µl Standard-Taq polymerase (New England Biolabs), 1 µl template cDNA (all samples have been adjusted to the same final concentration of cDNA (4ng/µl) to have comparable results), 2.5 µl 10X reaction buffer (New England Biolabs), nuclease-free water to fill up to 25 µl total volume. The reaction was set up on ice and run in a thermocycler (BioRad), using a touchdown PCR program: 94°C, 3 min; (94°C, 20 sec; annealing temperature, 30 sec; 68°C, 30 sec) x 35; 68°C, 5 min; 4°C∞. Annealing temperature for all primer pairs started at 55°C, decreasing by 1°C per cycle until 51°C for the remaining cycles. The PCR products were run on a 1.5% agarose gel, containing 2% midori green (BioZym) or 4% ethidium bromide (Carl Roth) in tris-borate-EDTA buffer (TBE) and visualized using normal UV excitation and filters for ethidium bromide (Figure 5-1. C).

Table 4-3: RT-PCR primer details

gene name	primer	sequence (5' --> 3')	Tm (°C)*	primer length	amplicon size	reference
plp1	PLP1_for PLP1_rev	GTGATTCATGCTTTCCAGTATGTC GGGAGAACACCATACATTCTGG	60.48 60.93	24 22	443+338	*
tbp	tbp_for tbp_rev	TGCTGAATATAATCCCAAGCGA CTGGCTCATAGCTACTGAACTG	60.14 60.72	22 22	289	*

***calculated by Perl Primer**

4.3. Electron Microscopy

Eyes of P21 days old Jimpy mutant and wild type mice were prepared for electron microscopy according to the protocol of Schraermeyer et al (Schraermeyer, Schnichels et al. 2009).

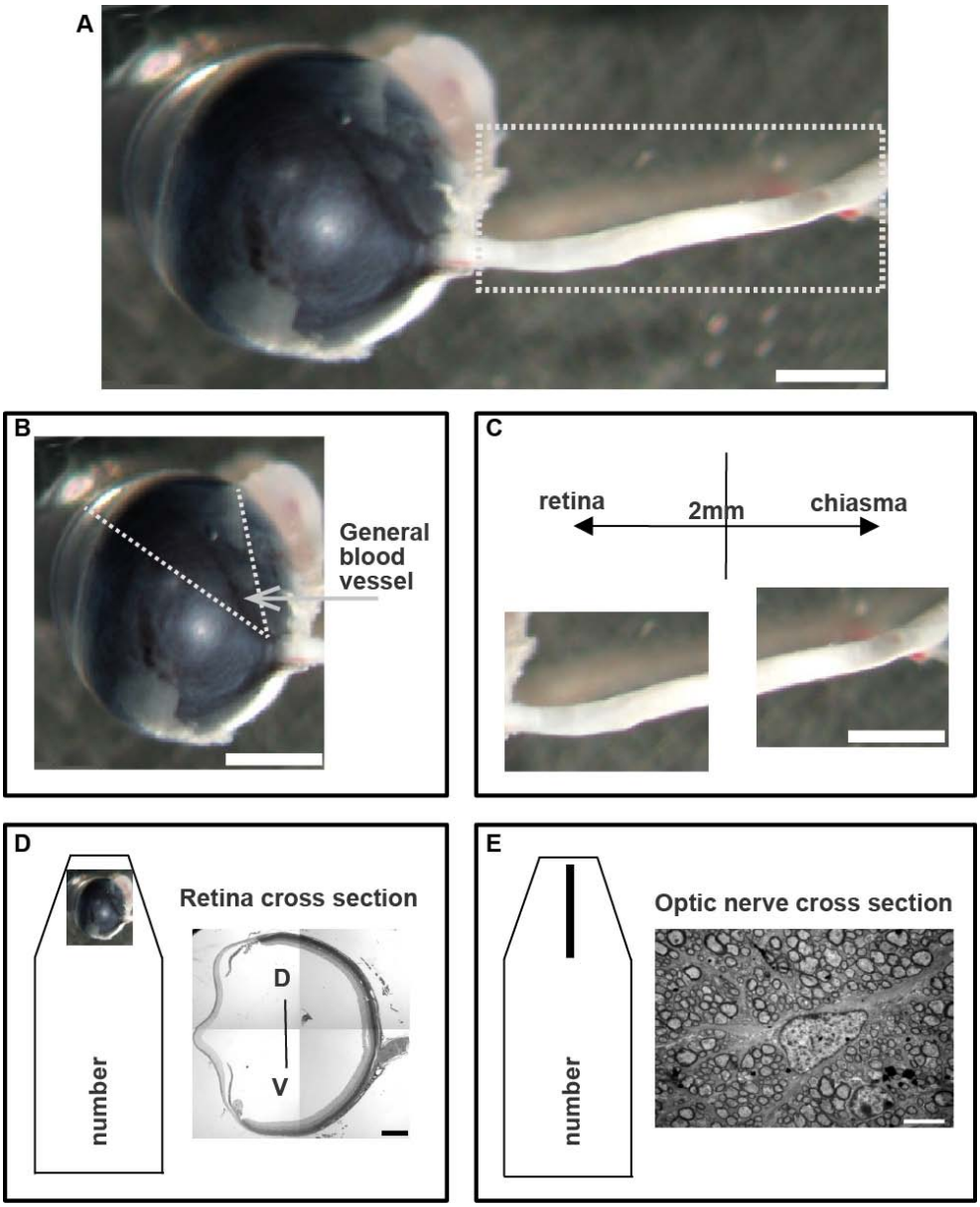

Figure 4-3. Eyecup and optic nerve preparation for EM analyses.

A: The eye cup and optic nerve preparation. White dotted square indicates the optic nerve piece (C) fixated for EM analyses. B: The isolated eye cup white arrow points on the general blood vessel on the temporal part of eye cup. White dotted lines indicate the cut of the eye cup with scissors. C: The optic nerve cut into two pieces each 2 mm length. Arrows indicate the direction to the retina and to the chiasm. D: The position of the eyecup in the EPON block. The "number" in D and E stands (on the left) for EPON block number. On the right of D is a cross section of the retina which corresponds to the orientation of the eye cup fixed in the EPON block. (D) stands for dorsal and (V) for ventral orientation. E: The position of optic nerve in the EPON block. On the right is the EM micrograph of cross section of the optic nerve. Scale bars in A,B,C is 1 mm, in D 400 µm, in E 5 µm.

Figure 4-3. shows the eye cup and optic nerve preparation protocol for EM. Briefly, after fixation of the eye cup with optic nerve still attached, staining with 1% osmium tetroxide, and dehydration steps up to 70% ethanol, the tissue was further stained with uranyl acetate, and further dehydrated (Schraermeyer, Schnichels et al. 2009). Then, the optic nerve was separated from the eye cup, and both eye cup and optic nerve were embedded in Epon. Semithin sections (0.5 µM) of retinas (dorso-ventral direction) and optic nerve were stained with toluidine blue and examined by light microscopy (LSM 710 confocal microscope). For analyses of retina gross morphology and cell number in each layer, I selected cross sections of 400 µm length of dorsal and ventral retina (Figure 4-4).

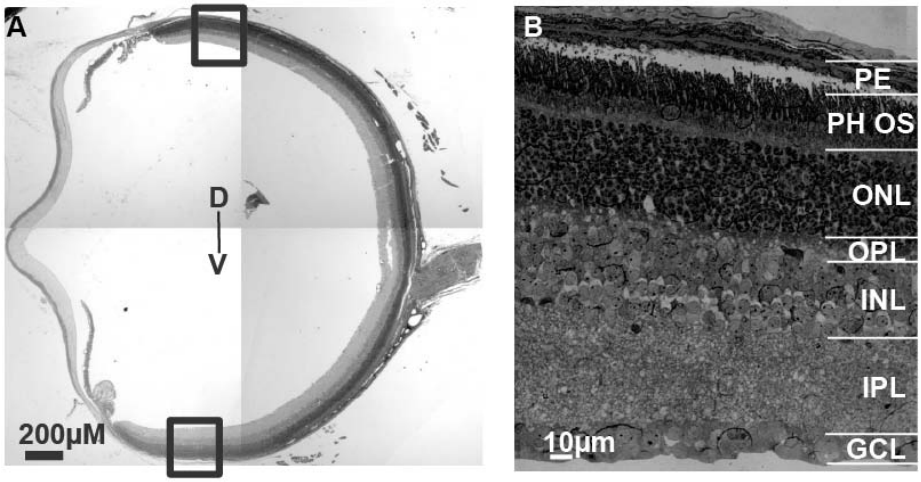

Figure 4-4. The cross section of the retina for light microscopy analyses. Toluidine blue stained retina cross sections. A: The cross section of the retina with orientation indication (D for dorsal, V for ventral). The black squares indicate the pieces of the retina's cross section chosen for analyses. B: More closer look to the cross section of the retina. RPE, retinal pigment epithelium; PR-OS, photoreceptor outer segments; ONL, outer nuclear layer; OPL, outer plexiform layer; INL, inner nuclear layer; IPL, inner plexiform layer; GCL, retinal ganglion cell layer. Scale bars 400 µm (A) and 10 µm (B, C).

In these sections, I counted the cell number in the inner and outer nuclear layers and the ganglion cell layer (Figure 4-5 the cell body count examples for ONL and INL), using a custom-written Matlab script and ImageJ software.

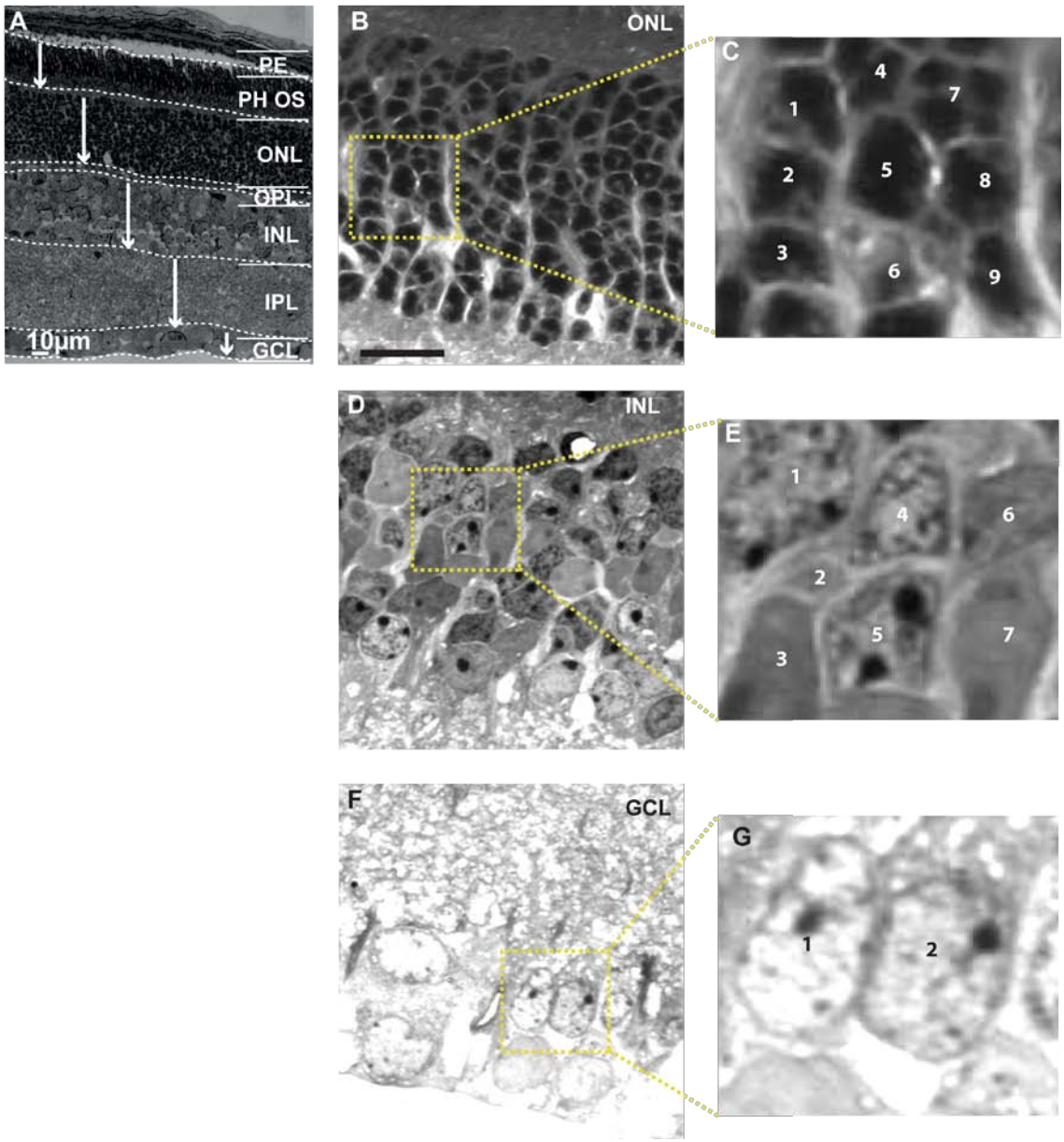

Figure 4-5. Measuring the thicknesses of retina layers and counting of the cells in the ONL, INL and GCL.

Toluidine blue stained retina cross sections. A: Cross section of the retina. The arrows indicate the example of the retina layers thickness that has been measured. The dashed lines are pointing on the borders of the retina layers. B, C: ONL cells. B: The overview of ONL and C: Closer view to the cells in ONL (the yellow dashed square in B). The numbers are indicating the counted cells. D, E: INL cells. D: The overview INL and E: Closer view to the cells in INL (the yellow dashed square in C). F, G: ONL cells. F: The overview of GCL and G: Closer view to the cells in GCL (the yellow dashed square in F). The numbers are indicating the counted cells (C,E,G). RPE, retinal pigment epithelium; PR-OS, photoreceptor outer segments; ONL, outer nuclear layer; OPL, outer plexiform layer; INL, inner nuclear layer; IPL, inner plexiform layer; GCL, retinal ganglion cell layer. Scale bars 400 µm (A) and 10 µm (B, C).

In these sections I have as well measured the area of the cells in the ONL, INL and GCL. In the Figure 4-6 there is an example of area measurement from ONL, INL, GCL cells. With the same approach I have measured the areas of the cell bodies in ONL and GCL.

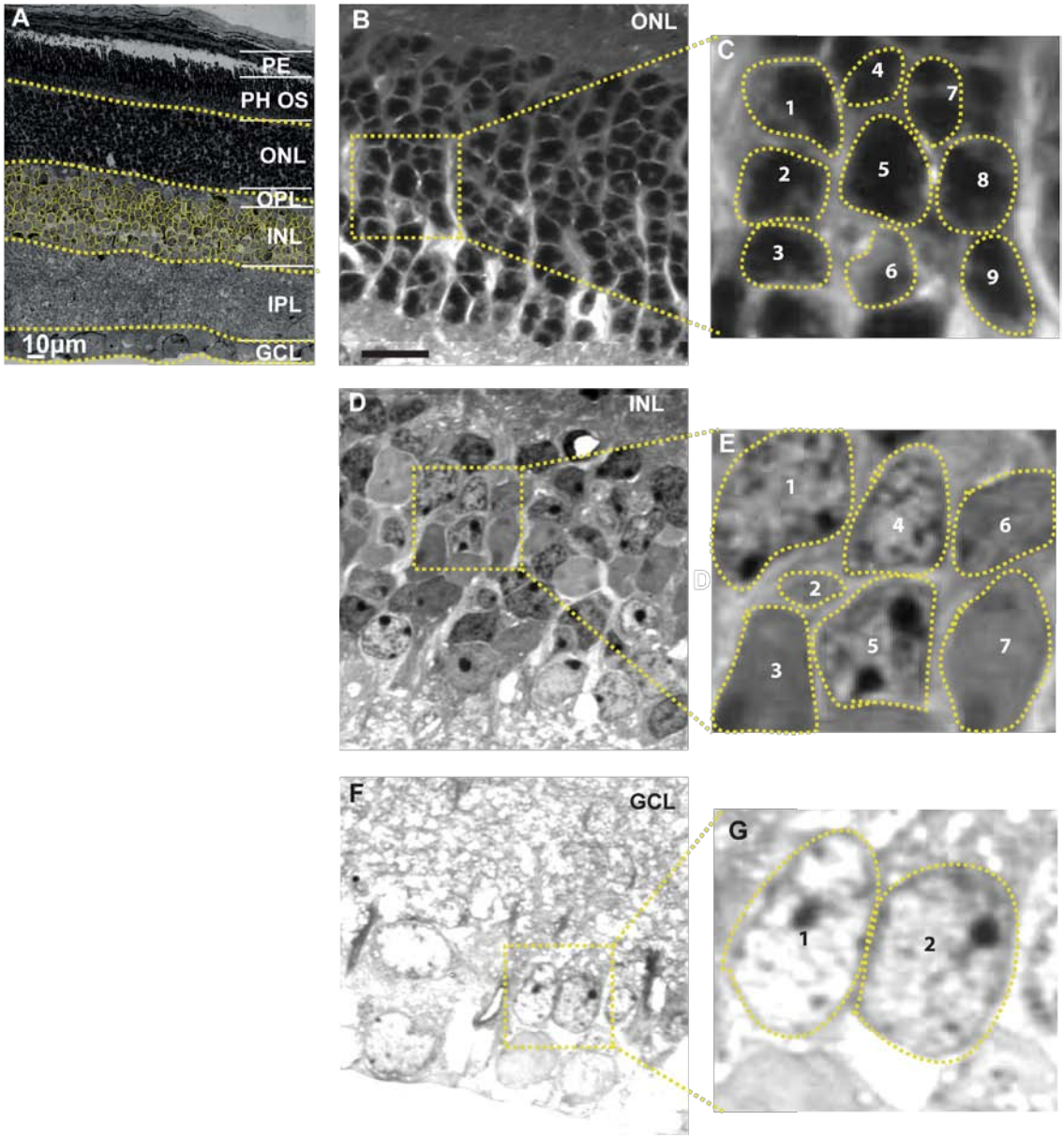

Figure 4-6. Measuring the cell body size in the ONL, INL and GCL.

Toluidine blue stained retina cross sections. A: Cross section of the retina. The dashed lines are pointing on the borders of the retina layers. Yellow circles are measured cell body areas. B, C: ONL cells. B: The overview ONL and C: Closer view to the cells in ONL (the yellow dashed square in B). D, E: INL cells. D: The overview INL and E: Closer view to the cells in INL (the yellow dashed square in D). F, G: GCL cells. F: The overview GCL and G: Closer view to the cells in INL (the yellow dashed square in F). The numbers and the yellow dashed circles are indicating the counted cells and their measured areas (C,E,G). The yellow doted circles are indicating the cell body area measurements (C,E,G). RPE, retinal pigment epithelium; PR-OS, photoreceptor outer segments; ONL, outer nuclear layer; OPL, outer plexiform layer; INL, inner nuclear layer; IPL, inner plexiform layer; GCL, retinal ganglion cell layer. Scale bars 400 µm (A) and 10 µm (B, C).

For electron microscopy, the sections were cut ultrathin (0.07 µM), stained with uranyl acetate and lead citrate and imaged using an electron microscope (model 902 A; Carl Zeiss). In the optic nerve cross sections, counting of ganglion cell axons has been performed in five 500 μm^2 regions (four peripheral and one central); the total number of ganglion cells in each retina was extrapolated based on these counts and on the cross sectional area of each optic nerve ($N_{\text{number of retinal ganglion cells}}=(A_{\text{whole optic nerve area}}*\sum N_{\text{axons counted per region}})/\sum A_{\text{counted region}}$).

4.4. Immunohistochemistry

P20-P22 days old Jimpy mutant and wild type mice were aneasthetized with 3-5% isoflurane and 4% O2 and killed by decapitation. The temporal side of each eye was marked with a cut, eyes were removed and cornea, lens and vitreous dissected out in solution consisting of the following (in mM): 87 NaCl, 2.5 KCl, 1.25 NaH_2PO_4, 7 $MgSO_4$, 0.5 $CaCl_2$, 25 $NaHCO_3$, 25 glucose, 75 sucrose, gassed with a 95% O_2/5% CO_2 mixture, pH 7.4. Cornea, lens and vitreous were removed and the eyecup was immersion fixed in 4% PFA at room temperature for 30 minutes. Subsequently the eyecup was washed over night in PBS. On the next day, retinas were dissected out and sucrose equilibration was done by immersion in 10% and 20% sucrose in PBS for several hours each and a final equilibration in 30% sucrose in PBS over night. On the following day, retinas were frozen three times at -150°C and thawed at room temperature for better antibody penetration. All following steps were carried out at room temperature. The retinas were washed three times for 30 minutes in PBS and blocking was done in 10% normal donkey serum (NDS, Sigma), 1% bovine serum albumine (BSA, Roth), 0.5% Triton X-100 (Sigma) and 0.02% sodium azide (Na-azide, Sigma) in PBS for one hour. Primary antibodies were diluted in 3% NDS, 1% BSA, 0.5% Triton X-100, 0.02% Na-azide in PBS. One retina of each animal was incubated in primary antibody solution for seven to ten days, gently shaked. The second retina served as a negative control and was incubated in the same solution without addition of primary antibodies. Antibodies and dilutions are summarized in Table 4-4. Retinas were washed three times for one hour in PBS. Secondary antibodies were diluted in 0.5% Triton X-100 in PBS

(antibodies and dilutions, see Table 4-4, the cell markers have been chosen based on (Haverkamp and Wassle 2000)) and retinas were incubated in secondary antibody solution for 24 hours, gently shaked. Retinas were washed three times for one hour in PBS after secondary antibody incubation. During mounting, the optic nerve was preserved for PLP and myelin basic protein (MBP) staining to have a positive control for protein expression in the retina. The retina was then mounted in Vectashield (Vector Laboratories) with the temporal side marked. Adhesive tape was used as a spacer before adding the coverslip and sealing with nail polish.

Table 4-4: Antibody list

Primary Antibodies				
antigen/conjugate	***Marker for cell***	***host species***	***supplier***	***dilution***
AA3 – PLP/DM20	Processes of oligodendrocytes	rat	Gift from B. Zalc, Hopital de la Salpetriere (Paris)	1:5
MBP	Processes of oligodendrocytes	rat	Abcam (ab7349)	1:125
PKC-α	Rod bipolar cell	mouse	Novus Biologicals (NB200-586)	1:50
ChAT	Starburst amacrine cell	goat	Millipore (AB144P)	1:100
Calbindin	Horizontal cell	rabbit	Swant (CB 38)	1:100
Glut Synth	Müller cell	mouse	BD Biosciences (610517)	1:100
Secondary Antibodies and other labels				
antigen/conjugate	***host species***		***supplier***	***dilution***
anti-mouse/Alexa 488	donkey		Invitrogen (A21202)	1:400
anti-mouse/Alexa 568	donkey		Invitrogen (A10037)	1:200
anti-goat/Alexa 555	donkey		Invitrogen (A21432)	1:400
anti-rat/Alexa 568	goat		Invitrogen (A11077)	1:250
anti-rabbit/biotin	goat		Dianova (111-065-003)	1:125
streptavidin/Cy5			Biomol/Rockland (S000-06)	1:200
streptavidin/Cy3			Dianova (016-160-084)	1:200
DAPI	(labels cell nuclei)		Sigma (D9542)	1:1000

The stained retinas and negative controls were evaluated on a normal upright epifluorescence microscope (Zeiss Imager Z1). Only the stained retinas were then visualized on a confocal laser scanning microscope in more detail (Zeiss LSM 710). Pinhole sizes were adjusted to the same optical Z-slice thickness for multichannel images. The following settings were used for imaging the various stainings:

MBP and PLP staining (Figure 5-1. A, B): 25x objective (LD LCI Plan-Apochromat 25x/0.8 Imm Korr DIC M27) (1.107 µm pixel size, 2830 x 2830µm^2), Z-stack

through the thickness of retina and optic nerve with 2 µm steps, covering ~6 mm^2 area of the retina with optic nerve. Figure 5-1. A,B are maximum intensity projections of the Z-stack.

Staining of horizontal cells, rod bipolar cells, starburst amacrine cells, Müller cells (Figure 7-4 and Figure 7-5): 40X objective (Plan-Apochromat 40x/1.3 Oil DIC M27) (0.346 µm pixel size, 350 x 350 $µm^2$), Z stacks through the whole mount retina covering the layers where the cells are located, separately for dorsal and ventral retina. The images were analyzed in a custom-written Wolfram Mathematica 9 script. For each cell type, individual analyses have been performed. The numbers of horizontal cells, rod bipolar cells and starburst amacrine cells were counted in maximal intensity projections of the image sections where cell bodies of the cells are located. Detection of the cell bodies and cell counting have been performed manually after optimally increasing the contrast of images (Figure 4-7. A-C). The number of Müller cells was approximated by counting the Müller cell processes in the proximal outer nuclear layer (ONL), where the processes of Müller cell come together (Figure 4-7. D and Figure 7-5.). Data analyses and statistics were done with Mathematica with Mann-Whitney test used.

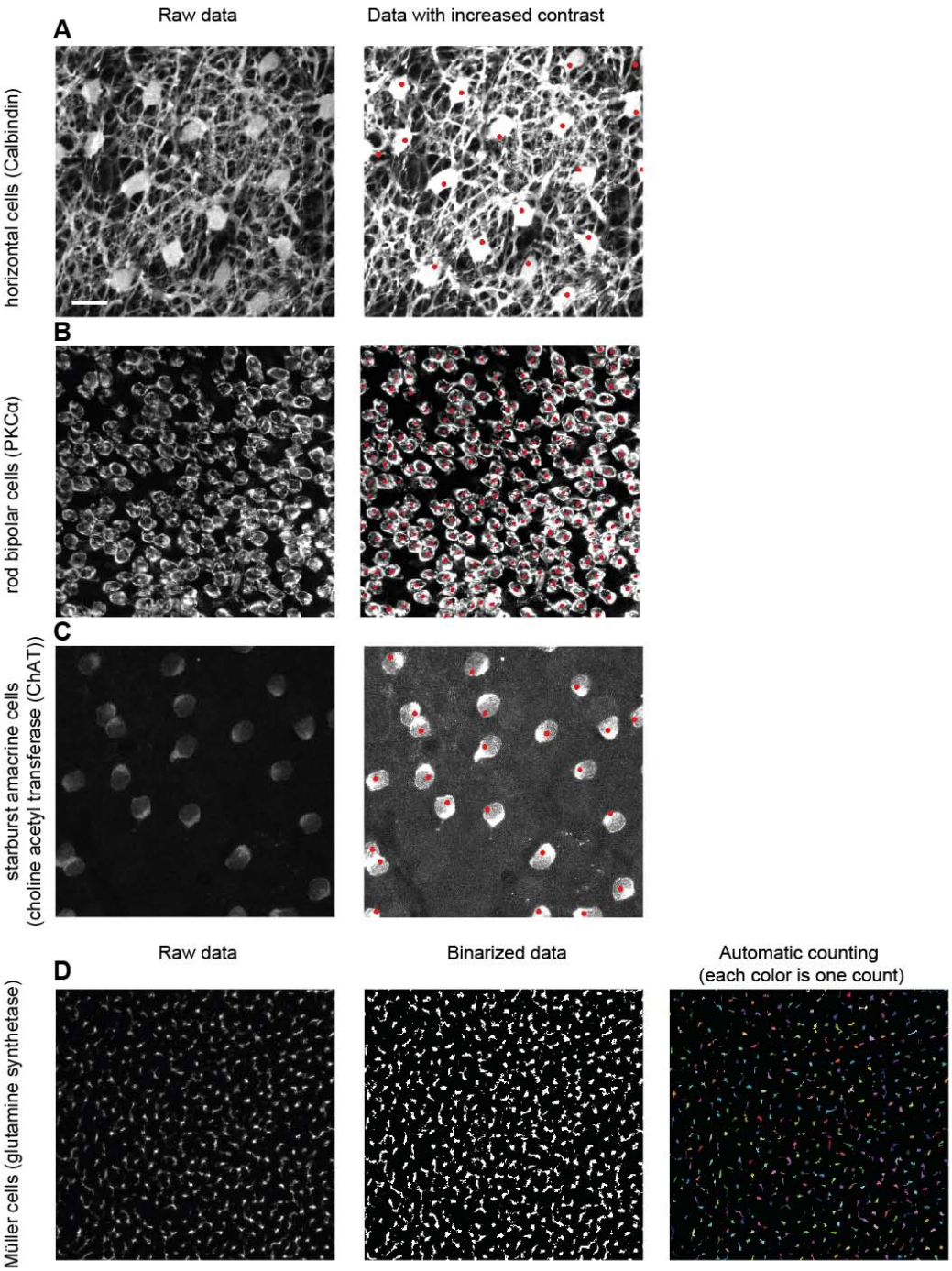

Figure 4-7. Cell count examples for horizontal, rod bipolar, starburst amacrine and Müller cells.

Left column is raw data and right column is modified data. (A-C) Images with increased contrast and (D) image with binarization of stained retinas. The red dots on the images are manually counted cells (A-C).
Maximal projection of confocal sections of A: calbindin staining for horizontal cells, B: PKCα staining for rod bipolar cells, C: choline acetyl transferase (ChAT) staining for starburst amacrine cells. D: Single confocal sections of glutamine synthetase staining for Müller cells, close to the ONL-OPL border. The third color image is false coloring of automatically counted Müller cell processes. Each color represents separate counted unit. Scale bar 20µm the same for all images.

4.5. MEA recordings: Experimental procedure

P20-P22 Jimpy and wild type mice were dark-adapted for at least 4 hours, killed by cervical dislocation and retinas were isolated under dim red light in Ringer's solution containing (in mM): 110 NaCl, 2.5 KCl, 1 $CaCl_2$, 1.6 $MgCl_2$, 10 D-glucose, 22 $NaHCO_3$; bubbled with 5% CO_2/95% O_2; pH 7.4. For visual overview for retina preparation to the MEA recordings see Figure 4-8.

Retinas were mounted on a nitrocellulose filter paper (Millipore) with a 2–3 mm rectangular aperture in the center and placed ganglion cell-side down on a 60-electrode perforated multi-electrode array (MEA) (60pMEA200/30iR-Ti-gr, Multichannel Systems). The inter-electrode distance was 200 µm, interspersed by holes through which gentle suction was applied. During the whole experiment the retina was continuously superfused with Ringer's solution pre-warmed to 38°C by an in-line heating system just before the MEA chamber (33-35°C inside the recording chamber). With this method, stable recordings over 8 hours and more could be obtained (Figure 4-8).

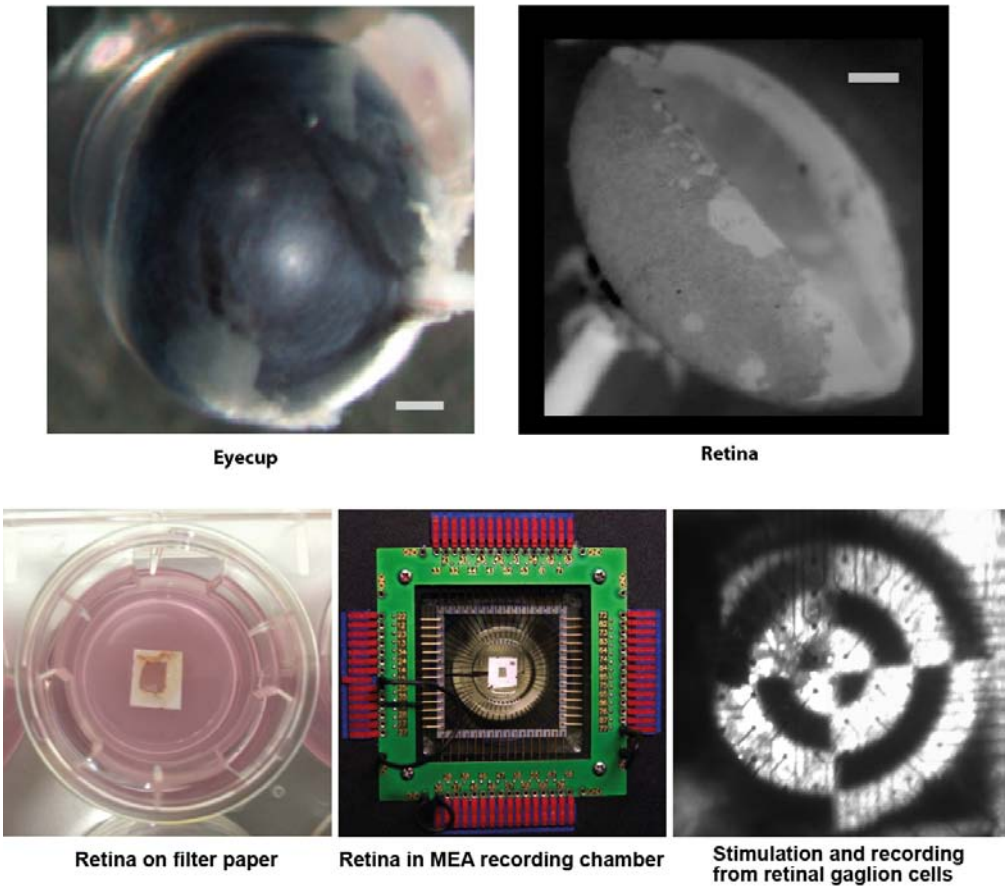

Figure 4-8. Retina preparation for MEA recordings.
From left to right: The whole eye cup; Isolated retina; Retina fixed on the filter paper; Retina on the MEA electrodes in the recording chamber; Retina, in the recording setup, with focused stimulus on photoreceptors layer.

4.6. MEA recordings: Stimuli

The MEA was put in an upright microscope, where light stimulation was supplied through the microscopes condensor by a digital light processing (DLP) projector (PG-F212X-L, Sharp), presenting a diverse set of visual stimuli focused through the transparent MEA onto the photoreceptors. Stimuli were presented at distinct brightness levels, achieved by inserting neutral density filters into the light path. The neutral density (ND) filters (Thorlabs NE10B-A to NE50B-A) had optical densities from 1 ("ND1", i.e. 10-fold light attenuation) to 5 ("ND5"). To achieve light attenuation stronger than 5 log units, two ND filters were combined in series.

Experiments started at ND8 (‘scotopic’; darkest setting, 10^8-fold attenuation) and continued over ND6 (‘mesopic’; 10^6-fold attenuation) and ND4 (‘photopic’; 10^4-fold attenuation). While changing ND filters, a shutter was closed to prevent intermittent exposure to unattenuated light (Figure 4-9).

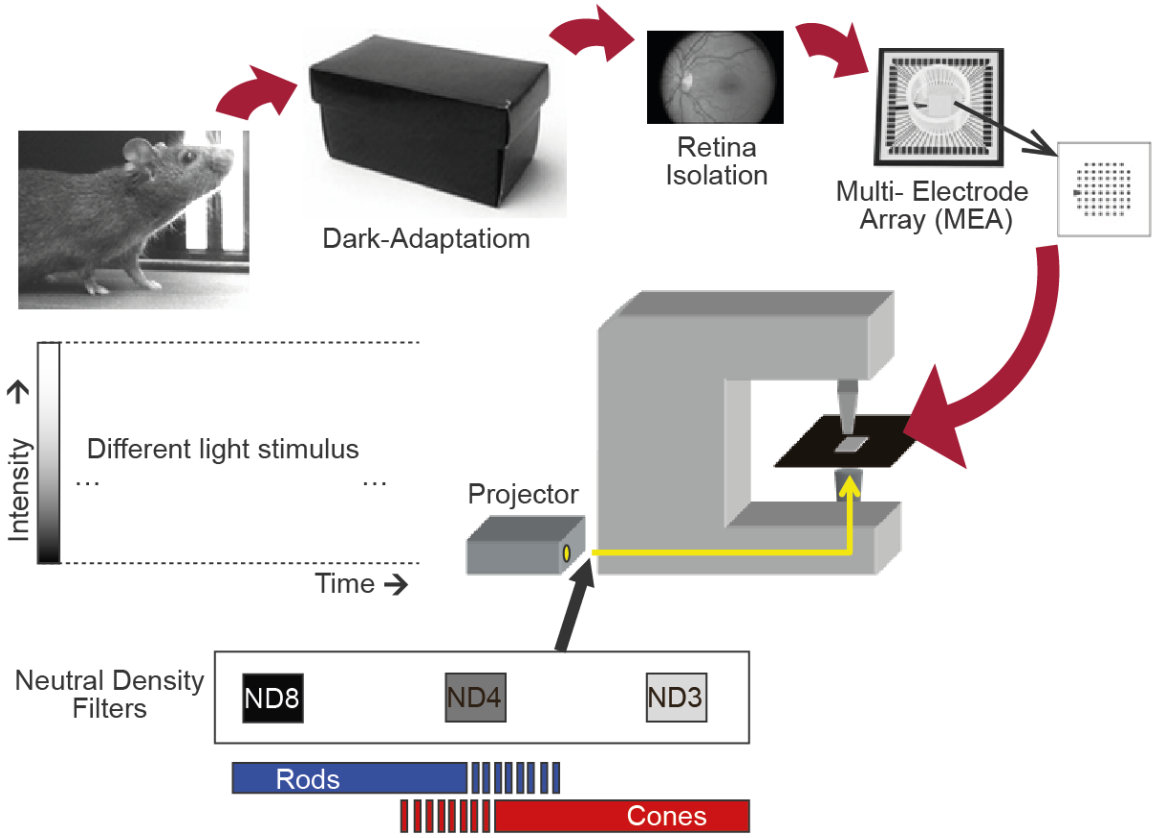

Figure 4-9. Experimental setup of MEA recordings.
From left to the right: Mouse from the animal facility; Dark adaptation of the mouse for 4-6 hours; Retina isolation from eye cup; Prepared retina positioning on the MEA. The different stimulus of different intensity presentation through the projector and the condenser to the centered retina; Natural density filter (ND8, ND6 and ND4) on front of the projector, to present the same stimuli in different brightness levels. This will activate different signal transduction circuits in the retina (Rod, Rod-Cone and only Cone driven).

I presented a diverse set of stimuli, including full-field flashes, moving bars, natural movies, full-field Gaussian white noise flicker and drifting sinusoidal gratings. One batch of stimuli lasted 40 minutes and was shown at least twice per brightness level (Figure 4-10, Figure 4-11).

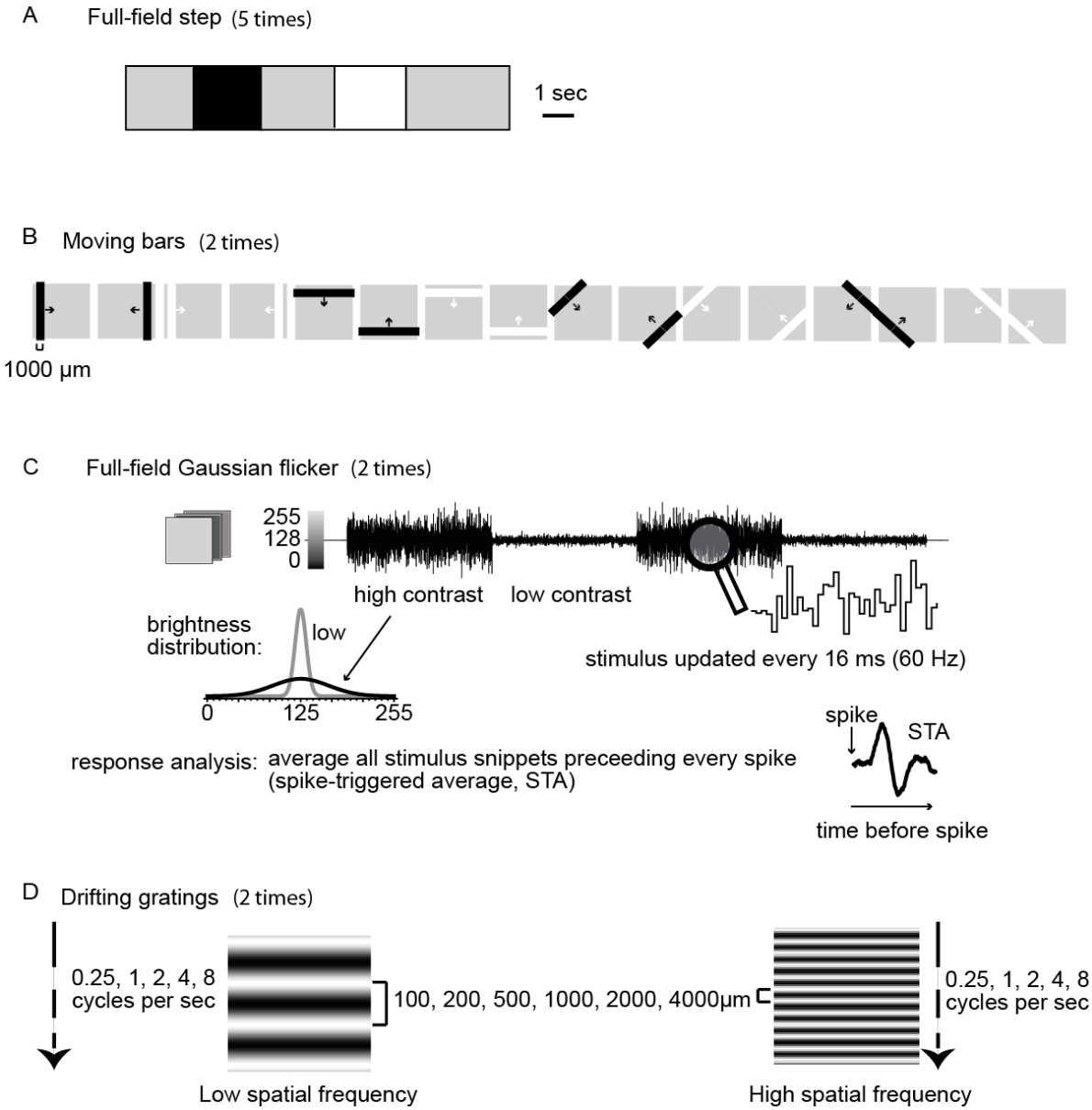

Figure 4-10. Stimulus used during MEA recordings, and included in the thesis.

A: Full field steps. B: moving bars. C: Full-field Gaussian ficker. D: Drifting gratings.

A: Fill field stimulation, used for unites/cells quality inspection (if the unit/cell is clean or not). B: Moving bars, used to define retinal ganglion cells direction selectivity. C: Full field Gaussian flicker, used for stimulus evoked spike rate calclulation and linear filter latency analyses. D: Drifting gratings, used for retinal ganglion cells response spatial and temporal preference analyses.

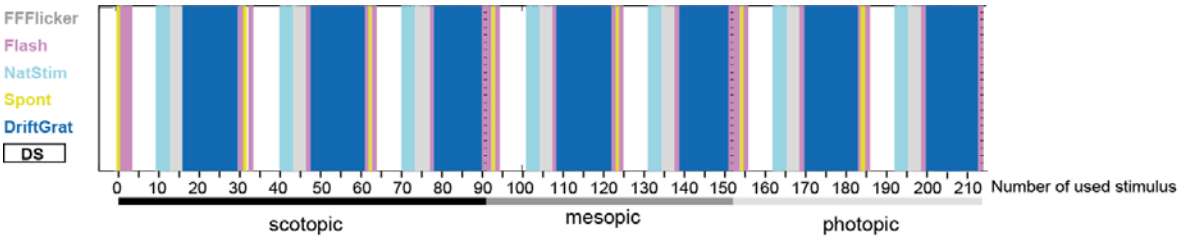

Figure 4-11. The time course of used stimuli during experiments.
The stimuli batch is 40 minutes and was shown at least twice per brightness level (scotopic, mesopic and photopic). Each stimuli batch was additionally repeated two times per brightness level. Only in scotopic brightness the batch was shown 3 times, and first batch is not included in the analyses, as the retina was settling down to the recording conditions. On the left of the figure is presented the used stimulus color code. FFFlicker: full-field Gaussian white noise flicker; Flash: full-field flashes; NatStim: natural movies; Spont: no stimulus; DriftGrat: drifting sinusoidal gratings; DS (what bars): moving bars. Responses to the all stimuli, except natural movies, have been analyzed, and the results are presented.

All stimuli were gray-scale images with pixel values between ‘0’ ("black") and ‘255’ ("white"). The stimulus projector produced an output spanning 3 log units of light intensities (i.e. 1000-fold difference between black (‘0’) and white (‘255’) pixels).I linearized the projector output, so that my mean background of ‘128’ corresponded to the physical light intensity middle between ‘0’ and ‘255’.

For this study I have used data from these following stimuli:

(1) Spontaneous activity: 1s interval before each presented stimuli I have shown background (gray value ‘128’) to analyze the spontaneous activity of retinal ganglion cells.

(2) Full-field-flashes (gray-black-gray-white-gray): The duration of each flash was 2s. Each stimuli set (gray-black-gray-white-gray) was repeated for one round five times per brightness level. (Figure 4-10. A).

(3) Moving bars: Black/white bars with 1000µm thickness and 1000 µm/s speed was used. The bar moved eight directions through full-field length of the screen. Each moving paradigm and the moving sequences of the bars were repeated for one round two times per brightness level (Figure 4-10. B).

(4) Full-field Gaussian white noise stimulus (“flicker”) (Chichilnisky 2001): Each flicker stimulus was presented two times per brightness level. It consisted of five 20-s episodes of high-contrast flicker interleaved with five 20-s episodes of low-contrast flicker. Screen brightness was updated every frame (60 Hz), and drawn from a Gaussian distribution with mean ‘128’ and sigma of 38.4 (high contrast) or 7.68 (low contrast). For the current analysis, I have only considered the high-contrast episodes (Figure 4-10. C).

(5) Drifting sine-gratings: Drifting sine-wave gratings of different speed and width (0.25, 1, 2, 4,8 cycles/sec; 100, 200, 500, 1000, 2000, 4000 µm) spatial period was used. Each combination of speed and width was presented for 12 seconds, moving from top to bottom two times per brightness level. The gratings were presented at full contrast, i.e. the maximum and minimum intensity of the sine-wave grating was black and white, respectively (Figure 4-10. D).

4.7. MEA recordings: Light Intensity Measurements

I measured the spectral intensity profile (in $\mu W \cdot cm^{-2} \cdot nm^{-1}$) of my light stimuli with a calibrated USB2000+ spectrophotometer (Ocean Optics). I then transformed the stimulus intensity into equivalents of photoisomerizations per rod per second, assuming dark-adapted rods, as described previously (Munch, da Silveira et al. 2009). Briefly, the spectrum was converted to photons $\cdot cm^{-2} \cdot s^{-1} \cdot nm^{-1}$, convolved with the normalized spectrum of rod sensitivity (Umino et al., 2008), and multiplied with the effective collection area of rods (0.5 µm²) (Nikonov et al., 2005). The results range from 8 $Rh^* \cdot s^{-1}$ per rod (ND8), to $8 \cdot 10^2$ $Rh^* \cdot s^{-1}$ per rod (ND6) , to $8 \cdot 10^4$ $Rh^* \cdot s^{-1}$ per rod (ND4) for the background ‘128’.

4.8. MEA recordings: Spike sorting and data analyses

Data was recorded at 25 kHz with a USB-MEA-system (USB-MEA1060, Multichannel Systems), high-pass filtered (500Hz, 10th-order butterworth filter) and spikes extracted by thresholding (Figure 4-12).

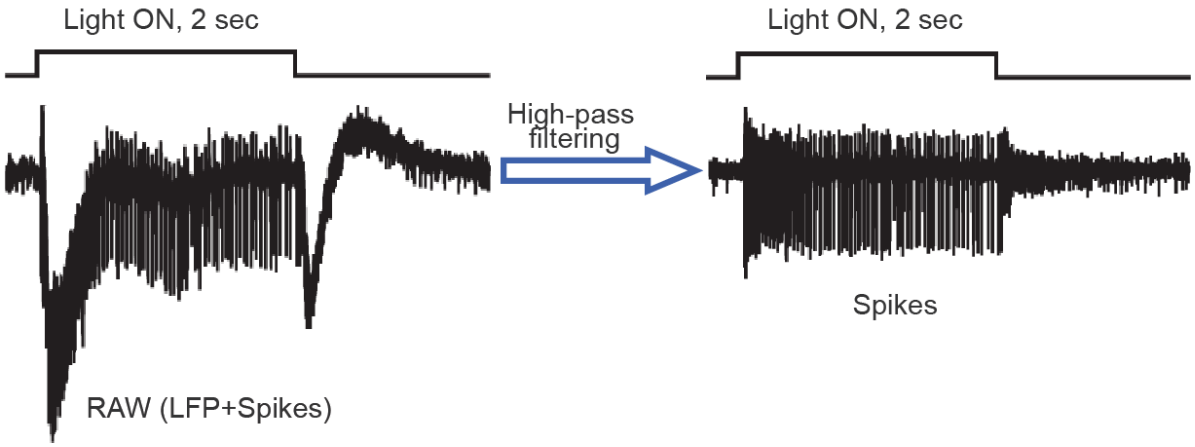

Figure 4-12. The raw data high pass filtering.

Spike sorting (assignment of spikes to individual "units", i.e. individual ganglion cells) was performed semi-manually with a custom-written Matlab (Mathworks) script. Quality of each unit was assessed manually by interspike interval, spike shape and the coherence of responses to my set of stimuli. Data analyses was based on the spike times of individual units. The instantaneous spike rate of each unit was calculated by convolving the spike train with a Gaussian with sigma = 40 ms and amplitude = 0.25 $\sqrt{e}$ sigma^{-1} (≈ 10 Hz for sigma = 40 ms) and was used for further analyses in Matlab. For the sake of simplicity, single units will be referred to as individual "cells".

(1) Spontaneous firing rate was calculated during 1s interval before each presented stimuli over whole experiment, and in all brightness levels. During recording constant background intensity was shown (gray value '128').

(2) The moving bars for eight different directions were used for estimation of retinal ganglion cells direction selectivity. For this the mean spike rate for each direction was extracted and the sum vector calculated.

(3) Calculated linear filters (Chichilnisky 2001) in response to the Gaussian flicker by summing the 500 ms stimulus history before each spike during high-contrast episodes. For this, the stimulus intensity was normalized to range from -1 to 1 (instead of '0' to '255'). Linear filter polarity was assessed manually for each cell and brightness level. For the analyses, I have only considered cells that had clear linear filters.

Peak latency and amplitude of the linear filter were determined by latency and amplitude of the first peak. To make those estimates more robust against noise, the first peak of the filter was fit with a Gaussian. The latency was then taken as the position of the Gaussian fit along the time axis; the amplitude was read from the apex of the Gaussian fit. Another latency parameter was taken as the time of the first zero crossing after the first peak of the filter.

(4) For retinal ganglion cells spatial and temporal preference analyses the responses from Drifting sine-gratings stimuli were used. To calculate the firing rate, the spike train was convolved with a Gaussian, and plotted against the presented stimuli. Additionally, Fourier transforms of the spike rate were calculated for all presented drifting sine-wave grating stimuli. The amplitude of the Fourier transform at the frequency corresponding to the presented stimulus was taken as the response strength of the cell. For retinal ganglion cells spatial preference calculation I have taken maximum response strength of different drifting grating bar size (100, 200, 500, 1000, 2000, 4000 µm) over the different drifting grating speeds (0.25, 1, 2, 4,8 cycles/sec). It was for temporal preference the other way around: maximum response strength of different drifting grating bar size (0.25, 1, 2, 4,8 cycles/sec) over the different drifting grating speeds (100, 200, 500, 1000, 2000, 4000 µm).

Statistics. I used the Wilcoxon signed-rank or the identical Mann-Whitney test to assess the significance of difference between distributions. It is mentioned in the manuscript which test was used in each case.

4.9. Behavioral tests: Optokinetic drum[1]

We examined the visual performance of wild type and Jimpy mice by using the optokinetic response (OKR) task as described earlier (Benkner, Mutter et al. 2013). Briefly, a projection of a virtual cylinder with black and white stripes was presented on four screens surrounding the animal, positioned on an elevated platform. The animal tracks the rotating “cylinder” and follows it with head movements, which we analyzed quantitatively. Rotation speed was kept constant at the optimum of 12 °/s. (Mitchiner, Pinto et al. 1976; Abdeljalil, Hamid et al. 2005; Lagali, Balya et al. 2008; Benkner, Mutter et al. 2013), while contrast and stripe width was varied to estimate the visual performance of the animals (Figure 4-13).

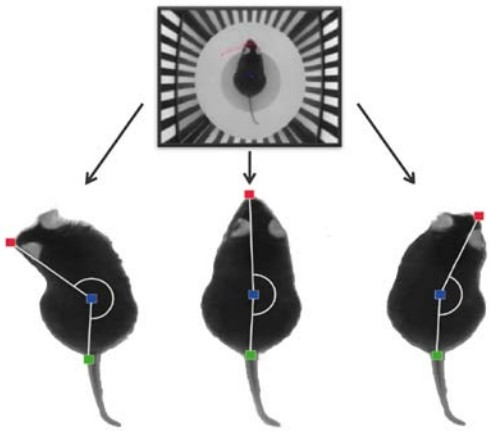

Figure 4-13. The optokinetic reflex measurement.
Mouse is sitting in the optokinetic drum surrounded by four screens. The red dot on the mice is the nose, the blue dot the middle of the body and the green one the beginning of the tail. Measured angle between head and the tale is indicated with white curly line, which has been used for the tracking analyses.

[1] Optokinetic Reflex measurements performed by Boris Benkner

5. Effect of Jimpy mutation on retinal ganglion cells and optokinetic reflex

5.1. Introduction

As has been introduced above, the Jimpy mouse model is a dysmyelination model, where PLP1 protein has point mutation and more than 90% of axons in the CNS are not myelinated. This mouse model has been used to investigate the effect of the absence of myelination on the CNS, in particular to find out the mechanisms of oligodendrocytes death (Knapp, Skoff et al. 1986; Ghandour, Feutz et al. 2002).

Because of severe lack of myelination Jimpy mouse model can be used to investigate the effects of dysmelination on neurons morphology and physiology. The retina and its ganglion cells can serve as a model for this purpose as, it has been mentioned in the introduction, axons of retinal ganglion cells are myelinated, but only after they leave the retina, thus any adverse effects of dysmyelination should therefore be caused by the lack of myelin itself.

5.2. Results

In this section I made preliminary experiments to check if Jimpy mouse model is suitable for investigation of influence of dysmyelination on neurons morphological, functional properties: I first looked at expression of PLP1 protein in mRNA and in protein level in the retina; Then I tested if ganglion cells are affected by Jimpy mutation (morphology and number); And finally if the visual input, that Jimpy mutant mice receive, is having functional visual output to the higher brain regions (optokinatic reflex measurement).

5.2.1. Myelin based protein and proteolipid protein expression in the retina

PLP1 is expressed by oligodendrocytes. Since the retina does not contain myelinated axons (axons of retinal ganglion cells are myelinated only after they leave the retina at the optic nerve head, Figure 5-1. A, n=3, shows staining for myelin (MBP)), it is not expected for PLP1 to be present inside the retina. Staining for PLP1 protein in wild type (Kalwy and Smith 1994) supported this hypothesis. The pattern of PLP1 immunoreactivity (Figure 5-1. B, n=3) coincided with the pattern for MBP immunoreactivity (Figure 5-1. A), which is another marker for myelination. Staining for neither protein yielded positive results in the wild type retina or in the lumina part of the optic nerve, the initial optic nerve segment where ganglion cell axons are not myelinated. In the optic nerve itself, staining was positive for both MBP and PLP1. As a more sensitive measure for potential expression of the *plp1* gene, I also looked for *plp1* mRNA in both wild-type and Jimpy retinas (Figure 5-1. C). I performed RT-PCR on total RNA isolated at P21, using cDNA-specific primers for the *plp1* gene (Table 4-4, in methods) (Figure 5-1. D). Optic nerve served as positive control. The ubiquitously expressed TATA-box binding protein (*tbp*) was used on retinal and optic nerve samples as a positive control for the PCR procedure itself. Negative controls were done with water as template and never gave a visible band. The *plp1* gene has 2 splice variants resulting in PCR products of 443 and 338 base pairs (bp), respectively. *plp1* mRNA was present in the optic nerve but not in the retina, for both wild type and Jimpy, as expected (Siegert, Cabuy et al. 2012). In summary, I found no expression of *plp1* on the mRNA or protein level in the retina. Ganglion cells do therefore not receive synaptic input from any neurons directly affected by dysmyelination, except potentially from histaminic retinopetal projections from the posterior hypothalamus (Gastinger, Barber et al. 2006).

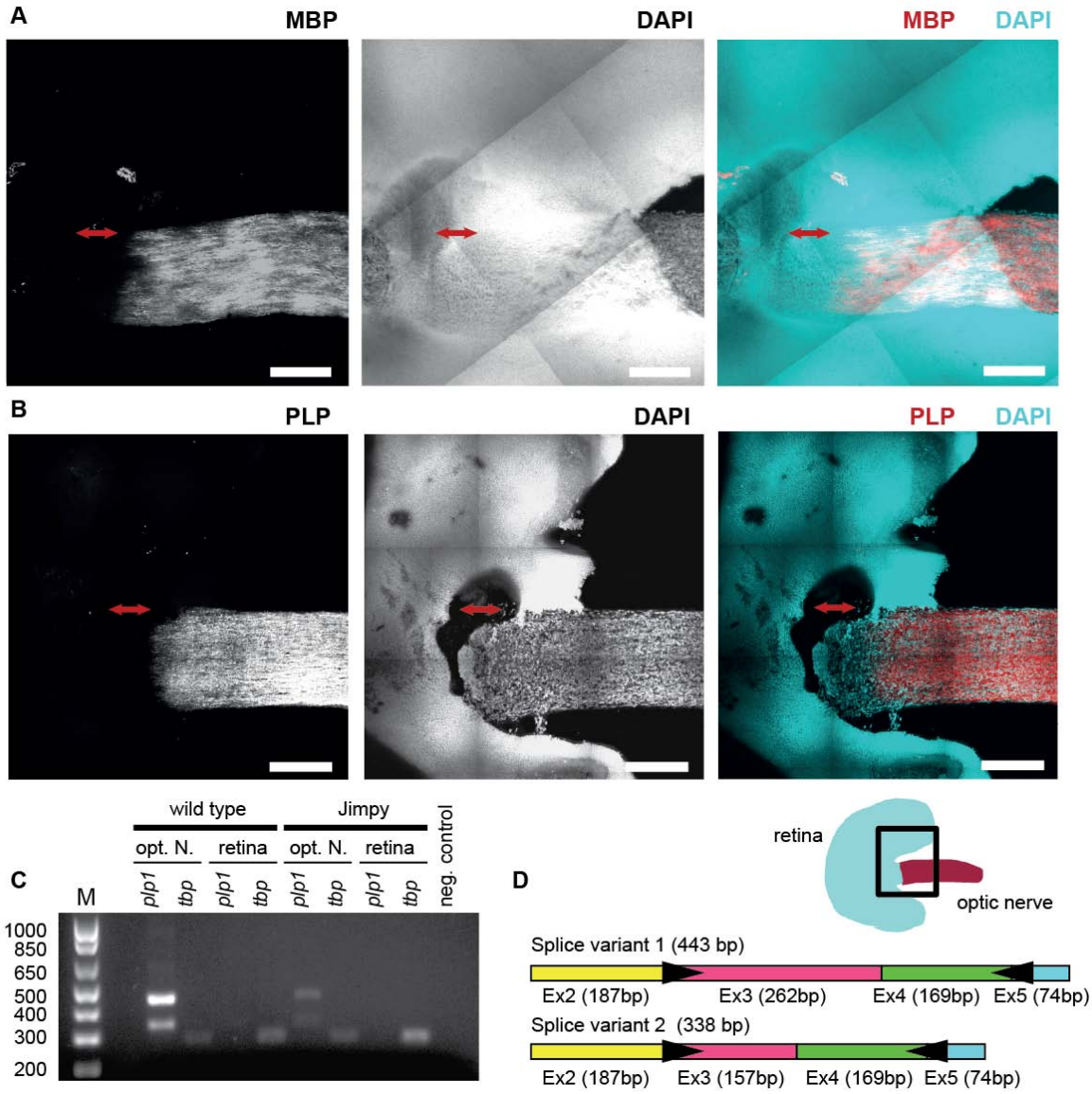

Figure 5-1.: Expression and localization of MBP and PLP in the retina and optic nerve.

A: Maximum intensity projection of MBP and DAPI staining in wild type. Red arrows: lumina of optic nerve. B: Maximum intensity projection of PLP and DAPI staining in wild type. Red arrows: lumina of optic nerve. The cartoon illustrates the layout of the retina-optic nerve preparation, for A and B. C: plp1 gene expression in mouse retina and optic nerve. RT-PCR on total RNA. plp1 gene is expressed in Jimpy mutant ("Jimpy") and wild type mouse optic nerves, but not in the retina. M: marker. Amplicon sizes: plp1: 350 bp and 499 bp (two different splice variants), tbp: 300 bp. D: Cartoon of the plp1 splice variants. Arrows indicate primer binding sites. All scale bars: 200µm.

5.2.2. Effects of the Jimpy mutation on the ganglion cells body and axons morphology

Next, I examined the ultrastructure of ganglion cell axons in optic nerve cross section in wild type (n=5) and Jimpy mutant (n=4) mice at age P21. While in the wild type optic nerves most axons were myelinated (Figure 5-2. A), in Jimpy optic nerve only a very small minority of axons had a myelin sheath (0.5 % ± 0.35 %, mean ± std, Figure 5-2. B), consistent with previous reports (Meier and Bischoff 1975; Omlin and Anders 1983). Furthermore, the myelination, when present, was less compact than in wild type (Figure 5-2. F,G), consistent with the proposed function of PLP1 (see Introduction).

Lack of myelination might have a detrimental effect on the ganglion cells themselves, therefore I next checked whether ganglion cells are dying in Jimpy mutant retinas. I counted the number of axons in five ~500μm^2 regions in each optic nerve, four peripheral and one central (Figure 5-2. A,B, boxes in the insets). I estimated the total number of ganglion cells based on these counts and the total cross-sectional area of the optic nerve. There was a large variation in the axon number in both wild type and Jimpy optic nerves. Overall, there was no significant difference between wild type and Jimpy mice (P = 0.39, Mann-Whitney test, Figure 5-2. C).

Consistent with the apparent lack of ganglion cell death, the ultrastructural appearance of the axons in Jimpy mutants seemed normal, including the appearance of their mitochondria (labeled ‘M’, Figure 5-2. D,E). Some oligodendrocytes (labeled ‘OLG’ in Figure 5-2.) also seemed normal in appearance (see Figure 5-2. H for a wild type oligodendrocyte), while others were filled with varying numbers of lipid inclusions (Figure 5-2. I, lipofuscin granules), an indication of dying cells. In contrast to the oligodendrocytes, astrocyte cell bodies (labeled ‘AC’) showed normal ultrastructural morphology.

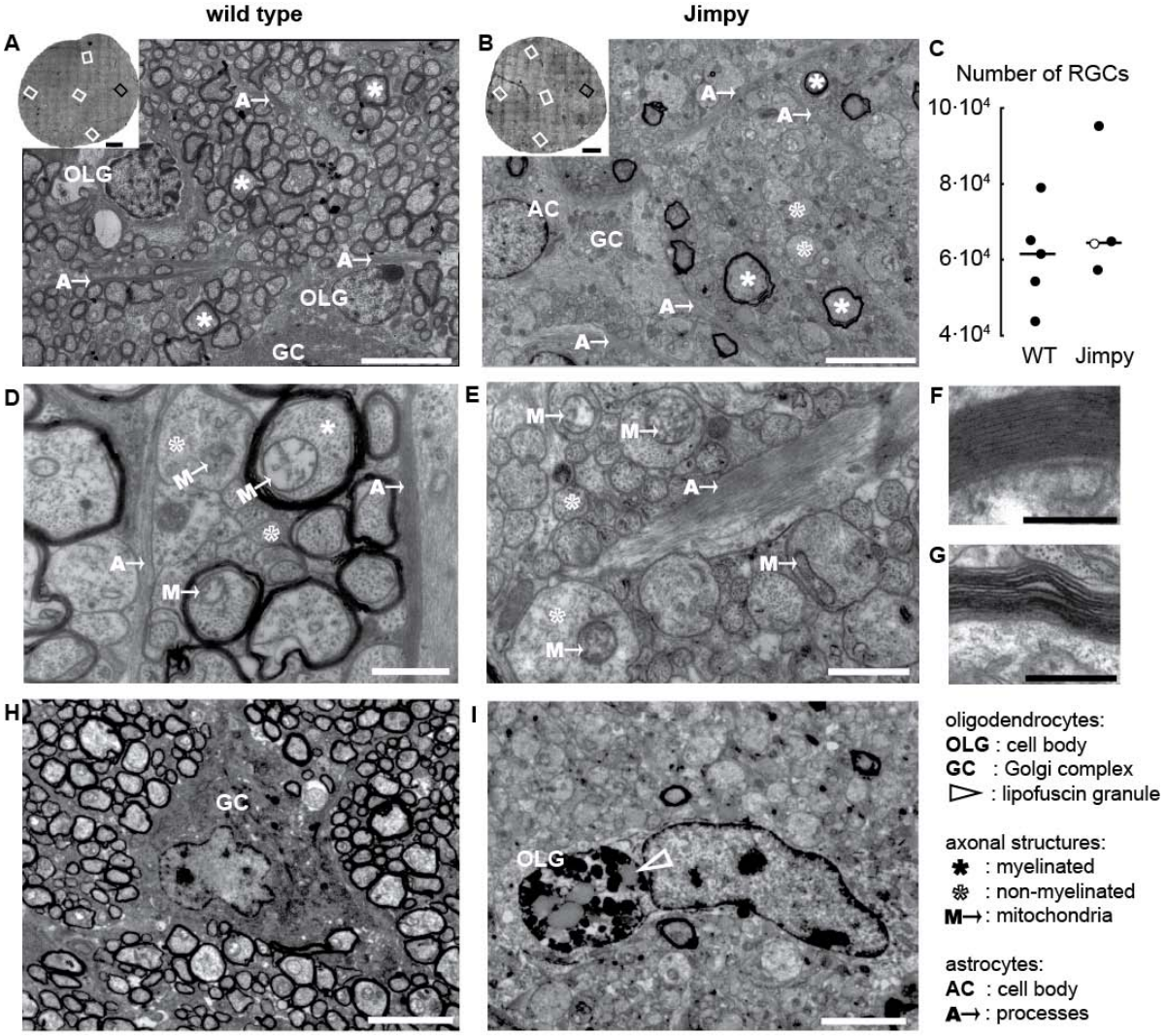

Figure 5-2.: Electron micrographs of optic nerve cross-sections.

The micrographs are from wild type (A, D, H, F) and Jimpy mutant (B, E, I, G) mice. A, B: Insets show entire optic nerve cross-section (EM tile scans). White and black boxes in the insets represent regions where axons have been counted. Black boxes: regions depicted at higher magnification in A and B. C: Number of ganglion cells (RGCs) in entire nerve of wild type (n=5) and Jimpy mutant (n=4) mice based on counting of optic nerve axons. Line indicates median values. The photomicrographs in the Jimpy panels are taken from the mutant indicated by the open circle that carries only the plp^{jp} but not the Eda^{TA} mutation. D, E: High magnification of optic nerve cross-sections. F, G: Myelin sheath around an axon in wild type (F) and Jimpy mutant (G) mouse optic nerve. H: Normal morphology of oligodendrocyte with Golgi complex. I: Abnormal morphology of oligodendrocyte in Jimpy mouse optic nerve. Scale bars 50 µm (insets), 5 µm (A, B, H, I), 1 µm (D,E), 0.2 µm (F,G).

Next, I examined the cell bodies of retinal ganglion cells (Figure 5-3). From the ultrastructural analyses they appeared normal; the membrane around their nuclei was intact (arrow) and the cisternae of the rough endoplasmic reticulum looked normal (arrowheads).

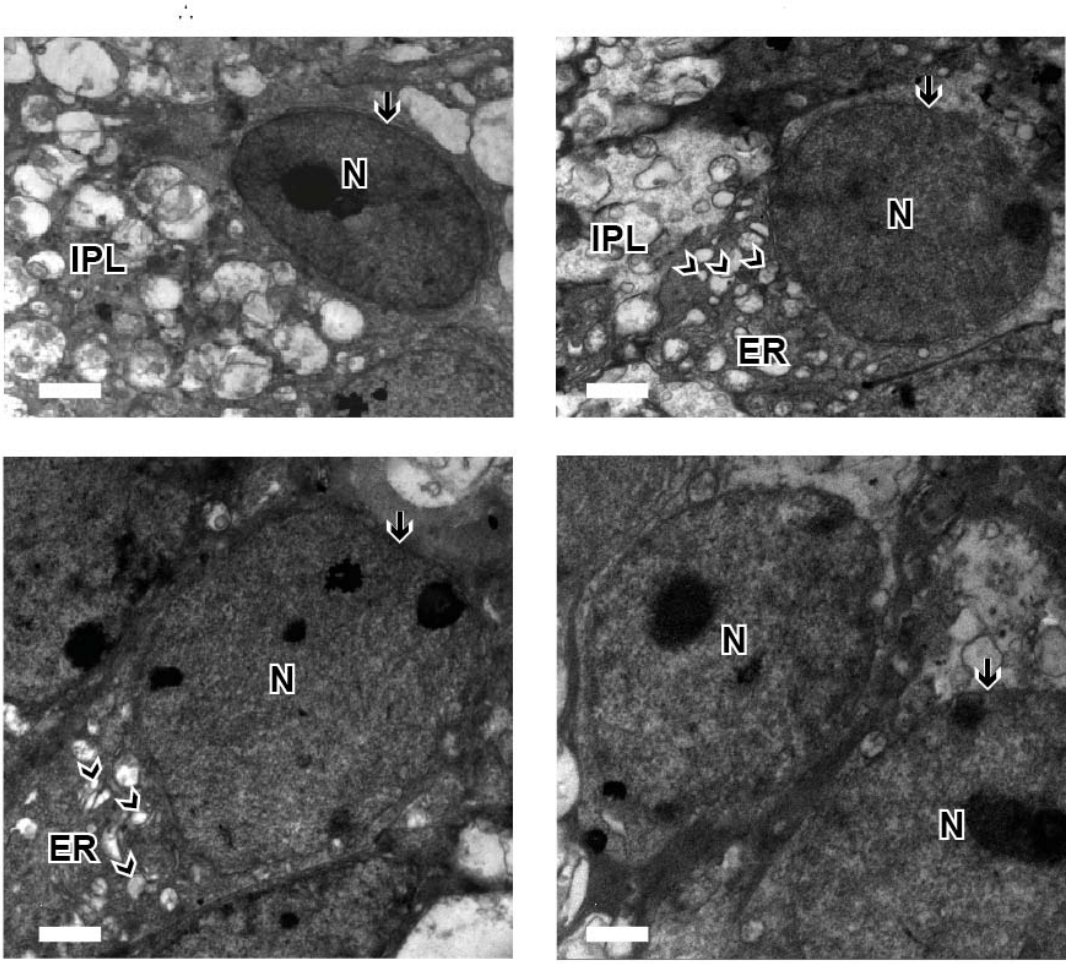

Figure 5-3. Electron micrographs of ganglion cell bodies from retina cross-sections of wild type (left) and Jimpy mutant mice (right).
N, cell nuclei; IPL, inner plexiform layer; ER, endoplasmic reticulum; arrow, the membrane of nuclei; arrow head, cisternae of the rough endoplasmic reticulum. Scale bars 2 µm.

In light microscope images, the cell body size and cell number of cells in the ganglion cell layer (presumably a combination of ganglion cells and amacrine cells) showed no significant difference in Jimpy mutants compared to wild type controls

(Figure 7-3. G, P>0.05, Mann-Whitney test). Hence, I found no indication of dying ganglion cells with this analysis.

Taken together, despite massive death of oligodendrocytes and near lack of myelination, neither the ultrastructural appearance of cell bodies and axons of ganglion cells nor their number was significantly affected in Jimpy mice at P21.

5.2.3. General functional characterization of visual system

Given the severe lack of myelination in the optic nerve, I wondered whether in Jimpy mutant mice visual information was transmitted to the brain. The optokinetic reflex is a simple reflex behavior which is often used to test for visual function (Benkner, Mutter et al. 2013). This reflex is based on the head movement of the animals to track moving visual stimuli. The input to the brain is a neural signal, which encodes information about visual motion on the retina. This is transformed to a motor command mainly via a subcortical neural pathway (i.e., the accessory optic system (AOS) and the nucleus of the optic tract (NOT)) (Wallman 1993; Tabata, Shimizu et al. 2010). Thus, the OKR plays an essential role in stabilizing the visual images on the retina.

If the optokinetic reflex is normal, a rotating stripe pattern is followed by the gaze of the animal (“tracking”) either with eye or head movement. Our analysis evaluated the animal’s head movements to determine correct tracking behavior. Visual acuity was tested over a range of 0.025-0.3 cycles per degree (Figure 5-4. B). Contrast was varied between 1.9% and 99.7% Michelson contrast (0.04 - 641.2 Weber contrast). 18 Jimpy mice (P18- P21) were compared to 22 wild type mice (P18-P23).

Due to their shaking phenotype and spasms, it is almost impossible for the Jimpy mutant mice to perform smooth tracking motions. It is thus quite difficult to analyze their performance in this task, as such tracking motion is often disrupted by spasms.

Despite this, 60% of the Jimpy mice reached our strict criterion threshold of successfully performing the optokinetic test (Benkner, Mutter et al. 2013) for at least one tested condition. This suggests that in general, the optokinetic reflex is working and that visual information is indeed transmitted along the optic nerve. For comparison, 90% of the wild type mice reached the criterion threshold for at least one condition, and they reached the same contrast sensitivity as C57Bl/6 mice (Benkner, Mutter et al. 2013) (Figure 5-4. A).

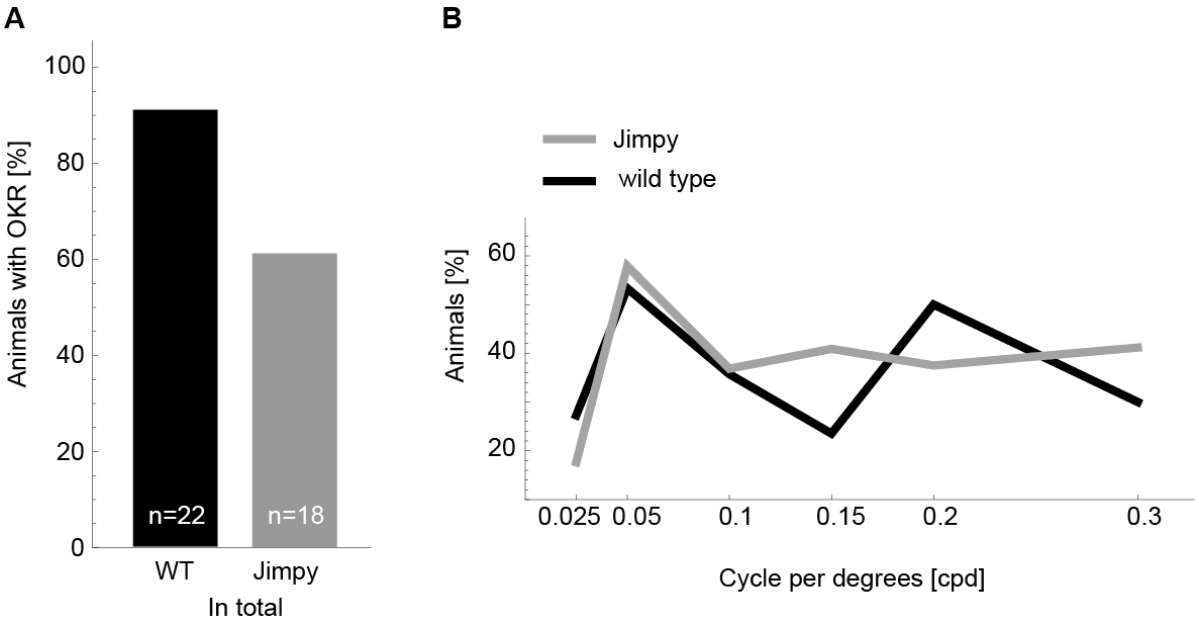

Figure 5-4.: Tested animals that show optokinetic reflex.
For the OKR test 22 wild type and 18 Jimpy mutant mice have been used. A: The % of total tested wild type and Jimpy mutant mice, which show the OKR. B: The % of tested wild type and Jimpy mutant mice which show visual acuity for tested 0.025-0.3 cycles per degree range of stimulus.

5.3. Discussion

In this section I have performed several preliminary experiments to confirm that the Jimpy mouse model is suitable for addressing the question whether dysmyelination has an effect on function and morphology of neurons.

I confirmed that PLP1 is not expressed neither on the protein nor the mRNA level in the retina. I found very few myelinated axons in the optic nerve of Jimpy mutant

mice, as expected. The few axons with myelination showed a rather non-compact myelin sheath (Figure 5-2. B, F) (Meier and Bischoff 1975; Omlin and Anders 1983). I did not observe any difference in the ultrastructure of the optic nerve axons and the ganglion cell bodies in Jimpy mutant and wild type mice. The cell number count in the ganglion cell layer and the axon count in the optic nerve was not altered either (Figure 5-2. C, Figure 7-3. G).

These findings, regarding to cell number and morphology of retinal ganglion cell bodies and axons, were rather surprising, as Jimpy mutant mice have severe problem with myelination, which is supposed to isolate axons from each other and help them to perform sufficient signal transduction. The conclusion of this section is that the lack of myelin does not lead to obvious ganglion cell damage or death, at least not at the testable age (P22) before the affected animals die. This conclusion was supported by the behavioral optokinetic reflex test. It showed that visual information can be transmitted along the optic nerve in Jimpy mutant mice (Figure 5-4).

6. Effects of the Jimpy mutation on retinal function

6.1. Introduction

The retina is part of the CNS. It is a complex system and consists of light sensitive input cells (photoreceptors), inter-neurons (cells which participate in linear and non-linear transduction of input signal in lateral (horizontal and amacrine cells) and perpendicular (bipolar cells) directions) and output neurons (retinal ganglion cells) (Møller 2003). There are more than 20 types of retinal ganglion cells characterized based on their morphological and physiological properties (Masland 2001; Volgyi, Chheda et al. 2009; Zhang, Kim et al. 2012).

Extracellular recordings from retinal ganglion cells by using MEA systems are widely used. This allows to investigate light induced electrophysiological properties of retinal ganglion cells (cell types, temporal and spatial properties, etc.) by stimulating retina with different visual stimuli and simultaneously recording from many retinal ganglion cells (Meister, Pine et al. 1994; Reinhard, Tikidji-Hamburyan et al. 2014). This is done by using different light stimuli, which probe different components of the retinal circuits (e.g., full field flashes (ON and OFF responses), moving bars (direction selectivity), different brightness of the same stimulus: scotopic, mesopic, photopic (to activate rods and cones by different amounts, which means different signal transduction pathways), etc.).

6.2. Results

After establishing that Jimpy mutant mice are able to transmit visual information to the brain, I next investigated whether the lack of myelination might affect the physiology of retinal ganglion cells. I recorded the activity of retinal ganglion cells by

placing isolated retina (n = 7 wild type retinas and n = 4 retinas of Jimpy mutants, each retina from a different animal) onto flat 60-electrode multi-electrode arrays (MEAs). With this arrangement I could characterize ganglion cell activity while the retina was exposed to different ambient light levels (scotopic, mesopic, photopic). In addition, I also recorded the activity of ganglion cells when presenting time-varying visual stimuli. From the raw data, spiking activity from each electrode was extracted, and single units were isolated by spike sorting (see Methods). In total, I have extracted and isolated 266 units from wild type retina, and 119 units from Jimpy mutant retina. These units presumably correspond to individual ganglion cells.

6.2.1. Spontaneous spike rate

To investigate the physiological properties I have first looked at the spontaneous spike rate of retinal ganglion cells of Jimpy mutant and wild type mice. Spontaneous activity was measured in the 1s interval before each presented stimulus over whole experiment. During this 1s only background was shown (gray value ‘128’) (Figure 6-1).

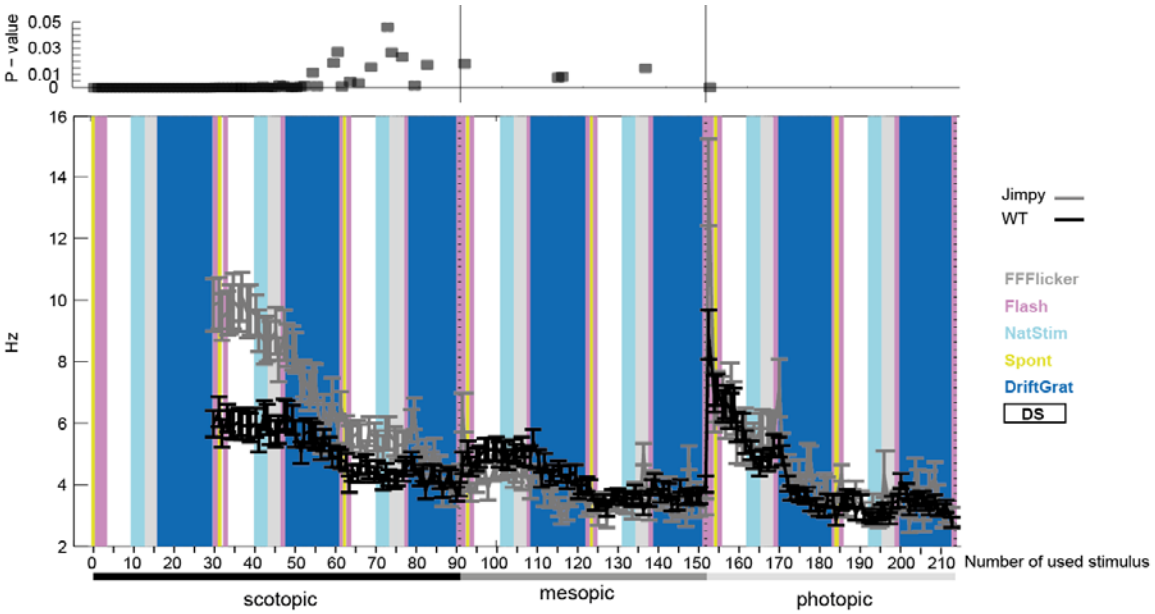

Figure 6-1. Spontaneous firing rate of retinal ganglion cells.
The spontaneous activity was measured before each applied stimulus in 1 s time frame over whole experiment. The upper panel is a P-value from Wilcoxon rank sum test. Early In the scotopic range there is a significant difference, as the retina is not settled down yet. In the mesopic and photopic brightness levels there is almost no difference. The bottom part of the figure is spontaneous spike rate over whole experiment. On the right of the figure the used stimulus color code presented. FFFlicker: Gaussian white noise flicker; Flash: full-field flashes; NatStim: natural movies; Spont: no stimulus; DriftGrat: drifting sinusoidal gratings; DS (white bars): moving bars. Responses to the all stimuli, except natural movies, have been analyzed, and the results are presented.

We haven't observed significant difference in the spontaneous firing rate of ganglion cells in Jimpy mutant and wild type mice at any ambient illumination (scotopic, mesopic, and photopic ambient brightness levels, Figure 6-1). The only difference that I have seen was early in the scotopic brightness level. I cannot exclude that at the beginning of the experiment the reason for this difference is that the retina is still settling down, as the spontaneous spike rate is not different in the other brightness levels.

In conclusion the background firing rate was not different in both mouse lines.

6.2.2. Stimulus evoked spike rate

When exposed to full-field Gaussian White Noise flicker, ganglion cells increased their firing rate compared to their spontaneous activity both in wild type and Jimpy mutant mice. Remarkably, by the transition from scotopic to mesopic ambient luminance the stimulus-evoked spike rate of Jimpy mutant ganglion cells decreased more than in wild type ganglion cells. While the wild type mice ganglion cells stimulus-evoked spike rate at the early mesopic range increased and then slowly decreased trough the brightness, the Jimpy mutants ganglion cells first decreased and then increased their spike rate (Figure 6-2). As a result, stimulus-evoked spike rate was clearly higher for wild-type ganglion cells than for Jimpy mutant ganglion cells in mesopic conditions, while they did not differ in other conditions.

For the direction selectivity of recorded ganglion cells to response moving bars stimuli, in both mouse lines I did not found significant difference differences between two mouse lines (in wild type mice 26 cells out of 119, and in Jimpy mutant mice 23 cells out of 266 cells were direction selective).

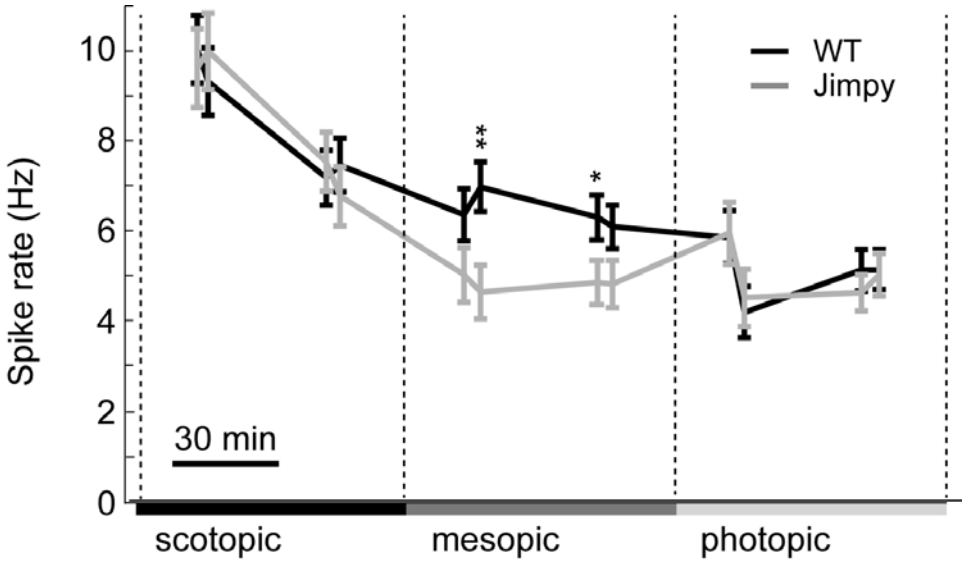

Figure 6-2. Stimulus evoked spike rate of retinal ganglion cells to white noise full flicker stimulation.

The ambient light level was increased every hour. Median ± s.e.m of ganglion ell spike rate across all retinas (Jimpy mutant retina: 119 cells in 4 retinas, wild type retina: 266 cells in 7 retinas). *P<0.05, **P<0.01.

Neither of these stimuli revealed significant differences between Jimpy mutant and wild type retinas for the parameters I have measured: direction selectivity, polarity.

In conclusion, the only difference that I have found in Jimpy mutant mice compared to their wild type littermates, was lower spike rate in the mesopic brightness level. The spike rate of Jimpy mutant mice was lower. This can suggests that changes in signal processing in the Jimpy mutant retina may be altered at a level preceding the ganglion cells.

6.2.3. Linear filter

From the ganglion cell activity in response to the full-field Gaussian White Noise flicker I calculated the linear filter (spike-triggered average stimulus) of each ganglion cell for each presentation of the flicker stimulus. The linear filter allows to inspect linear temporal response characteristics of each ganglion cell. I have analyzed two kinetic parameters of the linear filter (time-to-peak and time-to-zero-crossing). This analysis showed only minor differences between both mouse lines. As it is shown in Figure 6-3, the linear filter latencies (time-to-peak and time-to-zero-crossing) curves for Jimpy mutant and wild type mice are mostly overlapping.

This means that the Jimpy mutation has no effect on the signal processing of the retina by influencing on linear filter latencies.

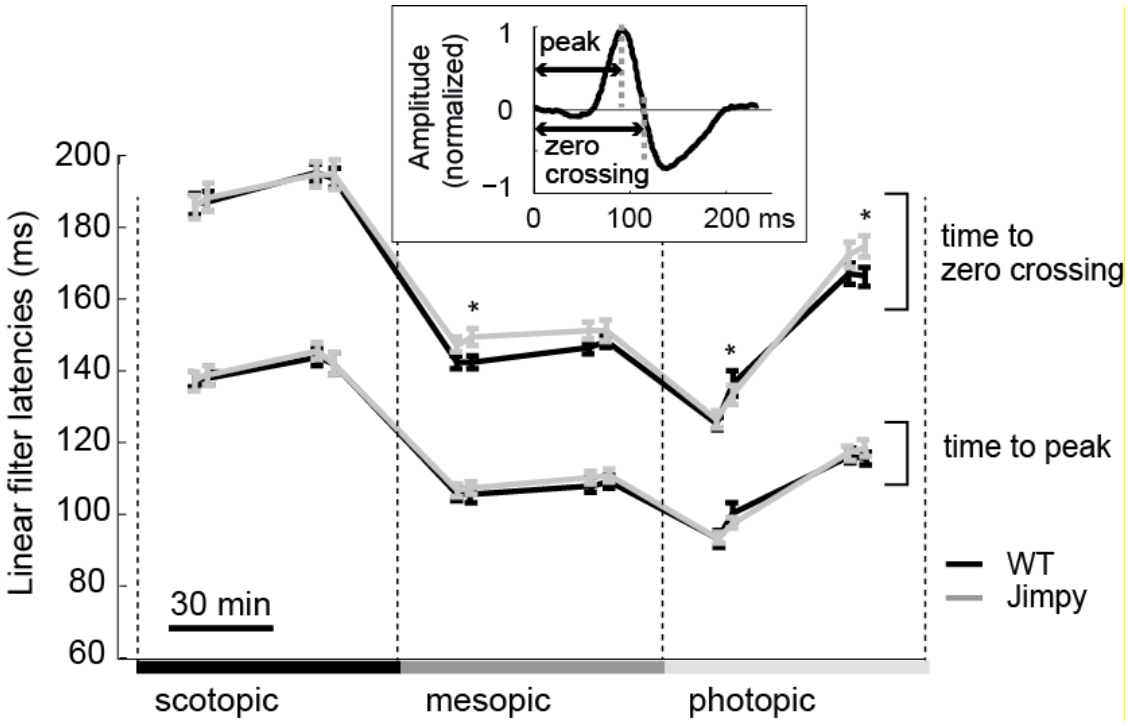

Figure 6-3. Linear filters latencies of retinal ganglion cells.
Temporal properties of linear filters of wild type and Jimpy mutant ganglion cells. Inset: Representative linear filter of ganglion cells calculated from Gaussian white noise. Time-to-peak and time-to-zero-crossing are indicated. *: P<0.05

6.2.4. Spatial and Temporal preference of retinal ganglion cells

To investigate spatial and temporal tuning of retinal ganglion cells I have used their responses to drifting sine-gratings stimuli (for analyses see methods section). To assess the response strength of a cell to each stimulus, I have taken the Fourier transform of the response, and measured the strength of the Fourier transform at the frequency of the periodic drifting grating stimulus. For spatial tuning curves I have taken the maximal response across all different temporal frequencies (0.25, 1, 2, 4,8 cycles/sec, Figure 6-4. B), and for the temporal tuning curve I have taken the maximum across all spatial frequencies (100, 200, 500, 1000, 2000, 4000 µm per

cycle, Figure 6-4. C). In both wild type and Jimpy mutant mice retina ganglion cells preferred bigger than 500μm size of the stimulus and 0.25-4 cycle/s speed of stimulus.

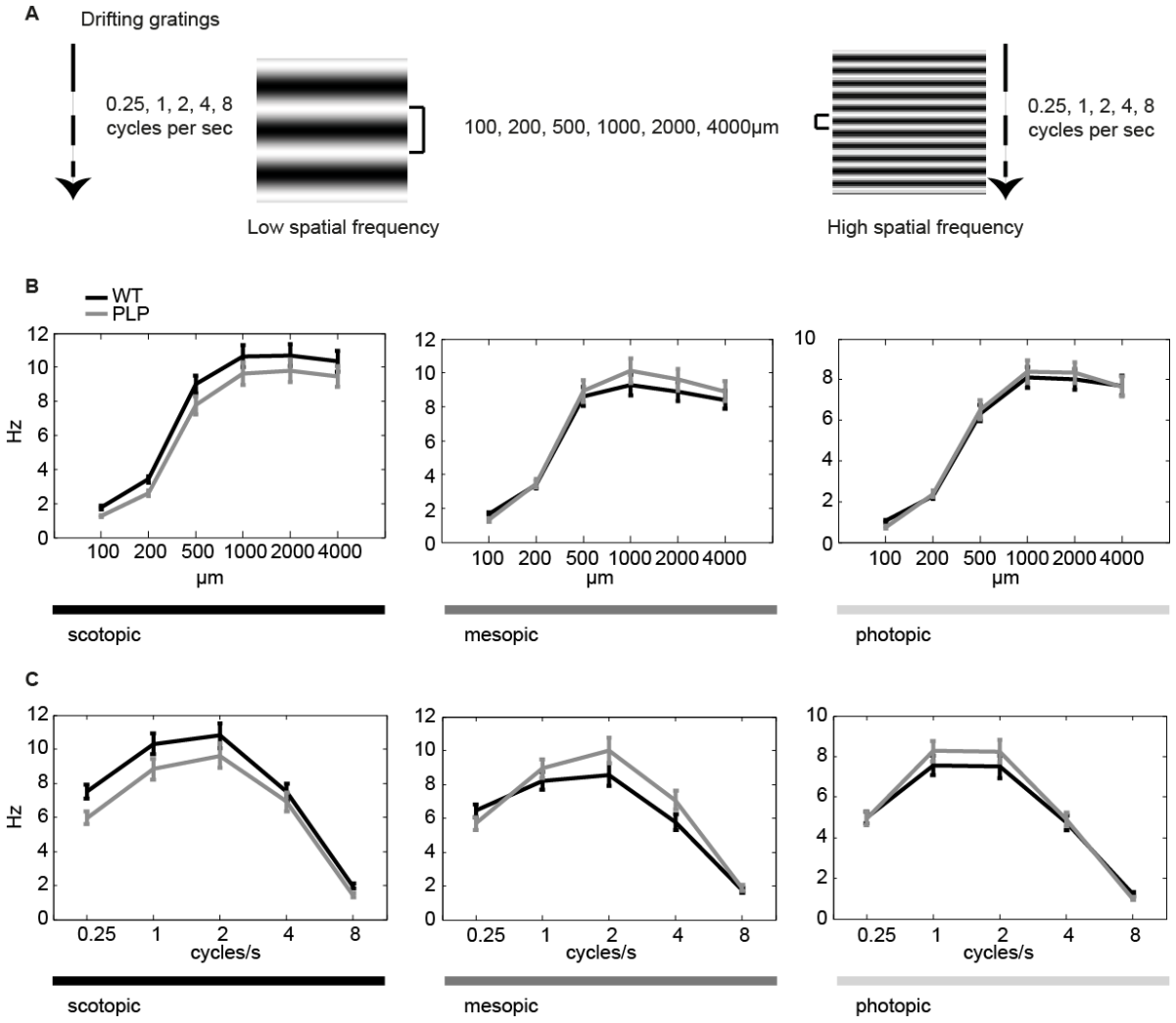

Figure 6-4. Spatial and temporal preference of retinal ganglion cells.
A: Drifting gratings stimulus for five different speeds (0.25, 1, 2, 4, 8 cycles/sec) and six different sizes (100, 200, 500, 1000, 2000, 4000 μm). B: Spatial preference of the retinal ganglion cells, over different brightness levels. In all cases preferred size of the stimulus is up to 500μm. C: Temporal preference of the retinal ganglion cells, over different brightness levels. In all cases preferred speed of the stimulus is 0.25-4 cycles/sec.

In summary, for both Jimpy mutant and wild type mouse retina, ganglion cells do not differ in their speed and size preference of the stimulus.

6.3. Discussion

The results from retinal ganglion cells spontaneous and stimulus evoked spike rate did not show a difference (except for the stimulus evoked lower spike rate of Jimpy mouse retinal ganglion cells in mesopic brightness range). The spatial and temporal preference of the retinal ganglion cells was also similar to the wild type mice. The response latencies from the linear filter analysis were as well the same. Taken this all together the conclusion is, that the $plp1^{jp}$ mutation resulted in only minor changes in the retina of Jimpy mutant mice. The physiology of ganglion cells were hardly affected. This suggests that dysmyelination has minor effects on the involved neurons (the retinal ganglion cells), at least within the timeframe measurable in the Jimpy mouse model before the mutant animals die.

7. Effects of the Jimpy mutation on retinal morphology

7.1. Introduction

The retina is a multilayer complex tissue. It consists of different cell types, which have distinct location in the retina. The retina has morphologically very well distinguished layers and each of them has certain cell types, which have specific function. The photoreceptor layer consists of the outer segments of photoreceptors (rods and cones) and the outer nuclear layer of nuclei of the same cells. The outer plexiform layer contains synaptic connections of all the photoreceptors and some inner nuclear layer cell (horizontal and bipolar cells) processes. In the inner nuclear layer most of the cell bodies of retinal inter-neurons and glia cells are located (horizontal, bipolar, and amacrine cells, Müller glia and microglia cells). The tuning of signal from photoreceptor outputs takes place here. The inner plexiform layer consists of inner nuclear layer cell (bipolar and amacrine cells) processes and their synaptic connections with ganglion cell layer cells. In this layer complex computations from the lateral interactions of upper retina layers are brought together. And finally, the ganglion cell layer contains different ganglion cell types, some amacrine cells and astrocytes. From the ganglion cells, the output of the retina is transmitted to higher brain regions.

The thickness of the retina layers and the cell number within them are defined during development and stays the same during the lifetime of the animal (in mammals), unless some pathological processes are taking place in the retina e.g., in case of retinitis pigmentosa (Cronin, Raffelsberger et al. 2010). That is why a change of thickness or cell number in any of these layers can be an indication for the existence of a pathology in the retina. Screening the retina for cell number,

thickness and morphology of the cells layers can help to find out if there is any pathology taking place.

7.2. Results

7.2.1. Retina gross morphology

The gross morphology of the retina was examined at the light microscopic level in cross sections of the whole retina along the central meridian (n=7 for wild type and n=4 for Jimpy mutant, Figure 7-1). Specifically, for each retina I analyzed two 400 µm long cross sections, one each from the dorsal and from the ventral retina (boxes in Figure 7-1. A); Figure 7-1 B and C show examples of ventral sections from wild type and Jimpy mutant retina, respectively. In these sections, I have measured the thickness of the retinal layers and counted the number of cell bodies in the inner nuclear layer (INL), outer nuclear layer (ONL), and ganglion cell layer (GCL) (Figure 7-1. D-G). None of these parameters showed a significant difference between wild type and Jimpy mutant retinas ($P > 0.05$ in all cases, Mann-Whitney Test). I have also measured cell body sizes in the ONL, INL, and GCL (Figure 7-1. E-G). I found no differences in the GCL between Jimpy mutant and wild type retina (Figure 7-1. G). The cell body sizes in ONL (Figure 7-1. E) were slightly larger in ventral Jimpy retina than ventral wild type retina ($P=0.042$). In the INL, I found that cell bodies were larger in Jimpy retinas by approximately 25% (Figure 7-1. F, $P=0.007$ for ventral retina, $P=0.042$ for dorsal retina, $P=0.01$ when combining dorsal and ventral retina, Mann-Whitney Test).

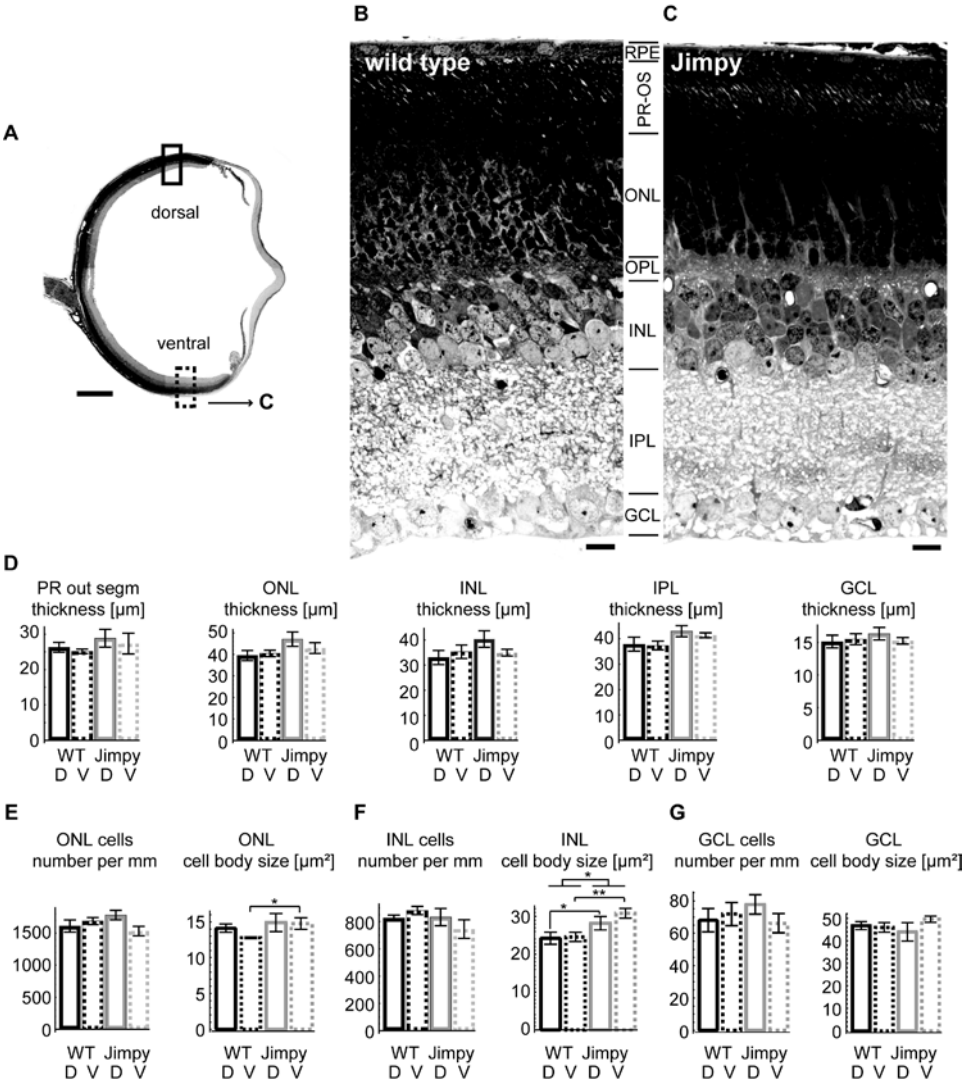

Figure 7-1. General morphology of wild type and Jimpy mutant retinas.

A: Overview of retinal cross section along the central meridian from EPON embedded retina. Boxes indicate ventral and dorsal regions where measurements have been made. Dashed box indicates high magnification ventral retina shown in C. B,C: Toluidine blue-stained transverse sections of wild type (B) and Jimpy mutant (C) retina showing the organization of the retinal layers. D: Thickness of retinal layers, measured in 400µm long cross sections in dorsal (D) and ventral (V) retina of wild type ('WT', n=7) and Jimpy mutant ('Jimpy', n=4). E-G: The number of cells per mm length of retinal cross section and cell body size (cross-sectional area) from wild type (n=7) and Jimpy mutant (n=4) mice in ventral (V) and dorsal (D) cross sections for cells in the outer nuclear layer (ONL, E), inner nuclear layer (INL, F), and ganglion cell layer (GCL, G). All bar graphs show mean ± s.e.m. RPE, retinal pigment epithelium; PR-OS, photoreceptor outer segments; ONL, outer nuclear layer; OPL, outer plexiform layer; INL, inner nuclear layer; IPL, inner plexiform layer; GCL, retinal ganglion cell layer. *P<0.05, **P<0.01. Scale bars 400 µm (A) and 10 µm (B, C).

Since the number of cells and the thickness of the layers in INL and ONL were not significantly different in Jimpy retinas (even though there was a non-significant tendency that thickness of Jimpy mouse retina was increased), I expected that the spacing between cell bodies would be compressed in Jimpy mutant retinas to allow for the larger cell bodies; this was indeed the case in the INL (P = 0.018, Mann-Whitney Test).

As I have already mentioned in the methods section, because of the way my data was distributed, I was unfortunately not able to exclude mice carrying the *Eda*^{Ta} mutation form the retina gross morphology analyses (Figure 7-1). This data contained n=4 mutant samples each, with one sample from a *plp1*^{jp} mouse, and 3 samples from *plp1*^{jp} *Eda*^{Ta} mice.

In the gross morphology analysis, the only difference between Jimpy and wild type mice I found was in the cell body size in the INL. The one *plp*^{jp}-only retina in my data set was actually the one with the most extreme phenotype (i.e. with the largest cell bodies in the INL of all mutant mice (Figure 7-2. B). For the retina layers thickness, cell number and as well for cell body size measurements (Figure 7-2. A, C) the data from only *plp*^{jp} mutant mouse was laying within the data distribution.

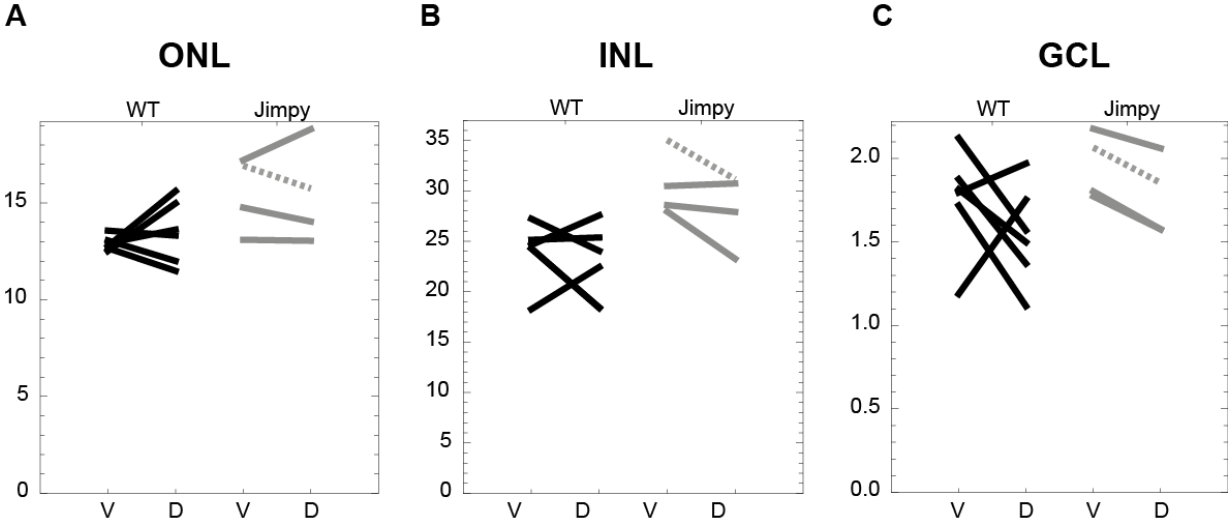

Figure 7-2. Mean cell body size from the individual retinas.
A, B,C: Mean cell body size in ONL, INL and GCL. The dashed line is from the only *plp*^{jp} mutant mouse. ONL, outer nuclear layer; INL, inner nuclear layer; GCL, retinal ganglion cell layer; V, ventral; D, dorsal.

On the ultrastructural level, in general, the Jimpy mutant retina looked normal, except that I sporadically observed lipofuscin granules in the INL, indicating that some cells are dying (Figure 7-3).

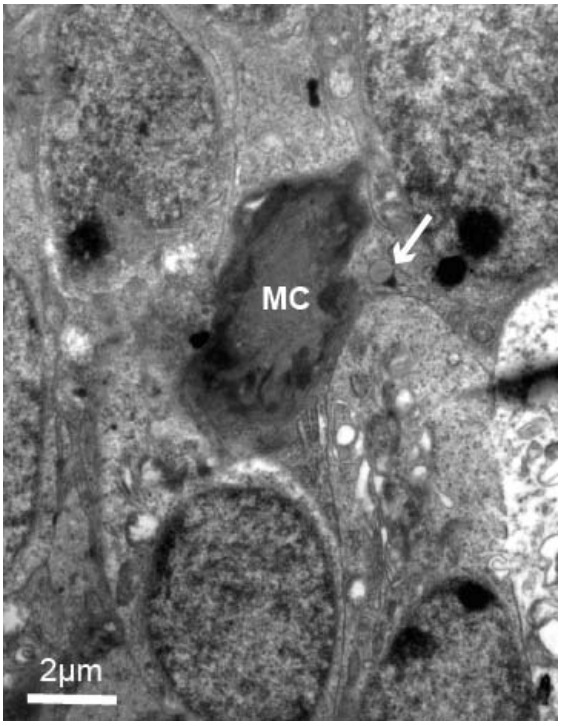

Figure 7-3. EM micrograph of Müller cell in the retina cross section. The Müller glia cell can be distinguished by its darker nuclei (MC). The arrow is pointing on the lipofiscin granule.

7.2.2. Cell type-specific comparison

The larger size of cell bodies in the INL of Jimpy mutant retinas could be explained by two factors. First, all or some cell types in the Jimpy mutant retina could have larger cell bodies than normal, i.e., the morphology of individual cells could be changed. Second, some cell type(s) with large cell bodies could increase in number, while at the same time, some cell type(s) with small cell bodies could decrease in number, i.e. the composition of cell types could be changed without changing the morphology of any one cell type. For a number of retinal cell types with established markers, I have therefore performed immunolabeling in the wholemount retina to

investigate whether their numbers are changing in the Jimpy mutant retina. The following cell types were labeled and the retina imaged with a confocal microscope: Horizontal cells (Figure 7-4. A, marker: calbindin), rod bipolar cells (Fig. 6.3. B, marker: protein kinase C-alpha), Müller glia cells (Figure 7-5. A, marker: glutamine synthetase), and starburst amacrine cells (Figure 7-5. B for INL, Figure 7-5.C for GCL, marker: choline acetyl transferase). For each cell type, I labeled between six and seven retinas each for wild type and Jimpy mutant mice, and counted the number of labeled cells in a defined area to calculate the cell number per mm², and I compared cell densities statistically with the Mann-Whitney test.

Horizontal cells (Figure 7-4. A) and rod bipolar cells (Figure 7-4. B) had increased density in Jimpy mutant mice than in wild type (horizontal cells: P=0.003, P=0.017 when comparing ventral retinas; rod bipolar cells: P=0.0001, P=0.0053 for dorsal as well as ventral retina, Mann-Whitney-Test). I did not find significant differences ($P > 0.05$, Mann-Whitney Test) neither for the number of Müller cells (Figure 7-5. A) nor for the number of starburst amacrine cells (neither OFF starburst cells in the INL, Figure 7-5. B, nor ON starburst cells in the GCL, Figure 7-5. C).

In conclusion, I have found some cell types to have increased density in the Jimpy mutant retina (rod bipolar and horizontal cell). None of the labeled cell types showed a decreased density in Jimpy mutant retina.

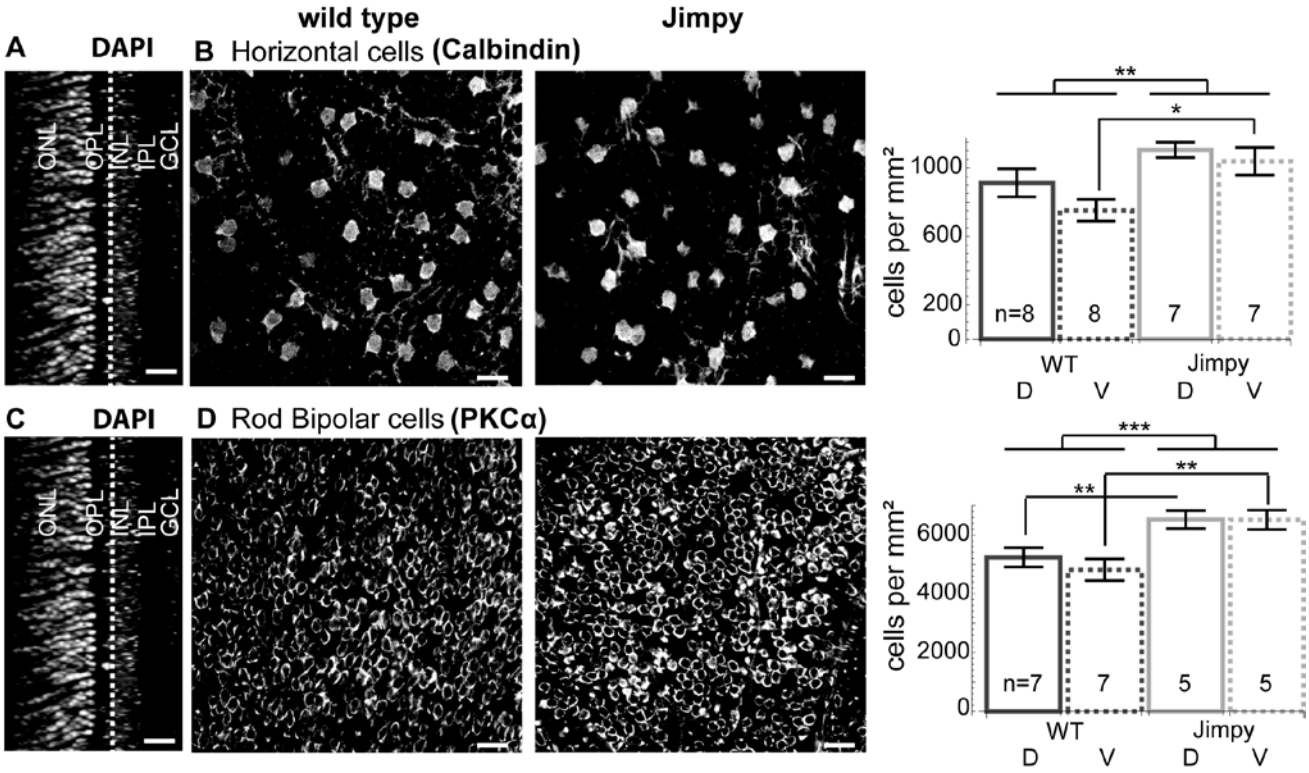

Figure 7-4. Density of horizontal and rod bipolar cells in wild type and Jimpy mutant ventral and dorsal retina.

A,C: Counter staining (with DAPI) reveals retinal layers. Dashed line: retinal layers where cells have been counted, depicted in B and D.B: Single confocal sections of calbindin staining for horizontal cells in wild type (left) and Jimpy mutant (middle) mouse retina. Bar chart (right) shows density of horizontal cells (mean ± s.e.m.) in ventral (V) and dorsal (D) retinas. D: Single confocal sections of PKCα staining for rod bipolar cells in wild type (left) and Jimpy mutant (middle) mouse. Bar chart (right) shows density of rod bipolar cells (mean ± s.e.m.) in ventral (V) and dorsal (D) retinas. *P<0.05, **P<0.01, ***P<0.001. Scale bars 20 µm.

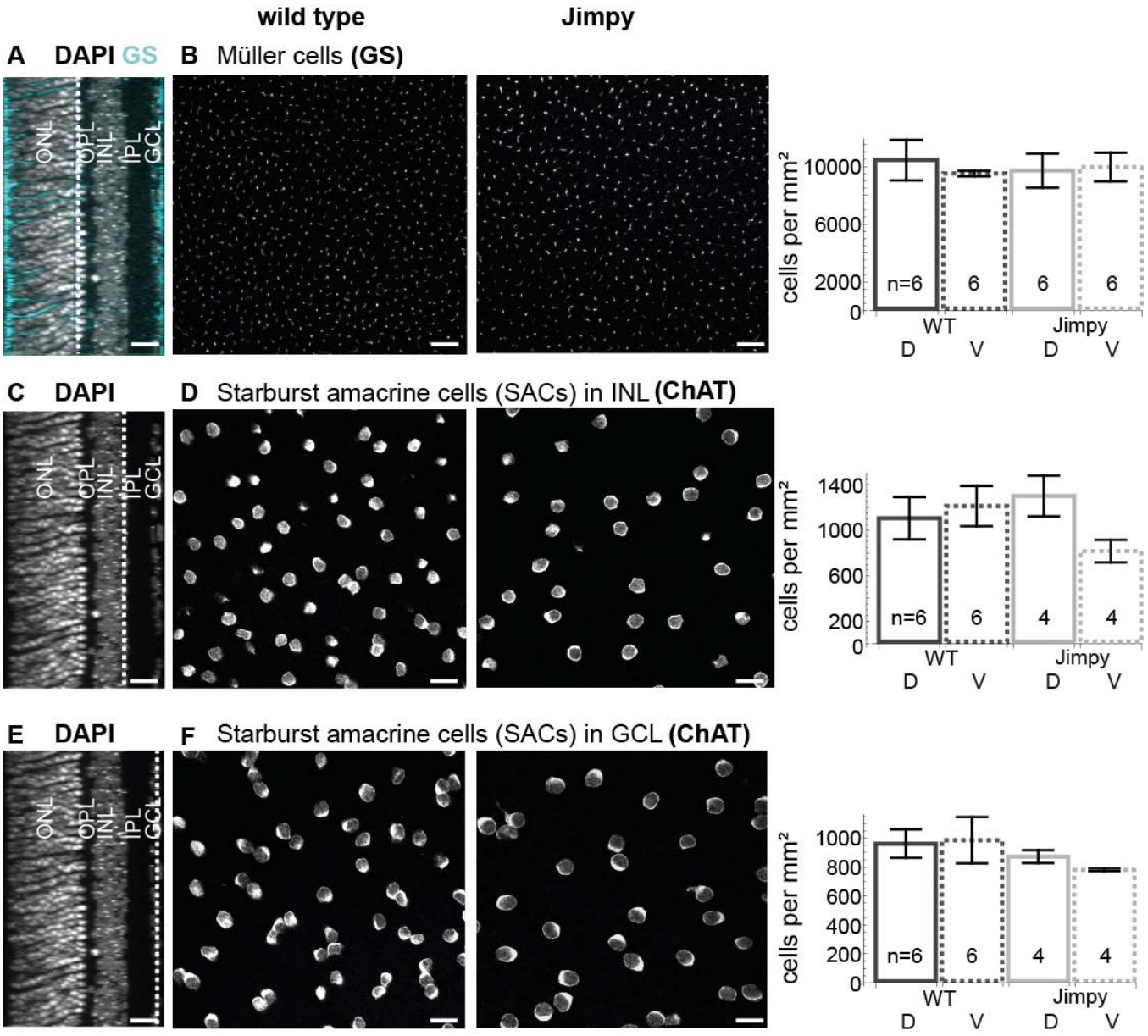

Figure 7-5. Density of Müller cells and starburst cells in wild type and Jimpy mutant ventral and dorsal retina.

A,C,E: Counter staining (with DAPI) reveals retina layers. Dashed line: retinal layer where cells have been counted, depicted in B, D, F. B: Single confocal sections of glutamine synthetase staining for Müller cells in wild type (left) and Jimpy mutant (middle) mouse retina. Bar chart (right) shows density of Müller cells (mean ± s.e.m.) in ventral (V) and dorsal (D) retinas. D,F: Single confocal sections of choline acetyl transferase (ChAT) staining for starburst amacrine cells in the inner nuclear layer (INL, D) and ganglion cell layer (GCL, F) in wild type (left) and Jimpy mutant (middle) mouse retina. Bar charts (right) show density of starburst cells (mean ± s.e.m.) in ventral (V) and dorsal (D) retinas. Scale bars 20 µm.

7.3. Discussion

The only difference that I have found from retina gross morphology analyses was increase of cell body size in INL (Figure 7-1. F). There can be two possible explanations for larger cell bodies on the population level: first, the cell body size of individual neurons is changes and *second,* balance in cell composition is changed, e.g. cells with smaller cell bodies could be less numerous, and cells with larger cell bodies more numerous. To test for this, I have immunolabeled four retinal cell types with cell bodies in the INL: horizontal cells, rod bipolar cells, starburst amacrine cells, and Müller glia cells (Figure 7-4 and Figure 7-5). Only horizontal cells and rod bipolar cells had increased cell number (Figure 7-4. A, B). Horizontal cells are cells with big cell bodies, which is consistent with the overall increased size of cell bodies in the INL as measured in retinal cross sections (Figure 7-1. D). Rod bipolar cells, on the other hand, are cells with small cell bodies. An increase in their number is inconsistent with the observed changes in cell body size distribution.

It should be noted that overall cell number in the Jimpy retina is not increased (Figure 6-1. E,F). Although, both individual cell types, horizontal cells and rod bipolar cells, increased their number. This suggests that other cell types, so far not identified, possibly decrease in number.

8. General discussion

De- and dys-myelination have severe consequences in the central and peripheral nervous system (Klugmann, Schwab et al. 1997; Vela, Gonzalez et al. 1998). It is not well understood whether detrimental effects on individual neurons are caused by the lack of myelin itself, or whether secondary effects (changed signaling between brain areas, changed physiological conditions in the surrounding tissue) play the major role. The retina and its ganglion cells can serve as a model to investigate this question. Axons of retinal ganglion cells are myelinated, but only after they leave the retina. While traversing the retina and until leaving the eye at the optic disc, they remain non-myelinated. Indeed, no myelination is found in the retina, as I have also confirmed in this study by staining for MBP and PLP1, two major myelin proteins. (Figure 5-1). Thus, ganglion cells receive no input from myelinated neurons, potentially with the exception of few centrifugal histaminergic neurons which target processes in the inner and outer plexiform layer. Any adverse effects of dysmyelination should therefore be caused by the lack of myelin itself.

We investigated the retina and optic nerve of a mouse model for Pelizaeus-Merzbacher disease, the Jimpy mouse. It carries a point mutation in the plp1 gene. The mutated protein accumulates in the Golgi complex and eventually causes death of the expressing oligodendrocytes (Gow, Friedrich et al. 1994; Jung, Sommer et al. 1996; Thomson, Montague et al. 1997; Gow, Southwood et al. 1998; Kramer, Schardt et al. 2001; Southwood and Gow 2001; Bauer, Bradl et al. 2002; Ghandour, Feutz et al. 2002; Dhaunchak and Nave 2007).

As expected, I found little myelination in the optic nerve of Jimpy mutant mice, and the few axons with myelination showed a rather non-compact myelin sheath (Fig. 4.2.B, F) (Meier and Bischoff 1975; Omlin and Anders 1983). However, I did not observe any difference in the ultrastructure of the optic nerve axons and the ganglion cell bodies. The number of the cells in the ganglion cell layer and the axon

count in the optic nerve was not altered either (Figure 4-2. C, Figure 6-1. G). I conclude that the lack of myelin does not lead to obvious ganglion cell damage or death, at least not at the very young age that is still testable (P21) before the affected animals die. This conclusion was supported by the behavioral optokinetic reflex test, which showed that visual information can be transmitted along the optic nerve in these animals.

Recording ganglion cell activity in retinas from wild type and Jimpy mutant mice revealed minor differences. Jimpy mutant ganglion cells tended to have a slightly lower friring rate in mesopic ambient luminance (Figure 6-2), which might be caused by dysmyelination. Note, however, that during MEA recordings, the retina is isolated, and the largest part of the axon, including the myelinated part, has been cut off. Therefore, any difference in spiking properties cannot be explained by a difference in the acute myelination status. Rather, such differences must stem from changed cellular properties of the neurons. One possibility might be that unmyelinated ganglion cells of the Jimpy mutant express a different complement of voltage gated sodium channels (or other channels involved in spike generation and propagation) than normal myelinated ganglion cells, or that the expression density of such channels is changed. Such a change in channel composition might lead to different spiking properties. However, it should be noted, that the differences between wild type and Jimpy mutant ganglion cell activity is not fixed, but influenced by the ambient light level. Potentially, activation of different retinal circuits in those different conditions (rod-driven vs. rod/cone-driven circuitry) leads to different polarization states in the ganglion cells, so that the observed difference in spike rate could be explained by ganglion cell autonomous differences. Alternatively, visual processing in the retina might also be different between the two genotypes. Interestingly, I mainly see differences of the stimulus-evoked spike rate in the mesopic brightness level, when rods and cones interact in the outer retina, and rod-pathways and cone-pathways interact in the inner retina. The two cell types for which I have seen a change in cell number – horizontal cells and rod bipolar cells (Figure 7-4) – are involved at both levels of these interactions (Rieke 2001; Baccus and Meister 2002; Chichilnisky and Kalmar 2002; Demb 2002; Demb 2008).

On the histological level, the retina seemed unaffected in Jimpy mice at first sight, which would be consistent with the mutated gene not being expressed in the retina. The gross retinal morphology was normal, the layering of the retina intact, and the thickness of the individual layers did not differ between Jimpy mice and their wild type littermates, although there was a (non-significant) tendency for the Jimpy retinal layers to be slightly thicker (Figure 7-1. D). The number of neurons in the three nuclear layers was also not affected, suggesting the absence of significant cell death. However, closer inspection revealed that the cell bodies in the inner nuclear layer (INL) in Jimpy retina appeared larger (Figure 7-1. E,F). The larger cell bodies could not be attributed to artifacts of the staining procedure (e.g., swelling), because, first, staining was performed in parallel on Jimpy and wild type retinal sections, and second, other cell bodies in the same tissue were not affected or affected to a much smaller degree. I cannot fully exclude that the increase in cell-body size is partly influenced by the EdaTA mutation: 3 out of the 4 Jimpy mutant mice used for these particular experiments carried that mutation in addition of the plp1jp mutation. However, the one retina lacking EdaTA mutation (i.e. pure plp1jp mutation) had the largest cell bodies of all mutants (Figure 7-2. B).

Larger cell bodies on the population level could be explained by changes in cell body size of individual neurons, or by a changing balance in cell composition: cells with smaller cell bodies could be less numerous, and cells with larger cell bodies more numerous. To test for this, I have immunolabeled four retinal cell types with cell bodies in the INL: horizontal cells, rod bipolar cells, starburst amacrine cells, and Müller glia cells (Figure 7-4 and Figure 7-5).

Starburst and Müller cells had unchanged cell densities in Jimpy retinas compared to wild type (Figure 7-5). The other two cell types, horizontal cells and rod bipolar cells, both had increased cell densities (Figure 7-4. A, B). Horizontal cells are cells with big cell bodies; the increase in their density, as measured in wholemount retina, is consistent with the overall increased size of cell bodies in the INL, as measured in retinal cross sections (Figure 7-1. D). Rod bipolar cells, on the other hand, are cells with small cell bodies. An increase in their density is inconsistent with the observed changes in cell body size distribution.

It should be noted that I did not see an increase in overall cell number in the Jimpy retina (Figure 7-1. E,F). Nevertheless, both individual cell types that showed changes, horizontal cells and rod bipolar cells, increased their density. This suggests that further cell types, so far not identified, possibly decrease in number.

It is not clear why I see changes in the inner retina at all. The mutated gene in the Jimpy mouse, plp1, is not expressed in the retina. One possible reason might be a difference in proliferation of cells in Jimpy and wild type mouse lines. It is known that the mutated gene is first expressed during development when oligodendrocytes start to be differentiated (in the optic nerve starting from P5 (Meier and Bischoff 1975; Omlin and Anders 1983)). This takes place when the retina is still immature and, potentially, developmental mechanisms and pathways might somehow be altered.

A second mechanistic possibility of how the retina of Jimpy mice might be influenced by the plp1 mutation might be through sparse centrifugal innervation. The existence of these projections from the brain into the retina has been shown in primates (Gastinger, O'Brien et al. 1999), birds (Nickla, Gottlieb et al. 1994) , in Xenopus tadpoles (Du, Wei et al. 2009) and rats (Feigenspan and Bormann 1994; Gastinger, Barber et al. 2001; Gastinger, Barber et al. 2006). It has been suggested that these neurons are histaminergic and serve to modulate the operational state of the retina. In rats they have varicose terminal branches in the inner and outer plexiform layer (IPL, OPL) (Gastinger, Barber et al. 2006). Thus, the retina might be innervated by neurons that experience dysmyelination, that might therefore be in a changed physiological state, and that therefore – by their modulatory action – affect the retina.

My data do neither support nor refute any of the two mechansims suggested above. What these mechanisms have in common is that they have to act at an earlier stage during development, preceeding the time point at which I have made my observations (P20-P22). To gain more clarity on potential mechanism, it would be necessary to observe the affected cell types (horizontal cells and rod bipolar cells) throughout development.

In summary, I found that the plp1jp mutation resulted in only minor changes in the retina of Jimpy mutant mice. In particular, both the physiology and morphology of ganglion cells was hardly affected, despite a very severe dysmyelination phenotype in the optic nerve. This suggests that dysmyelination has minor effects on the involved neurons (the retinal ganglion cells), at least within the timeframe measurable in the Jimpy mouse model before the mutant animals die.

9. References

Abbott, N. J., L. Ronnback, et al. (2006). "Astrocyte-endothelial interactions at the blood-brain barrier." Nat Rev Neurosci 7(1): 41-53.

Abdeljalil, J., M. Hamid, et al. (2005). "The optomotor response: a robust first-line visual screening method for mice." Vision Res 45(11): 1439-1446.

Baccus, S. A. and M. Meister (2002). "Fast and slow contrast adaptation in retinal circuitry." Neuron 36(5): 909-919.

Bauer, J., M. Bradl, et al. (2002). "Endoplasmic reticulum stress in PLP-overexpressing transgenic rats: gray matter oligodendrocytes are more vulnerable than white matter oligodendrocytes." J Neuropathol Exp Neurol 61(1): 12-22.

Baumann, N. and D. Pham-Dinh (2001). "Biology of oligodendrocyte and myelin in the mammalian central nervous system." Physiol Rev 81(2): 871-927.

Benkner, B., M. Mutter, et al. (2013). "Characterizing visual performance in mice: an objective and automated system based on the optokinetic reflex." Behav Neurosci 127(5): 788-796.

Bergles, D. E., J. D. Roberts, et al. (2000). "Glutamatergic synapses on oligodendrocyte precursor cells in the hippocampus." Nature 405(6783): 187-191.

Billon, N., C. Jolicoeur, et al. (2002). "Normal timing of oligodendrocyte development depends on thyroid hormone receptor alpha 1 (TRalpha1)." EMBO J 21(23): 6452-6460.

Bradl, M. and H. Lassmann (2010). "Oligodendrocytes: biology and pathology." Acta Neuropathol 119(1): 37-53.

Butt, A. M., M. Pugh, et al. (2004). "Functions of optic nerve glia: axoglial signalling in physiology and pathology." Eye (Lond) 18(11): 1110-1121.

Campagnoni, A. T. and W. B. Macklin (1988). "Cellular and molecular aspects of myelin protein gene expression." Mol Neurobiol 2(1): 41-89.

Chichilnisky, E. J. (2001). "A simple white noise analysis of neuronal light responses." Network 12(2): 199-213.

Chichilnisky, E. J. and R. S. Kalmar (2002). "Functional asymmetries in ON and OFF ganglion cells of primate retina." J Neurosci 22(7): 2737-2747.

Coco, S., F. Calegari, et al. (2003). "Storage and release of ATP from astrocytes in culture." J Biol Chem 278(2): 1354-1362.

Colello, R. J., U. Pott, et al. (1994). "The role of oligodendrocytes and myelin on axon maturation in the developing rat retinofugal pathway." J Neurosci 14(5 Pt 1): 2594-2605.

Dangata, Y. Y., G. S. Findlater, et al. (1996). "Postnatal development of the optic nerve in (C57BL x CBA)F1 hybrid mice: general changes in morphometric parameters." J Anat 189 (Pt 1): 117-125.

Dawson, M. R., A. Polito, et al. (2003). "NG2-expressing glial progenitor cells: an abundant and widespread population of cycling cells in the adult rat CNS." Mol Cell Neurosci 24(2): 476-488.

De Biase, L. M., A. Nishiyama, et al. (2010). "Excitability and synaptic communication within the oligodendrocyte lineage." J Neurosci 30(10): 3600-3611.

Demb, J. B. (2002). "Multiple mechanisms for contrast adaptation in the retina." Neuron 36(5): 781-783.

Demb, J. B. (2008). "Functional circuitry of visual adaptation in the retina." J Physiol 586(Pt 18): 4377-4384.

Dhaunchak, A. S. and K. A. Nave (2007). "A common mechanism of PLP/DM20 misfolding causes cysteine-mediated endoplasmic reticulum retention in oligodendrocytes and Pelizaeus-Merzbacher disease." Proc Natl Acad Sci U S A 104(45): 17813-17818.

Diniz, L. P., J. C. Almeida, et al. (2012). "Astrocyte-induced synaptogenesis is mediated by transforming growth factor beta signaling through modulation of D-serine levels in cerebral cortex neurons." J Biol Chem 287(49): 41432-41445.

Du, J. L., H. P. Wei, et al. (2009). "Long-range retrograde spread of LTP and LTD from optic tectum to retina." Proc Natl Acad Sci U S A 106(45): 18890-18896.

Duncan, I. D., J. P. Hammang, et al. (1989). "Myelination in the jimpy mouse in the absence of proteolipid protein." Glia 2(3): 148-154.

Eric R. Kandel, J. H. S., Thomas M. Jessell (2000). "Principles of Neural Science."

Farkas-Bargeton, E., O. Robain, et al. (1972). "Abnormal glial maturation in the white matter in Jimpy mice. An optical study." Acta Neuropathol 21(4): 272-281.

Feigenspan, A. and J. Bormann (1994). "Facilitation of GABAergic signaling in the retina by receptors stimulating adenylate cyclase." Proc Natl Acad Sci U S A 91(23): 10893-10897.

Ferguson, B. M., N. Brockdorff, et al. (1997). "Cloning of Tabby, the murine homolog of the human EDA gene: evidence for a membrane-associated protein with a short collagenous domain." Hum Mol Genet 6(9): 1589-1594.

Fisher, L. J. (1979). "Development of synaptic arrays in the inner plexiform layer of neonatal mouse retina." J Comp Neurol 187(2): 359-372.

Frohlich, N., B. Nagy, et al. (2011). "Fate of neuron-glia synapses during proliferation and differentiation of NG2 cells." J Anat 219(1): 18-32.

Gao, L., W. Macklin, et al. (2006). "Intrinsic and extrinsic inhibition of oligodendrocyte development by rat retina." Dev Biol 290(2): 277-286.

Gastinger, M. J., A. J. Barber, et al. (2001). "Abnormal centrifugal axons in streptozotocin-diabetic rat retinas." Invest Ophthalmol Vis Sci 42(11): 2679-2685.

Gastinger, M. J., A. J. Barber, et al. (2006). "Histamine receptors in mammalian retinas." J Comp Neurol 495(6): 658-667.

Gastinger, M. J., J. J. O'Brien, et al. (1999). "Histamine immunoreactive axons in the macaque retina." Invest Ophthalmol Vis Sci 40(2): 487-495.

Ge, W. P., W. Zhou, et al. (2009). "Dividing glial cells maintain differentiated properties including complex morphology and functional synapses." Proc Natl Acad Sci U S A 106(1): 328-333.

Genetics. (2008). "PLP1." from http://ghr.nlm.nih.gov/gene/PLP1.

Gensert, J. M. and J. E. Goldman (1997). "Endogenous progenitors remyelinate demyelinated axons in the adult CNS." Neuron 19(1): 197-203.

Ghandour, M. S., A. C. Feutz, et al. (2002). "Trafficking of PLP/DM20 and cAMP signaling in immortalized jimpy oligodendrocytes." Glia 40(3): 300-311.

Godement, P., J. Salaun, et al. (1984). "Prenatal and postnatal development of retinogeniculate and retinocollicular projections in the mouse." J Comp Neurol 230(4): 552-575.

Gow, A., V. L. Friedrich, Jr., et al. (1994). "Many naturally occurring mutations of myelin proteolipid protein impair its intracellular transport." J Neurosci Res 37(5): 574-583.

Gow, A., C. M. Southwood, et al. (1998). "Disrupted proteolipid protein trafficking results in oligodendrocyte apoptosis in an animal model of Pelizaeus-Merzbacher disease." J Cell Biol 140(4): 925-934.

Greer, J. M. (2013). "Autoimmune T-cell reactivity to myelin proteolipids and glycolipids in multiple sclerosis." Mult Scler Int 2013: 151427.

Greer, J. M. and M. B. Lees (2002). "Myelin proteolipid protein--the first 50 years." Int J Biochem Cell Biol 34(3): 211-215.

Hartline, D. K. and D. R. Colman (2007). "Rapid conduction and the evolution of giant axons and myelinated fibers." Curr Biol 17(1): R29-35.

Hildebrand, C., S. Remahl, et al. (1993). "Myelinated nerve fibres in the CNS." Prog Neurobiol 40(3): 319-384.

Honjin, R., S. Sakato, et al. (1977). "Electron microscopy of the mouse optic nerve: a quantitative study of the total optic nerve fibers." Arch Histol Jpn 40(4): 321-332.

Hsieh-Wilson, G. (2002). "Neural Connections." from http://chemistry.caltech.edu/groups/hsieh/hsieh1/neuralco.htm.

Imaizumi, T., J. D. Kocsis, et al. (1998). "Resistance to anoxic injury in the dorsal columns of adult rat spinal cord following demyelination." Brain Res 779(1-2): 292-296.

Imaizumi, T., K. L. Lankford, et al. (1998). "Transplanted olfactory ensheathing cells remyelinate and enhance axonal conduction in the demyelinated dorsal columns of the rat spinal cord." J Neurosci 18(16): 6176-6185.

Jabr, F. (2012). Chapter 4: What is the Ratio of Glia to Neurons in the Brain?

Jahn, O., S. Tenzer, et al. (2009). "Myelin proteomics: molecular anatomy of an insulating sheath." Mol Neurobiol 40(1): 55-72.

Jung, M., I. Sommer, et al. (1996). "Monoclonal antibody O10 defines a conformationally sensitive cell-surface epitope of proteolipid protein (PLP): evidence that PLP misfolding underlies dysmyelination in mutant mice." J Neurosci 16(24): 7920-7929.

Kalwy, S. A. and R. Smith (1994). "Mechanisms of myelin basic protein and proteolipid protein targeting in oligodendrocytes (review)." Mol Membr Biol 11(2): 67-78.

Keenan, E. (2008). QUANTIFICATION OF RETINAL GANGLION CELL AXONS IN A MURINE MODEL OF DIABETIC RETINOPATHY

Kitagawa, K., M. P. Sinoway, et al. (1993). "A proteolipid protein gene family: expression in sharks and rays and possible evolution from an ancestral gene encoding a pore-forming polypeptide." Neuron 11(3): 433-448.

Klugmann, M., M. H. Schwab, et al. (1997). "Assembly of CNS myelin in the absence of proteolipid protein." Neuron 18(1): 59-70.

Knapp, P. E., R. P. Skoff, et al. (1986). "Oligodendroglial cell death in jimpy mice: an explanation for the myelin deficit." J Neurosci 6(10): 2813-2822.

Kramer, E. M., A. Schardt, et al. (2001). "Membrane traffic in myelinating oligodendrocytes." Microsc Res Tech 52(6): 656-671.

Kukley, M., E. Capetillo-Zarate, et al. (2007). "Vesicular glutamate release from axons in white matter." Nat Neurosci 10(3): 311-320.

Kukley, M., M. Kiladze, et al. (2008). "Glial cells are born with synapses." FASEB J 22(8): 2957-2969.

Kukley, M., A. Nishiyama, et al. (2010). "The fate of synaptic input to NG2 glial cells: neurons specifically downregulate transmitter release onto differentiating oligodendroglial cells." J Neurosci 30(24): 8320-8331.

Lagali, P. S., D. Balya, et al. (2008). "Light-activated channels targeted to ON bipolar cells restore visual function in retinal degeneration." Nat Neurosci 11(6): 667-675.

Lam, K., A. J. Sefton, et al. (1982). "Loss of axons from the optic nerve of the rat during early postnatal development." Brain Res 255(3): 487-491.

Lin, S. C. and D. E. Bergles (2004). "Synaptic signaling between GABAergic interneurons and oligodendrocyte precursor cells in the hippocampus." Nat Neurosci 7(1): 24-32.

Marquardt, T. and P. Gruss (2002). "Generating neuronal diversity in the retina: one for nearly all." Trends Neurosci 25(1): 32-38.

Masland, R. H. (2001). "The fundamental plan of the retina." Nat Neurosci 4(9): 877-886.

May, C. A. and E. Lutjen-Drecoll (2002). "Morphology of the murine optic nerve." Invest Ophthalmol Vis Sci 43(7): 2206-2212.

Meier, C. and A. Bischoff (1975). "Oligodendroglial cell development in jimpy mice and controls. An electron-microscopic study in the optic nerve." J Neurol Sci 26(4): 517-528.

Meister, M., J. Pine, et al. (1994). "Multi-neuronal signals from the retina: acquisition and analysis." J Neurosci Methods 51(1): 95-106.

Mitchiner, J. C., L. H. Pinto, et al. (1976). "Visually evoked eye movements in the mouse (Mus musculus)." Vision Res 16(10): 1169-1171.

Møller, A. R. (2003). Sensory Systems: Anatomy and Physiology.

Mooney, R., A. A. Penn, et al. (1996). "Thalamic relay of spontaneous retinal activity prior to vision." Neuron 17(5): 863-874.

Morgan, J. L., A. Dhingra, et al. (2006). "Axons and dendrites originate from neuroepithelial-like processes of retinal bipolar cells." Nat Neurosci 9(1): 85-92.

Munch, T. A., R. A. da Silveira, et al. (2009). "Approach sensitivity in the retina processed by a multifunctional neural circuit." Nat Neurosci 12(10): 1308-1316.

Nave, K. A. (2010). "Myelination and the trophic support of long axons." Nat Rev Neurosci 11(4): 275-283.

Nickla, D. L., M. D. Gottlieb, et al. (1994). "The retinal targets of centrifugal neurons and the retinal neurons projecting to the accessory optic system." Vis Neurosci 11(2): 401-409.

Nishiyama, A., M. Komitova, et al. (2009). "Polydendrocytes (NG2 cells): multifunctional cells with lineage plasticity." Nat Rev Neurosci 10(1): 9-22.

Nishiyama, A., X. H. Lin, et al. (1996). "Co-localization of NG2 proteoglycan and PDGF alpha-receptor on O2A progenitor cells in the developing rat brain." J Neurosci Res 43(3): 299-314.

Oberwahrenbrock, T., S. Schippling, et al. (2012). "Retinal damage in multiple sclerosis disease subtypes measured by high-resolution optical coherence tomography." Mult Scler Int 2012: 530305.

Ohsawa, R. and R. Kageyama (2008). "Regulation of retinal cell fate specification by multiple transcription factors." Brain Res 1192: 90-98.

Omlin, F. X. and J. J. Anders (1983). "Abnormal cell relationships in Jimpy mice: electron microscopic and immunocytochemical findings." J Neurocytol 12(5): 767-784.

Ono, K., Y. Yasui, et al. (1997). "Focal ventricular origin and migration of oligodendrocyte precursors into the chick optic nerve." Neuron 19(2): 283-292.

Perge, J. A., K. Koch, et al. (2009). "How the optic nerve allocates space, energy capacity, and information." J Neurosci 29(24): 7917-7928.

Peters, A., K. Josephson, et al. (1991). "Effects of aging on the neuroglial cells and pericytes within area 17 of the rhesus monkey cerebral cortex." Anat Rec 229(3): 384-398.

Poliak, S. and E. Peles (2003). "The local differentiation of myelinated axons at nodes of Ranvier." Nat Rev Neurosci 4(12): 968-980.

Psachoulia, K., F. Jamen, et al. (2009). "Cell cycle dynamics of NG2 cells in the postnatal and ageing brain." Neuron Glia Biol 5(3-4): 57-67.

Raff, M. C., R. Mirsky, et al. (1978). "Galactocerebroside is a specific cell-surface antigenic marker for oligodendrocytes in culture." Nature 274(5673): 813-816.

Reichenbach, A. and A. Bringmann (2013). "New functions of Muller cells." Glia 61(5): 651-678.

Reinhard, K., A. Tikidji-Hamburyan, et al. (2014). "Step-by-step instructions for retina recordings with perforated multi electrode arrays." PLoS One 9(8): e106148.

Rieke, F. (2001). "Temporal contrast adaptation in salamander bipolar cells." J Neurosci 21(23): 9445-9454.

Rivers, L. E., K. M. Young, et al. (2008). "PDGFRA/NG2 glia generate myelinating oligodendrocytes and piriform projection neurons in adult mice." Nat Neurosci 11(12): 1392-1401.

Rock, R. B., G. Gekker, et al. (2004). "Role of microglia in central nervous system infections." Clin Microbiol Rev 17(4): 942-964, table of contents.

Schraermeyer, M., S. Schnichels, et al. (2009). "Ultrastructural analysis of the pigment dispersion syndrome in DBA/2J mice." Graefes Arch Clin Exp Ophthalmol 247(11): 1493-1504.

Siegert, S., E. Cabuy, et al. (2012). "Transcriptional code and disease map for adult retinal cell types." Nat Neurosci 15(3): 487-495, S481-482.

Skoff, R. P. (1976). "Myelin deficit in the Jimpy mouse may be due to cellular abnormalities in astroglia." Nature 264(5586): 560-562.

Skoff, R. P., D. L. Price, et al. (1976). "Electron microscopic autoradiographic studies of gliogenesis in rat optic nerve. II. Time of origin." J Comp Neurol 169(3): 313-334.

Smith, R. (1992). "The basic protein of CNS myelin: its structure and ligand binding." J Neurochem 59(5): 1589-1608.

Southwood, C. and A. Gow (2001). "Molecular pathways of oligodendrocyte apoptosis revealed by mutations in the proteolipid protein gene." Microsc Res Tech 52(6): 700-708.

Spassky, N., F. de Castro, et al. (2002). "Directional guidance of oligodendroglial migration by class 3 semaphorins and netrin-1." J Neurosci 22(14): 5992-6004.

Sugimoto, Y., M. Taniguchi, et al. (2001). "Guidance of glial precursor cell migration by secreted cues in the developing optic nerve." Development 128(17): 3321-3330.

Sun, D., M. Lye-Barthel, et al. (2009). "The morphology and spatial arrangement of astrocytes in the optic nerve head of the mouse." J Comp Neurol 516(1): 1-19.

Tabata, H., N. Shimizu, et al. (2010). "Initiation of the optokinetic response (OKR) in mice." J Vis 10(1): 13 11-17.

Thomson, C. E., P. Montague, et al. (1997). "Phenotypic severity of murine Plp mutants reflects in vivo and in vitro variations in transport of PLP isoproteins." Glia 20(4): 322-332.

Tian, N. (2004). "Visual experience and maturation of retinal synaptic pathways." Vision Res 44(28): 3307-3316.

Tian, N. and D. R. Copenhagen (2001). "Visual deprivation alters development of synaptic function in inner retina after eye opening." Neuron 32(3): 439-449.

Trapp, B. D. and K. A. Nave (2008). "Multiple sclerosis: an immune or neurodegenerative disorder?" Annu Rev Neurosci 31: 247-269.

Tsai, H. H. and R. H. Miller (2002). "Glial cell migration directed by axon guidance cues." Trends Neurosci 25(4): 173-175; discussion 175-176.

Vela, J. M., B. Gonzalez, et al. (1998). "Understanding glial abnormalities associated with myelin deficiency in the jimpy mutant mouse." Brain Res Brain Res Rev 26(1): 29-42.

Velez-Fort, M., E. Audinat, et al. (2009). "Functional alpha 7-containing nicotinic receptors of NG2-expressing cells in the hippocampus." Glia 57(10): 1104-1114.

Volgyi, B., S. Chheda, et al. (2009). "Tracer coupling patterns of the ganglion cell subtypes in the mouse retina." J Comp Neurol 512(5): 664-687.

Wallman, J. (1993). "Subcortical optokinetic mechanisms." Rev Oculomot Res 5: 321-342.

Witkovsky, P. (2006). Chapter 20, Functional Anatomy of the Retina.

Young, K. M., K. Psachoulia, et al. (2013). "Oligodendrocyte dynamics in the healthy adult CNS: evidence for myelin remodeling." Neuron 77(5): 873-885.

Zhang, Y., I. J. Kim, et al. (2012). "The most numerous ganglion cell type of the mouse retina is a selective feature detector." Proc Natl Acad Sci U S A 109(36): E2391-2398.

Ziskin, J. L., A. Nishiyama, et al. (2007). "Vesicular release of glutamate from unmyelinated axons in white matter." Nat Neurosci 10(3): 321-330.